Coordination Chemistry Reviews, 83 (1988) 199–275
Elsevier Science Publishers B.V., Amsterdam – Printed in The Netherlands

ELECTROCHEMISTRY OF METAL–SULFUR CLUSTERS: STEREOCHEMICAL CONSEQUENCES OF THERMODYNAMICALLY CHARACTERIZED REDOX CHANGES

Part I. Homometal clusters

PIERO ZANELLO

Dipartimento di Chimica dell'Università di Siena, Pian dei Mantellini, 44 — 53100 Siena (Italy)

(Received 28 November 1986)

CONTENTS

0010-8545/88/$26.95

ABBREVIATIONS FOR SOLVENTS

AN	acetonitrile
BN	benzonitrile
DCE	1,2-dichloroethane
DCM	dichloromethane
DME	1,2-dimethoxyethane
DMF	*N*,*N*-dimethylformamide
DMSO	dimethylsulfoxide
NMP	*N*-methyl-2-pyrrolidinone
MeOH	methanol
TMU	tetramethylurea

INTRODUCTION

Metal–sulfur clusters play a prominent role as synthetic analogues of the active sites of important biological functions [1,2], but their chemistry is even more important because of their involvement in the fields of heterogeneous catalysis [3,4] and superconductivity [5–7], and for the novelty of their theoretical, structural and synthetic aspects.

Since for the most part, these polynuclear compounds undergo electron-transfer reactions, it is useful to have a thermodynamic survey of their ability to undergo redox changes, together with knowledge of the relevant structural effects. One of the most representative examples is the well-known [8] structural reorganization of the Fe_4S_4 core of the cubane-like tetranuclear anions $[Fe_4S_4(SR)_4]^{2-,3-}$ consequent to a one-electron charge transfer namely:

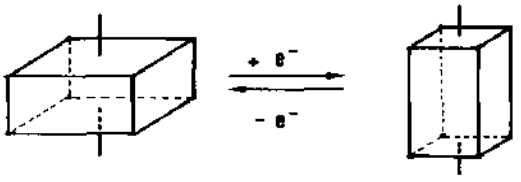

$[Fe_4S_4(SR)_4]^{2-}$ compressed D_{2d} $[Fe_4S_4(SR)_4]^{3-}$ elongated D_{2d}

AN solutions
R = Ph
$E^{\circ\prime} = -1.25$ V(vs. Fc^+/Fc)

For an easy comparison of the standard electrode potentials found in different solvents and with respect to different reference electrodes, we will report, unless otherwise specified, redox potentials with respect to the ferrocenium/ferrocene couple (Fc^+/Fc) [9,10], in view of the commonly accepted extrathermodynamic assumption that the redox potential of this couple is independent of the solvent.

B. IRON–SULFUR CLUSTERS

With the intent of modelling active sites of nonheme iron–sulfur proteins [1], a great deal of work has recently been devoted to the synthesis and physicochemical characterization of a variety of iron–sulfur assemblies.

(i) Fe_3S core

The carbonyl complex $H_2Fe_3(CO)_9S$ contains an Fe_3S core, in which a sulfur atom is triply bridged to an Fe_3 triangular unit, according to the proposed structure shown in Fig. 1 [11].

In polar solvents this complex behaves as a dibasic acid. The relevant dianion $[Fe_3(CO)_9S]^{2-}$ undergoes a quasi-reversible one-electron anodic oxidation in dichloroethane solvent [12]. The diagnostic parameters of the charge transfer (namely, the peak current ratio $i_{pc}/i_{pa} < 1$) are, however, indicative of the instability of the electrogenerable species $[Fe_3(CO)_9S]^-$.

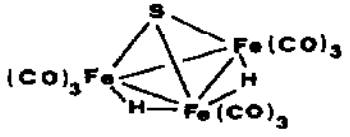

Fig. 1. Proposed structure of the complex $H_2Fe_3(CO)_9(\mu_3\text{-}S)$.

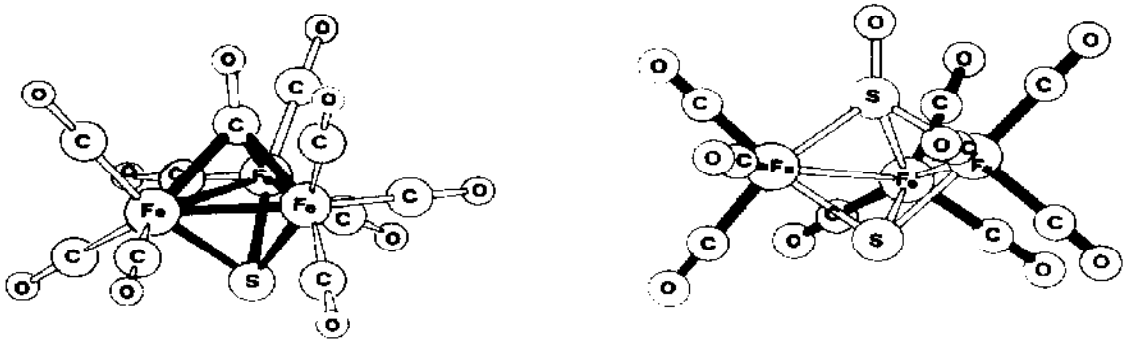

Fig. 2. Molecular structure of the complexes $Fe_3(CO)_9(S)(CO)$ (from ref. 14) and $Fe_3(CO)_9(S)(SO)$ (from ref. 15).

The redox properties of two other sulfur capped tri-iron complexes of formula $Fe_3(CO)_9(\mu_3\text{-}S)(\mu_3\text{-}X)$ (X = CO; X = SO) have been studied electrochemically [13].

In these cases too the Fe_3S core is formed by an apical triply bridging S atom lying over the trimetallic plane as shown in Fig. 2.

Interestingly, however, whilst in $Fe_3(CO)_9(S)(CO)$ the three iron atoms are in a closed triangle (i.e., three metal–metal bonds), in $Fe_3(CO)_9(S)(SO)$ they are in an open triangle (i.e., two metal–metal bonds).

In nonaqueous solvents, $Fe_3(CO)_9(S)(CO)$ undergoes a well-defined one-electron oxidation and a well-defined one-electron reduction. Both processes, however, appear as irreversible steps, probably because of the instability of the monocation $[Fe_3(CO)_9(S)(CO)]^+$ as well as of the monoanion $[Fe_3(CO)_9(S)(CO)]^-$. In fact, if we consider the molecular orbital diagram for the neutral parent [16] (Fig. 3), it is conceivable that the removal of one electron from the triply bridging CO leads to destruction of the molecule (leaving only one electron for three CO–Fe bonds). Likewise, it is likely that the addition of one electron to a highly destabilized antibonding orbital leads to an energetically unstable framework.

In a similar manner $Fe_3(CO)_9(S)(SO)$ undergoes two well-defined consecutive one-electron reductions, irreversible in character.

Another electrochemically studied Fe_3S structural unit is present in the sulfide–thiolate compound $[Fe_3S(1,2\text{-}(SCH_2)_2C_6H_4)_3](NEt_4)_2$, the structure of which is reported in Fig. 4 [17].

In the pyramidal fragment Fe_3S, the apical μ_3-S atom is 1.66 Å above the Fe_3 plane. Each metal atom is surrounded by a tetrahedron of sulfur atoms and each dithiolate ligand is involved with one bridging and one terminal sulfur atom. The three bridging and three terminal dithiolate sulfur atoms form two parallel planes situated below and above the trimetallic plane.

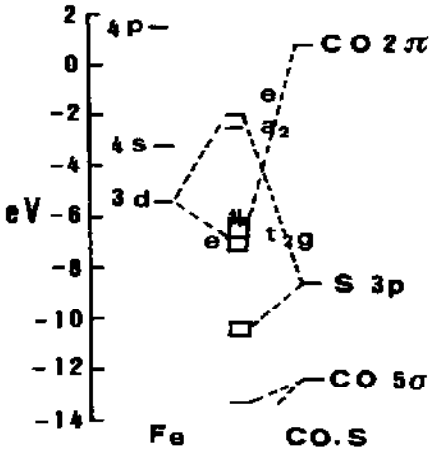

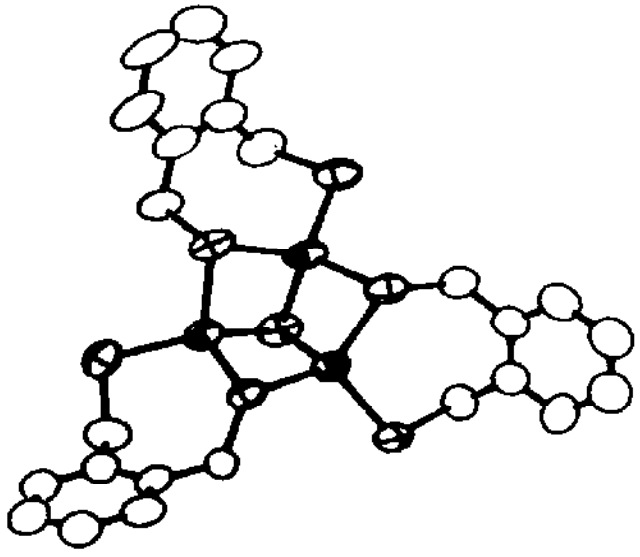

Fig. 3. MO diagram for $Fe_3(CO)_9(S)(CO)$.

Fig. 4. Crystal structure of the dianion $[Fe_3S(1,2\text{-}(SCH_2)_2C_6H_4)_3]^{2-}$ (from ref. 17).

In acetonitrile solution $[Fe_3S(1,2\text{-}(SCH_2)_2C_6H_4)_3]^{2-}$ undergoes a one-electron quasi-reversible anodic oxidation and an irreversible cathodic reduction. No attempts have been made to electrogenerate the monoanion $[Fe_3S(1,2\text{-}(SCH_2)_2C_6H_4)_3]^{-}$.

Table 1 summarizes the redox potentials for the charge transfers of the compounds containing an Fe_3S core.

(ii) Fe_3S_2 core

One of the first iron–sulfur clusters to be studied from the electrochemical viewpoint is the dithiolene complex $Fe_3S_2(S_2C_2\{CF_3\}_2)_4$ [18], for which

TABLE 1

Standard electrode potentials (in volts) for the redox processes observed in compounds containing the Fe_3S core

Complex	Redox processes				Solvent	Ref.
	1+/0	0/1−	1−/2−	2−/3−		
$[Fe_3(CO)_9S]^{2-}$			−0.80		DCE	12
$Fe_3(CO)_9(S)(CO)$	−0.07 [a]	−0.76 [a]			BN	13
$Fe_3(CO)_9(S)(SO)$		−0.81 [a]	−1.50 [a]		BN	13
$[Fe_3S(1,2\text{-}(SCH_2)_2C_6H_4)_3]^{2-}$			−0.84	−2.29 [a]	AN	17

[a] Half-wave (in polarography) or peak potential (in cyclic voltammetry) value for irreversible processes. [b] For solvent abbreviations, here and elsewhere, see list at beginning of article.

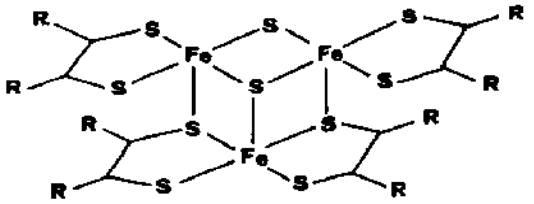

Fig. 5. Proposed structure for the compound $Fe_3S_2(S_2C_2\{CF_3\}_2)_4$.

the structure shown in Fig. 5 has been proposed (but not proven by X-ray diffraction).

In dichloromethane solution this complex undergoes two one-electron cathodic reductions. The chemically generated $[Fe_3S_2(S_2C_2\{CF_3\}_2)_4]^-$ monoanion seems stable in CH_2Cl_2 solution.

The redox behaviour of two other derivatives, namely $Fe_3(CO)_9S_2$ [13] and $Fe_3(CO)_8S_2(C_3H_2S_2)$ [19], containing the Fe_3S_2 core, has been reported.

The derivative $Fe_3(CO)_9(\mu_3\text{-}S)_2$ contains an open triangle of iron atoms, bound to two triply bridging sulfur atoms lying above and below the trimetallic plane as shown in Fig. 6 [20]. As shown in Fig. 7, in benzonitrile solution this sulfur-dicapped complex undergoes two well-defined one-electron reduction steps. The less cathodic step is electrochemically quasi-reversible, but chemically reversible; the more cathodic step is irreversible in character. This result is not entirely rationalizable on the basis of the molecular orbital diagram for $Fe_3(CO)_9S_2$ [16], given in Fig. 8. In fact, the first electron, likely entering the orbital e', increases the population of the Fe–Fe bonding orbitals with respect to the Fe–Fe antibonding orbital a_2'.

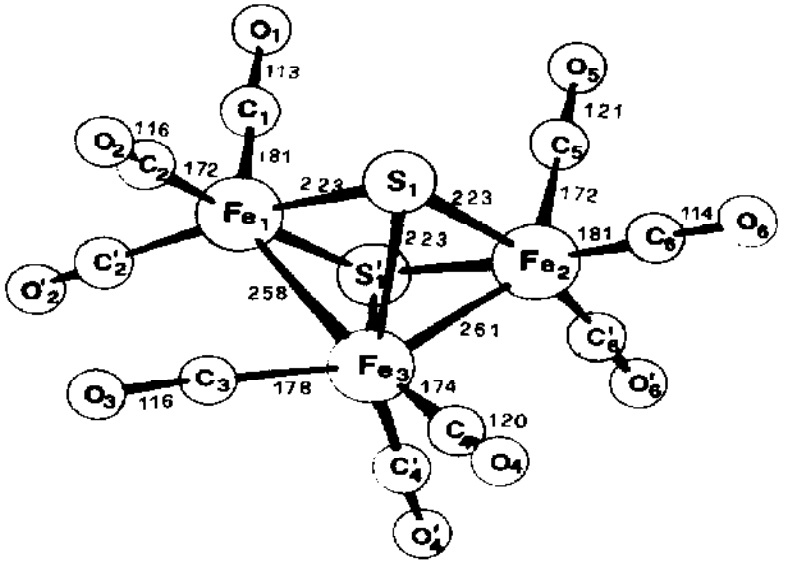

Fig. 6. Molecular structure of $Fe_3(CO)_9S_2$ (from ref. 20).

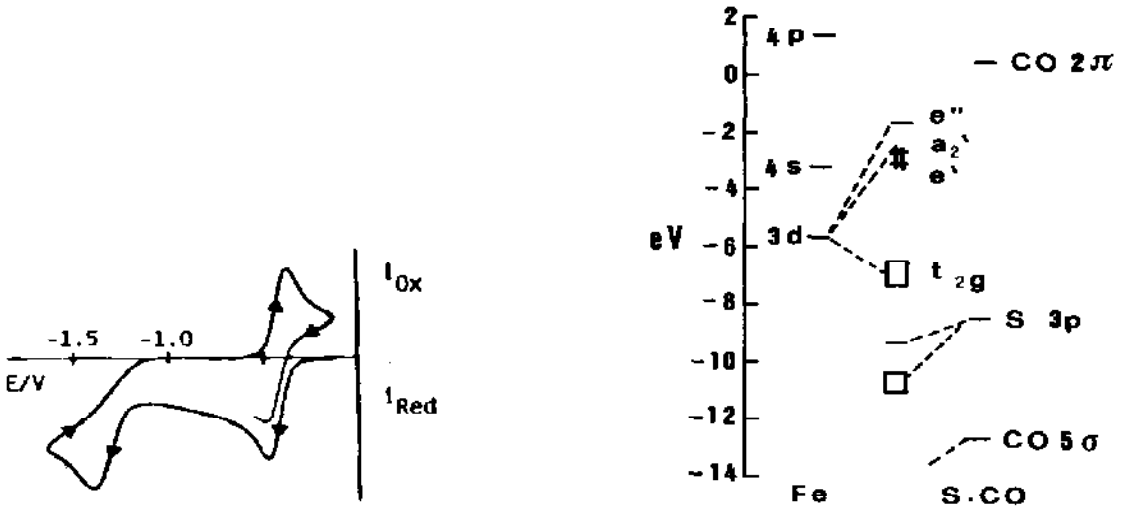

Fig. 7. Cyclic voltammetric behaviour of $Fe_3(CO)_9S_2$ in benzonitrile solution. Potential values vs. Ag/AgCl.

Fig. 8. MO diagram for $Fe_3(CO)_9S_2$.

On the contrary, it is difficult to foresee the rupture of the molecular framework following the addition of the second electron. We can invoke two arguments: (i) after the addition of the first electron, the MO ordering is quite different; (ii) the irreversibility of the second cathodic step is simply due to the slowness of the heterogeneous charge transfer, rather than to an extremely fast reaction coupled to the charge transfer (i.e., the structural reorganization of the molecule).

No attempts to characterize the electrogenerable stable monoanion $[Fe_3(CO)_9S_2]^-$ have been reported.

The structure of the closely related $Fe_3(CO)_8S_2(C_3H_2S_2)$ is shown in Fig. 9 [19].

In dimethylformamide this latter undergoes a reversible one-electron reduction, complicated by following, slow, chemical reactions (probably a decarbonylation reaction), and a multielectron irreversible oxidation. The redox chemistry of $Fe_3(CO)_8S_2(C_3H_2S_2)$ serves to illustrate the electrocatalytic substitution of carbonyl ligands by trimethylphosphite groups in carbonyl clusters.

A less common Fe_3S_2 core is present in the trinuclear species $Fe_3(\eta^5\text{-}C_5H_5)_3(CO)_2(S)(SR)$ ($R = CH_3$, C_2H_5) *. On the basis of their spectro-

* Strictly speaking, if one considers only inorganic sulfur atoms as participating in the metal–sulfur core, these derivatives would belong to the preceding section devoted to the Fe_3S core.

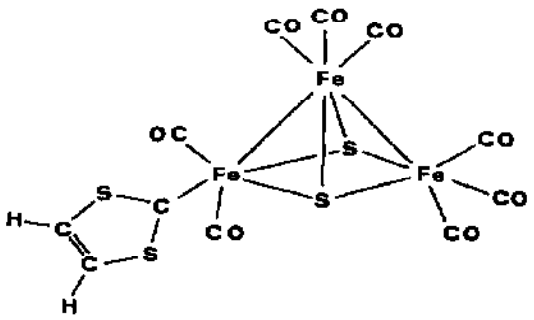

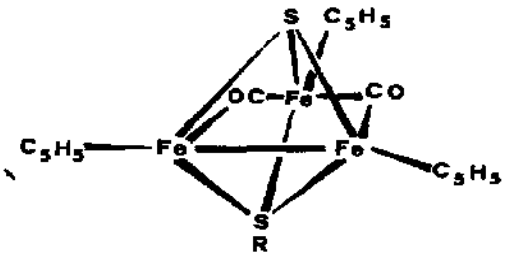

Fig. 9. Schematic representation of the molecular structure of $Fe_3(CO)_8S_2(C_3H_2S_2)$.

Fig. 10. Proposed structure for the species $Fe_3(C_5H_5)_3(CO)_2(S)(SR)$.

scopic properties, the structure illustrated in Fig. 10 has been proposed [21,22].

In dimethoxyethane these derivatives undergo two consecutive one-electron reversible charge transfers leading to $[Fe_3(\eta^5\text{-}C_5H_5)_3(CO)_2(S)SR]^+$ and $[Fe_3(\eta^5\text{-}C_5H_5)_3(CO)_2(S)SR]^{2+}$, respectively. The chemically obtained monocation decomposes fairly rapidly.

Table 2 summarizes the standard potentials evaluated for the redox changes in the compounds containing the Fe_3S_2 assembly.

(iii) Fe_3S_4 core

Two derivatives of formula $[Fe_3S_4(SR)_4](Et_4N)_3$ (R = Ph, Et) contain an electroactive $[Fe_3S_4]^+$ core. As shown in Fig. 11, in this fragment the three tetrahedral iron sites are nearly collinear. The central iron atom is bound to four sulfides, while each terminal iron atom binds two thiolate and two

TABLE 2

Standard potentials (in volts) for the redox processes observed in compounds containing the Fe_3S_2 core

Complex	Redox processes				Solvent	Ref.
	2+/1+	1+/0	0/1−	1−/2−		
$Fe_3S_2\{S_2C_2(CF_3)_2\}_4$			+0.39	−0.17	DCM	18
$Fe_3(CO)_9S_2$			−0.93	−1.88 [a]	BN	13
$Fe_3(CO)_8S_2(C_3H_2S_2)$			−1.18	–	DMF	19
$Fe_3(C_5H_5)_3(CO)_2(S)(SR)$	[b]	[b]	–	–	DME	22

[a] Peak potential value for irreversible charge-transfers. [b] Potential value unknown.

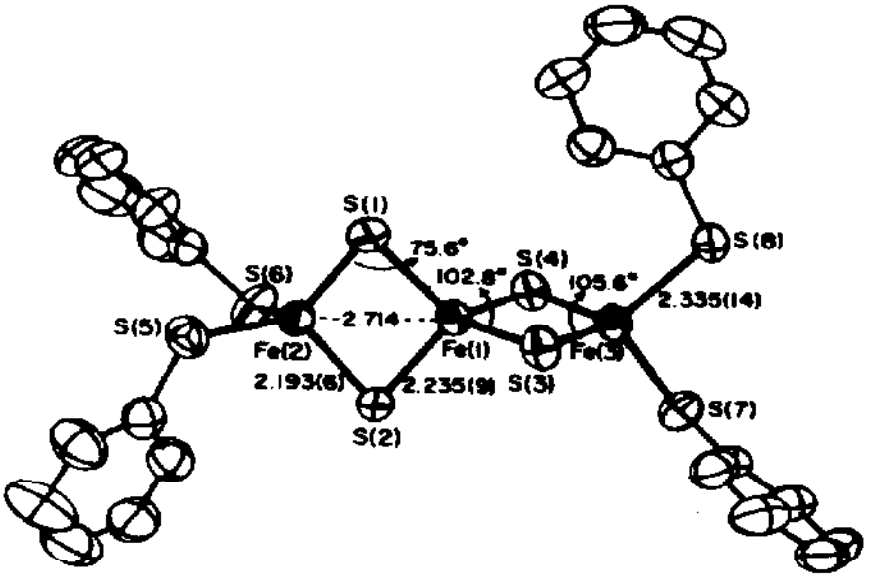

Fig. 11. Molecular structure of $[Fe_3S_4(SPh)_4]^{3-}$ (from ref. 23).

sulfide ligands [23]. Multiple cathodic reduction processes are displayed by these compounds in acetonitrile solvent, only the less cathodic one, however, being core centered and attributed to the redox change $[Fe_3S_4]^{+} \xrightarrow{+e^-} [Fe_3S_4]^{0}$. The presence of chemical complications following this charge transfer is probably due to a declustering reaction [24], which indicates no appreciable flexibility for the present Fe/S assembly. The relevant redox potentials are reported in Table 3.

The marked sensitivity of the redox potentials to the nature of the thiolate group (the alkylthiolate is more electron-donating than the arylthiolate) indicates that the ligands outside the Fe_3S_4 core contribute significantly to the LUMO of these complexes.

TABLE 3

Redox potentials (in volts) for the redox processes observed in acetonitrile solutions of $[Fe_3S_4(SR)_4]^{3-}$

Complex	Core centred redox process 3−/4−	Further reductions	
$[Fe_3S_4(SPh)_4]^{3-}$	−1.60	−1.73 [a]	−1.90 [a]
$[Fe_3S_4(SEt)_4]^{3-}$	−1.91	−2.04	–

[a] Peak potential values for irreversible processes.

(iv) Fe_4S_4 cores

The work devoted to Fe_4S_4 clusters is far more copious than that concerning all other metal–sulfur assemblies. This stems from the fact that cubane-like $|Fe_4S_4(SR)_4|^{1-/2-/3-}$ congeners are good analogs (see Scheme 1) of bacterial ferredoxins (Fd) and high-potential iron proteins (HP), which contain Fe_4S_4 cores attached to cysteinyl ligands able to undergo sequential one-electron redox changes [1].

$$|Fe_4S_4(SR)_4|^{3-} \rightleftarrows |Fe_4S_4(SR)_4|^{2-} \rightleftarrows |Fe_4S_4(SR)_4|^{-}$$
$$Fd_{red} \rightleftarrows Fd_{ox}$$
$$HP_{s\text{-}red} \rightleftarrows HP_{red} \rightleftarrows HP_{ox}$$

Scheme 1

The compounds containing an Fe_4S_4 core have been extensively studied from the redox viewpoint, and the structural reorganizations consequent to these redox changes have been accurately examined. Structural–redox relationships are affected by the type of terminal ligand coordinated to the Fe_4S_4 core.

(a) Fe_4S_4–dithiolene derivatives

The first electrochemical investigations devoted to derivatives containing an Fe_4S_4 core dealt with the isolated polynuclear dithiolene complexes $|Fe_4S_4(S_2C_2R_2)_4|^z$ ($R = CF_3$, $z = 0, 1-, 2-$; $R = Ph$, $z = 0, 1-$) [18,25].

The polarographic behavior of these complexes in nonaqueous solvents revealed the great facility of the Fe_4S_4–dithiolene assembly to undergo, reversibly, a large one-electron transfer series. The relevant redox potentials are summarized in Table 4.

The marked effect on the redox potentials of CF_3 electron-withdrawing groups gives evidence for the effective conjugation of the terminal ligands to the Fe_4S_4 core.

TABLE 4

Redox potentials (in volts) for the redox processes shown by $Fe_4S_4(S_2C_2R_2)$ $Fe_4S_4(S_2C_2R_2)_4$ species ($R = CF_3$, Ph)

Complex	Redox processes				Solvent	Ref.
	0/1	1−/2−	2−/3−	3−/4−		
$Fe_4S_4(S_2C_2\{CF_3\}_2)_4$	+0.49	+0.05	−0.59	−1.2	DCM	18
$Fe_4S_4(S_2C_2Ph_2)_4$	−0.36	−0.65	−1.25	–	DCM	18
	−0.52	−1.03	−1.74	−2.37	DMF	25 [a]

[a] Incorrectly formulated as $Fe_2S_2(S_2C_2Ph_2)_2$.

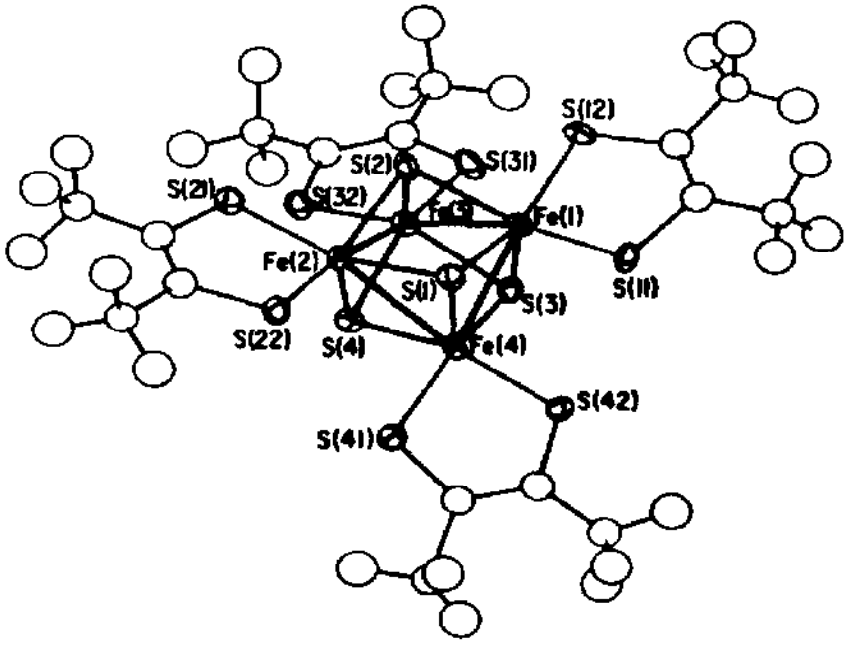

Fig. 12. Crystal structure of $[Fe_4(\mu_3\text{-}S)_4(S_2C_2\{CF_3\}_2)_4]^{2-}$ (from ref. 27).

On the basis of physico-chemical properties, a "cube" structure, with iron and sulfur atoms occupying alternate vertices, was preliminarily assigned to the cores of the isolated $[Fe_4S_4(S_2C_2R_2)_4]^z$ species [18]. Subsequent X-ray investigations on the dianion $[Fe_4(\mu_3\text{-}S)_4(S_2C_2\{CF_3\}_2)_4]^{2-}$ [26,27] confirmed this fundamental geometry, which ideally should be built by two concentric interpenetrating regular tetrahedra of iron atoms and sulfur atoms, respectively. The best refined structure of the dianion is presented in Fig. 12. The Fe_4S_4 core has a tetragonal D_{2d} symmetry compressed along the S_4 axis, with four equivalent Fe–Fe bonding distances shorter than the other two equivalent nonbonding distances (these latter being Fe(1)...Fe(2) and Fe(3)...Fe(4)), as well as four equivalent Fe–S bonds (the vertical Fe(1)–S(3), Fe(2)–S(4), Fe(3)–S(2), Fe(4)–S(1), near parallel to the S_4 axis) shorter than the other eight equivalent Fe–S bonds.

No other crystallographic data are available for either the monoanion or neutral precursors, which might allow one to spot some relationships between redox changes and structural consequences. However, Dahl and co-workers, on the basis of the similarity of both the crystallographic parameters of $[Fe_4(\mu_3\text{-}S)_4(S_2C_2\{CF_3\}_2)_4]^{2-}$ and $[Fe_4(\mu_3\text{-}S)_4(\eta^5\text{-}C_5H_5)_4]^{2+}$ and Mossbauer data on their congeners, $[Fe_4S_4(S_2C_2\{CF_3\}_2)_4]^{0/1-/2-}$ and $[Fe_4S_4(C_5H_5)_4]^{0/1+/2+}$ [27,28] have assumed the same qualitative MO bonding model to be valid [28]. This being true, they foresee then that the anodic oxidation of $[Fe_4(\mu_3\text{-}S)_4(S_2C_2\{CF_3\}_2)_4]^{2-}$ to $[Fe_4(\mu_3\text{-}S)_4(S_2C_2\{CF_3\}_2)_4]^{-}$

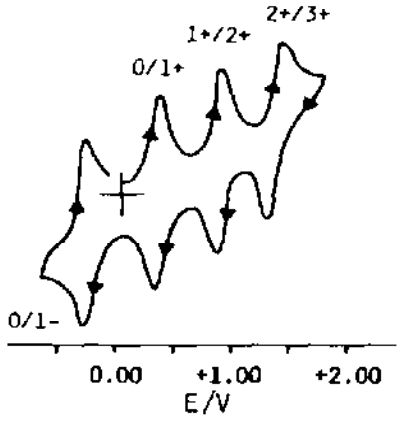

Fig. 13. Cyclic voltammetric response obtained at a platinum electrode in an acetonitrile solution of $Fe_4S_4(C_5H_5)_4$. Potential values vs. S.S.C.E.

would maintain the tetragonal D_{2d} geometry of the Fe_4S_4 core, or alternatively, a slight Jahn–Teller distortion may cause an orthorhombic D_2 configuration. The further oxidation to $Fe_4(\mu_3\text{-}S)_4(S_2C_2\{CF_3\}_2)_4$ would again lead to a tetragonal D_{2d} geometry with a shortening of the four equivalent Fe–Fe bonding distances.

(b) Fe_4S_4–cyclopentadienyl derivatives

The tetrameric cyclopentadienyl sulfide derivative $Fe_4(\eta^5\text{-}C_5H_5)_4(\mu_3\text{-}S)_4$ undergoes four electrochemically reversible charge transfers in acetonitrile [29]. The cyclic voltammogram (Fig. 13) illustrates this unusually rich redox behaviour [28]. The relevant redox potentials are summarized in Table 5.

Of the five, apparently stable, members of this series, up to now only the congeners $[Fe_4S_4(C_5H_5)_4]^{0/1+/2+}$ have been isolated and crystallographically characterized.

The X-ray structure of both the orthorhombic [30] and the monoclinic [31] phases of the neutral parent have been reported. In both phases the Fe_4S_4 core has a tetragonal D_{2d} symmetry, with an elongated cubane framework.

TABLE 5

Standard electrode potentials (in volts) for the redox processes of $Fe_4S_4(C_5H_5)_4$ in acetonitrile

Complex	Redox processes			
	3+/2+	2+/1+	1+/0	0/1−
$Fe_4S_4(C_5H_5)_4$	+1.03	+0.50	−0.05	−0.71

TABLE 6

Selected mean distances (Å) for the $[Fe_4S_4(C_5H_5)_4]^{0/1+/2+}$ congeners (from ref. 28) with the number of distances having the listed value given in brackets

Tetramer	$Fe_4(\eta^5\text{-}C_5H_5)_4(\mu_3\text{-}S)_4$		$[Fe_4(\eta^5\text{-}C_5H_5)_4(\mu_3\text{-}S)_4]^+$	$[Fe_4(\eta^5\text{-}C_5H_5)_4(\mu_3\text{-}S)_4]^{2+}$
	Monoclinic phase	Orthorhombic phase		
Crystallographic site symmetry	C_2-2	C_s-m	C_2-2	S_4-$\bar{4}$
Idealized geometry of Fe_4S_4 core	D_{2d}-$\bar{4}2m$	D_{2d}-$\bar{4}2m$	D_2-222	D_{2d}-$\bar{4}2m$
Fe–Fe	2.65 [2]	2.63 [2]	2.65 [2]	2.83 [4]
	3.36 [4]	3.36 [4]	3.19 [2]	3.25 [2]
			3.32 [2]	
S···S	2.88 [4]	2.88 [4]	2.88 [2]	2.82 [2]
	3.33 [2]	3.34 [2]	3.06 [2]	3.30 [4]
			3.39 [2]	
Fe–S	2.20 [8]	2.21 [8]	2.18 [4]	2.16 [4]
	2.25 [4]	2.26 [4]	2.21 [4]	2.21 [8]
			2.25 [4]	

In the monocationic species, the Fe_4S_4 core retains the cubane-like framework, but it undergoes an angular deformation with respect to the neutral parent, which leads to a D_2 geometry [32].

In the dicationic species, the Fe_4S_4 core again assumes a tetragonal D_{2d} geometry [28].

Figure 14 and Table 6 summarize both the structures and some salient parameters for the $[Fe_4S_4(C_5H_5)_4]^{0/1+/2+}$ homologues.

In the neutral derivative the iron tetrahedron is elongated so that it gives rise to two short Fe–Fe bonding distances and four long Fe–Fe non-bonding distances.

The one-electron oxidation causes the elongated iron tetrahedron to twist from tetragonal D_{2d} to orthorhombic D_2 symmetry, with the consequence that the four originally nonbonding Fe–Fe distances divide into two non-equivalent pairs of shorter non-bonding distances, the originally two short bonding distances remain practically unaltered. The further one-electron oxidation finally causes the elongated iron tetrahedron to transform to a flattened iron tetrahedron of D_{2d} symmetry, with four short Fe–Fe bonding distances and two long Fe–Fe non-bonding distances.

Interestingly, the Fe–S bonding distances follow the same trend in the course of the redox changes.

These crystallographic data fit the bonding description well and their variation with the redox changes [28] in these clusters. In this model [28] it is

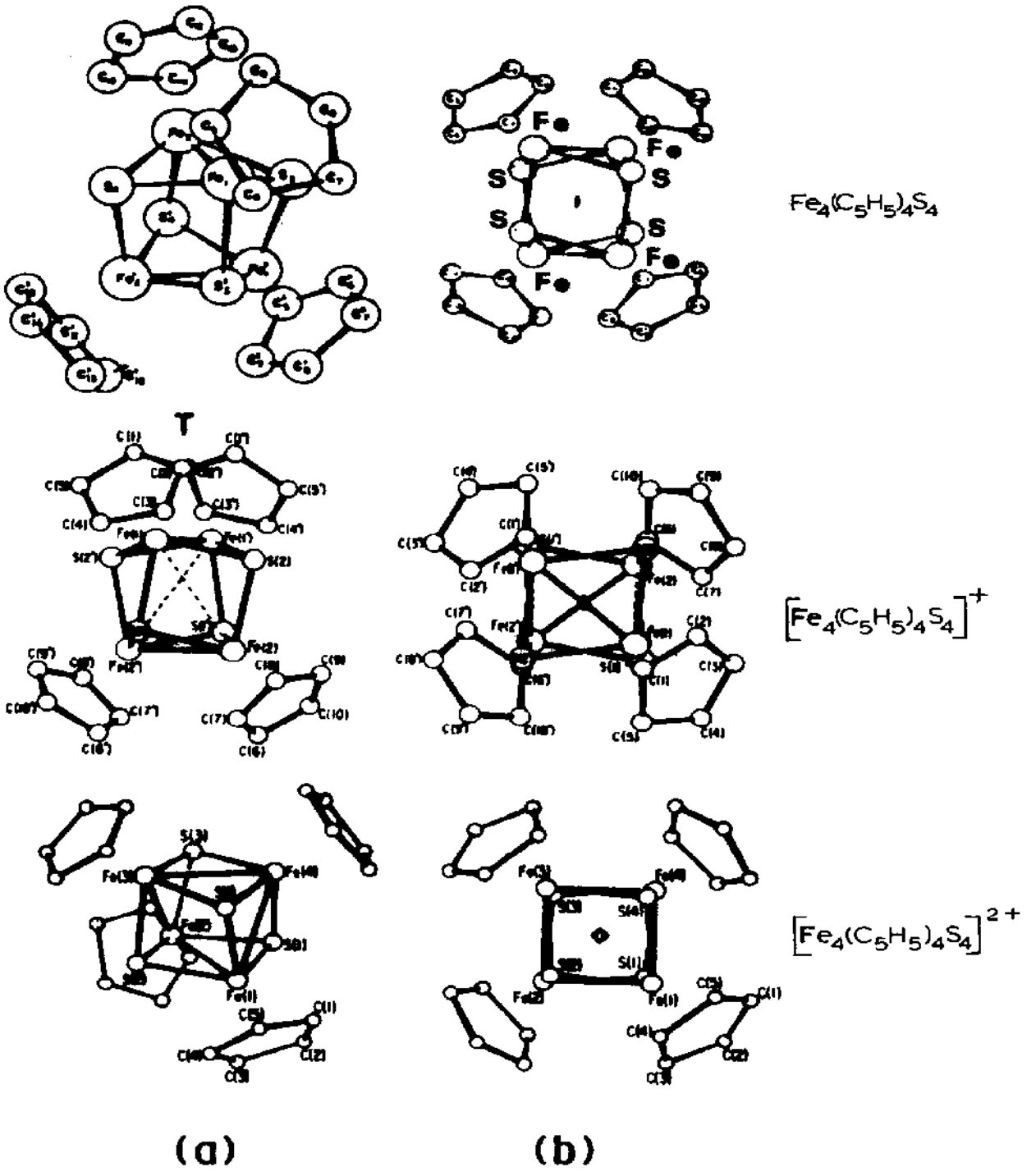

Fig. 14. (a) General views and (b) projections along the crystallographic axis of $[Fe_4S_4(C_5H_5)_4]^{0/1+/2+}$ (from refs. 28, 31, 32).

assumed that the 20 3*d* orbitals in a M_4S_4 core of cubic T_d symmetry split as follows: six bonding tetra-metal cluster orbitals ($a_1 + e + t_2$), six antibonding tetra-metal cluster orbitals ($t_1 + t_2$), eight symmetry orbitals ($e + t_1 + t_2$) essentially non-bonding with respect to direct metal–metal interactions but antibonding with respect to metal–ligand interactions. Hence, in the neutral $Fe_4S_4(C_5H_5)_4$, the 20 3*d* electrons from the four formally-Fe(III) atoms are so distributed: $(a_1 + e + t_2)^{12}(t_1 + t_2)^8(e + t_1 + t_2)^0$.

On the basis of this bonding description, Dahl and co-workers have attempted to predict the structural reorganizations for the non-isolated members $[Fe_4S_4(C_5H_5)_4]^-$ and $[Fe_4S_4(C_5H_5)_4]^{3+}$ [28]. For the trication the maintenance of a tetragonal D_{2d} symmetry is expected, with a further shortening of the four Fe–Fe bonding distances, or, alternatively, a slight Jahn–Teller distortion causing an orthorhombic D_2 geometry. For the monoanion, a Jahn–Teller distortion should lead to an orthorhombic D_2 geometry.

Note that the redox processes cited above are described as electrochemically reversible [28,29]. Since in these papers the electrochemical behaviour is only brief alluded to, we assume these charge transfers to be chemically reversible, but electrochemically quasi-reversible. In fact, the conformational changes accompanying these redox processes must raise the activation barrier of the electron-transfer, slowing down the rate of the heterogeneous charge transfer [33].

(c) Fe_4S_4– and $Fe_4S_2N_2$– nitrosyl derivatives

The cubane-like nitrosyl complex $Fe_4(NO)_4(\mu_3\text{-}S)_4$ undergoes two distinct one-electron reduction steps in dichloromethane, quasi-reversible in character [34]. These redox changes are shown in Fig. 15, and the relevant redox potentials are reported in Table 7.

From comparison with Table 5, the effect of the NO^+ groups make it easy, from a thermodynamic viewpoint, to add electrons to the Fe_4S_4 core compared with the $C_5H_5^-$ groups.

The crystal structures of both the $Fe_4S_4(NO)_4$ [35] and $[Fe_4S_4(NO)_4]^-$ species, obtained by chemical reduction [34], have been reported (Fig. 16).

TABLE 7

Standard electrode potentials (in volts) for the redox process of $Fe_4S_4(NO)_4$ in dichloromethane

Complex	Redox processes	
	0/1−	1−/2−
$Fe_4S_4(NO)_4$	−0.36	−1.14

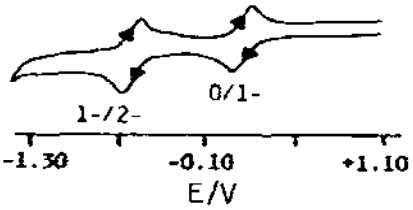

Fig. 15. Cyclic voltammetric behaviour of $Fe_4(NO)_4S_4$ in dichloromethane solvent. Potential values vs. S.S.C.E.

The neutral molecule possesses a cubane-like framework in which each triply bridging sulfur is apically bound to the three iron atoms of each face of the iron tetrahedron, with an almost exact cubic T_d symmetry. The iron atoms form a completely bonding tetrahedron with six Fe–Fe mean distances of 2.651 Å. The twelve chemically equivalent Fe–S bonds have a mean value of 2.217 Å.

In the one-electron reduced product, the Fe_4S_4 core is deformed towards a tetragonal D_{2d} symmetry. The six originally equivalent Fe–Fe distances are broken into two longer Fe–Fe distances (mean value of 2.704 Å) and four shorter Fe–Fe distances (mean value of 2.688 Å). The elongation of the Fe–S bonds is much smaller. The original twelve equivalent bonds would be expected to be partitioned into eight equivalent and four equivalent distances; indeed the two sets of Fe–S bonds have an identical mean value of 2.231 Å.

The stereochemical deformation occurring as a consequence of the addition of one electron to the Fe_4S_4 framework conforms to a general MO

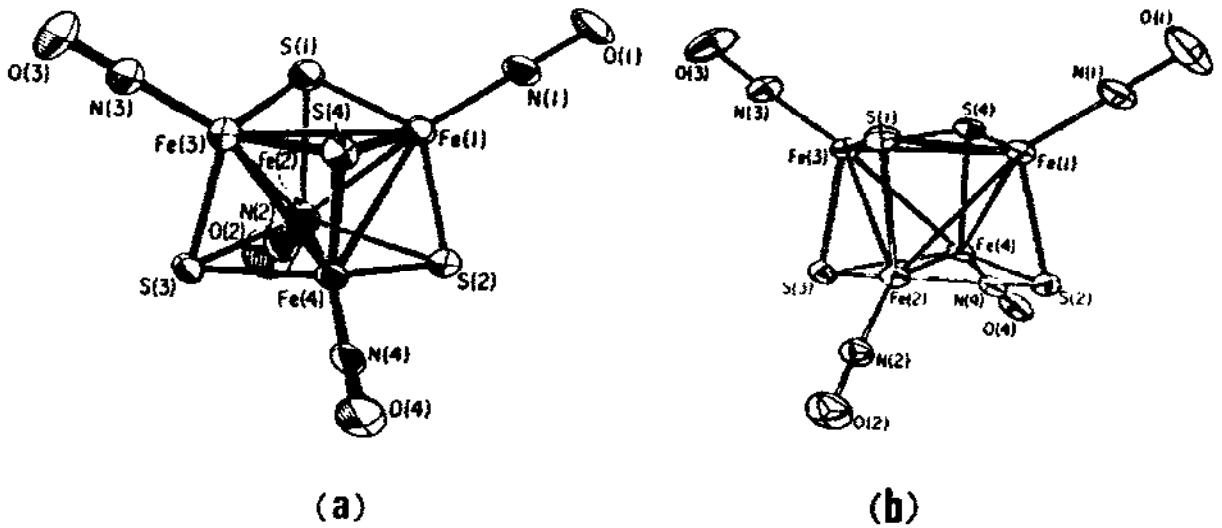

Fig. 16. Molecular structures of: (a) $Fe_4S_4(NO)_4$; (b) $[Fe_4S_4(NO)_4]^-$ (from ref. 34).

description of the bonding in these nitrosyl clusters [34]. According to this model, the 28 iron core electrons of the neutral cluster (from a d^7 Fe(I) configuration) under a cubic T_d symmetry are distributed in the following manner: $(e + t_1 + t_2)^{16}$ (non-bonding tetra-iron orbitals), $(a_1 + e + t_2)^{12}$ (bonding tetra-iron orbitals), $(t_1 + t_2)^0$ (antibonding tetra-iron orbitals). The addition of one electron causes the population of a t antibonding tetra-iron orbital. The system undergoes a Jahn–Teller distortion to a tetragonal D_{2d} configuration.

Strictly related to the above mentioned Fe_4S_4-nitrosyl clusters are the $[Fe_4(NO)_4(\mu_3\text{-}S)_2(\mu_3\text{-}NCMe_3)_2]^z$ ($z = 0, 1-$) congeners, in which two triply bridging tert-butyl nitrogens substitute two sulfur ligands [35,36].

From the electrochemical viewpoint, it has been briefly reported that $Fe_4(NO)_4(\mu_3\text{-}S)_2(\mu_3\text{-}NCMe_3)_2$ (probably in dichloromethane) undergoes four one-electron reduction steps [35]. No redox potential values are available.

The crystal structure of both $Fe_4(NO)_4S_2(NCMe_3)_2$ [35] and $[Fe_4(NO)_4S_2(NCMe_3)_2]^-$, obtained by chemical reduction [36], have been resolved. Figure 17 reports the relevant molecular views.

The neutral molecule, which possesses a C_{2v} symmetry, may be described as a completely-bonding iron tetrahedron dipped in a cubane-like $Fe_4S_2N_2$ core. This core can be thought to be an Fe_2S_2 moiety joined face-to-face to an Fe_2N_2 moiety. The Fe–Fe bond length in the Fe_2S_2 face is 2.642 Å. The Fe–Fe bond length in the Fe_2N_2 face is 2.496 Å. The remaining four Fe–Fe bond lengths for the SFeNFe faces have a mean value of 2.562 Å. The four Fe–S bond lengths in the Fe_2S_2 fragment and the two Fe–S mean bond lengths in the SFeNFe faces are 2.22 Å. The four Fe–N bond lengths in the Fe_2N_2 fragment and the two Fe–N mean bond lengths in the SFeNFe faces are 1.91 Å.

The mono-anion retains the C_{2v} geometry, but significant structural changes occur: the Fe–Fe distance in the Fe_2S_2 fragment increases to 2.701 Å; the Fe–Fe distance in the Fe_2N_2 fragment increases to 2.552 Å; the Fe–Fe distances in the SFeNFe faces increase to 2.574 Å. This results in a relative lengthening of the Fe–Fe bonds normal to the C_2 crystallographic axis, hence causing elongation of all six Fe–S bonds. Unexpectedly, however, all the six Fe–N bonds decrease.

The previously cited qualitative MO bonding description for $Fe_4S_4(NO)_4$ [34] under cubic T_d symmetry, now lowered to C_{2v} geometry because of the presence of *N*-tert-butyl groups, once again agrees with the structural reorganization following the one-electron reduction of $Fe(NO)_4S_2(NCMe_3)_2$ to $[Fe(NO)_4S_2(NCMe_3)_2]^-$; in fact, the additional electron enters an antibonding tetra-iron orbital, giving rise to a decrease in the total metal–metal bond order.

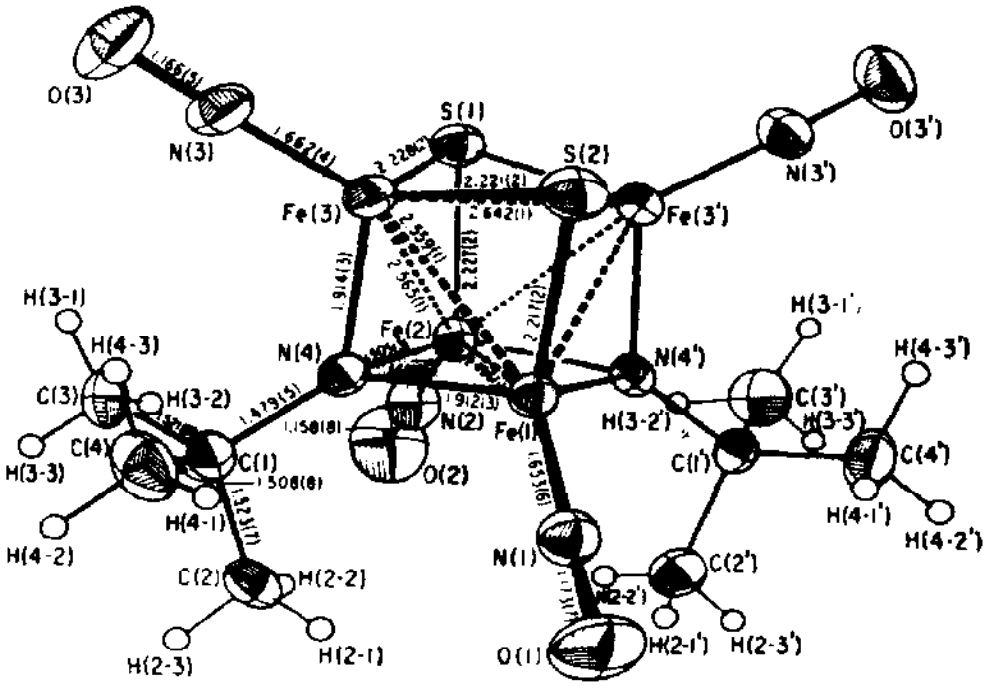

(a)

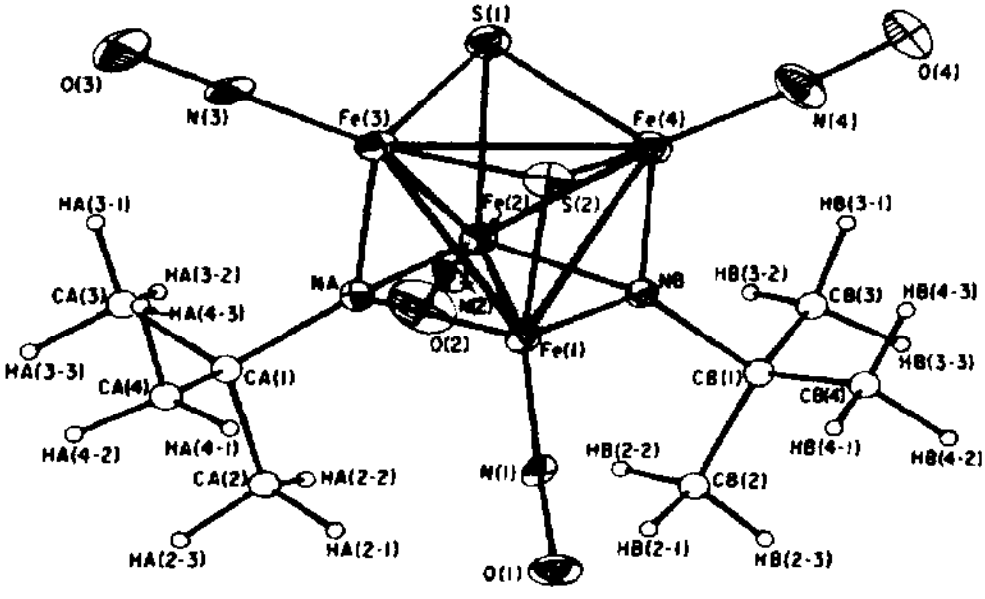

(b)

Fig. 17. Molecular structure of: (a) $Fe_4(NO)_4(\mu_3\text{-}S)_2(\mu_3\text{-}NCMe_3)_2$; (b) $[Fe_4(NO)_4(\mu_3\text{-}S)_2(\mu_3\text{-}NCMe_3)_2]^-$ (from ref. 36).

(d) Fe_4S_4–carbonyl derivatives

Only the carbonyl derivative $Fe_4(CO)_{12}(\mu_3\text{-}S)_4$ has been structurally characterized [37]. This species is insoluble in common solvents, and this prevented any test of its ability to undergo redox changes from being performed. Never the less, the dianion $[Fe_4S_4(CO)_{12}]^{2-}$ has been prepared and X-ray characterized [38]. The structures of both species are reported in Fig. 18.

The neutral molecule consists of a non-bonding iron tetrahedron with face-bridging sulfur atoms, with an Fe_4S_4 distorted cube (C_{2v} symmetry).

In the dianion, the Fe_4S_4 core is "linear", with the two Fe_2S_2 fragments linked by an S–S bond in a centrosymmetric butterfly structure.

Even if not strictly related to the purposes of this topic (no proven electrochemical change), this example is cited because it constitutes the first case in which a two-electron addition to an Fe_4S_4 core seems to cause the rupture of the cubane-like assembly.

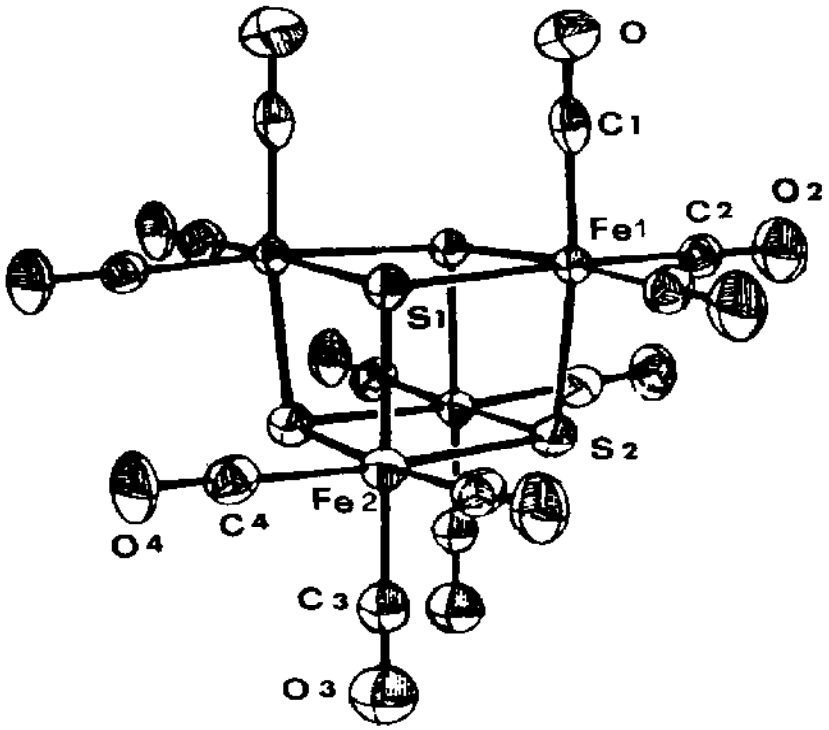

(a)

Fig. 18. Molecular structures of: (a) $Fe_4S_4(CO)_{12}$ (from ref. 37); (b) $[Fe_4S_4(CO)_{12}]^{2-}$ (from ref. 38).

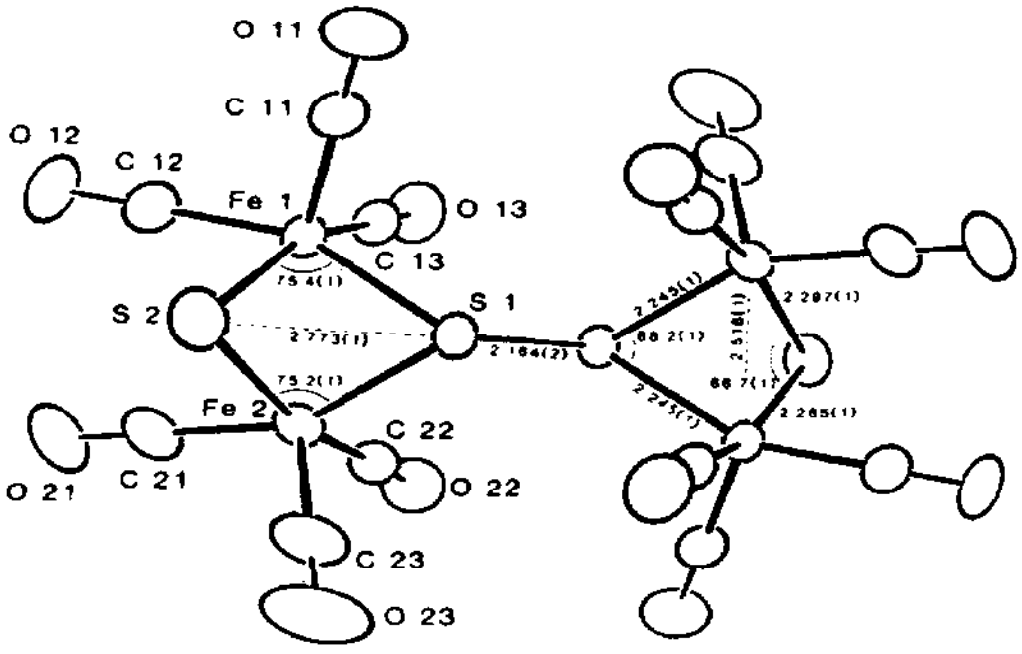

(b)

Dahl and co-workers proposed that the bonding in the neutral carbonyl cluster can be described through an MO model similar to the one for $Fe_4S_4(C_5H_5)_4$ [28]. Hence the 24 electrons of the iron core (from a d^6 Fe(II) configuration) have the following energy level ordering: $(a_1 + e + t_2)^{12}(t_1 + t_2)^{12}(e + t_1 + t_2)^0$. It is likely that the addition of two electrons in the $(e + t_1 + t_2)$ symmetry orbitals, which are antibonding with respect to metal–ligand interactions, weakens the Fe–S bonds up to the destruction of the cubane geometry.

(e) Fe_4S_4– thiolate derivatives

The resemblance of the physicochemical properties of the tetranuclear clusters $[Fe_4S_4(SR)_4]^{2-}$, which contain an $[Fe_4S_4]^{2+}$ core, to those of some non-heme iron–sulfur proteins led to wide investigation of these compounds. Since it is firmly established that, in their biological functions, such proteins undergo, in aqueous solutions, a one-electron reduction at about $E^{0\prime} = -0.4$ V vs. NHE (i.e. around -0.8 V vs. Fc^+/Fc couple), many studies have dealt with the redox behavior of these analogs. As exemplified in Fig. 19, most tetrathiolate compounds undergo, in non-aqueous solvent,

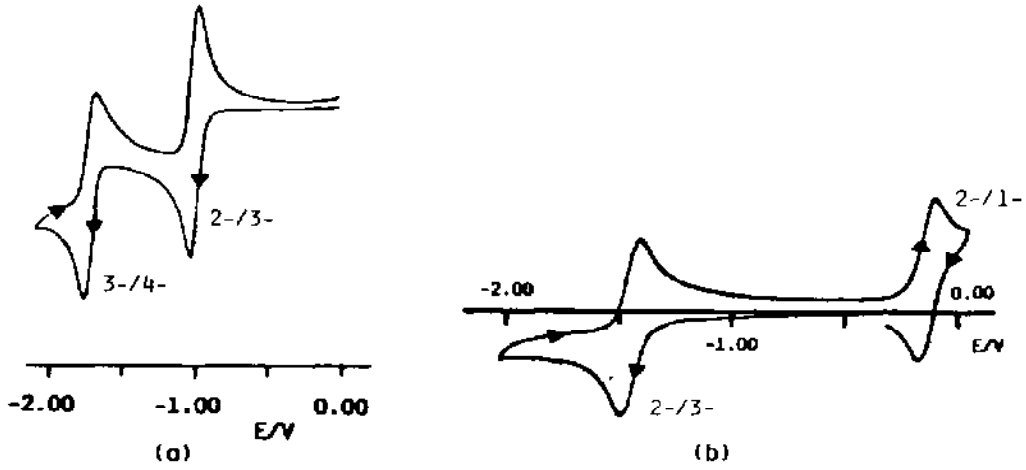

Fig. 19. Cyclic voltammetric responses obtained from: (a) $[Fe_4S_4(SPh)_4]^{2-}$ in acetonitrile solvent; (b) $[Fe_4S_4(S\text{-}t\text{-}Bu)_4]^{2-}$ in dimethylformamide solvent. Potential values vs. S.C.E.

two distinct near reversible one-electron reduction steps. In a very few cases a one-electron anodic process is also displayed.

It is commonly accepted that these one-electron charge transfers correspond to the four-membered sequence:

$$[Fe_4S_4]^{3+} \underset{-e^-}{\overset{+e^-}{\rightleftarrows}} [Fe_4S_4]^{2+} \underset{-e^-}{\overset{+e^-}{\rightleftarrows}} [Fe_4S_4]^{+} \underset{-e^-}{\overset{+e^-}{\rightleftarrows}} [Fe_4S_4]^{0}$$

Table 8 summarizes the standard potentials of the different redox changes in all the tetra-iron thiolate compounds studied. In addition to the inductive effects of the different ligands, two points deserve some comment. First of all, in non-aqueous solvents the redox potentials of the biologically significant $[Fe_4S_4]^{2+/1+}$ step in these synthetic complexes are notably more negative than those occurring in proteins; secondly, passing from non-aqueous to aqueous solutions, the redox potentials of the analogs approach the biological ones. Both the influence of hydrogen bonding in the protein matrix and the extent of dielectric of the environmental shell surrounding the iron–sulfur center have been proposed to account, in part, for both these effects [62].

Particular interest arises as far as the structural consequences accompanying the redox changes are concerned.

It can be assumed that all the $[Fe_4S_4(SR)_4]^{2-}$ species isolated exhibit compressed tetragonal structures of idealized D_{2d} symmetry. The $[Fe_4S_4]^{2+}$ core consists of nearly concentric imperfect Fe_4 and S_4 tetrahedra, the volume of the latter being about 2.3 times larger than that of the former. The departure from T_d symmetry results in four short Fe–S distances parallel to the $\bar{4}$ symmetry axis and eight longer Fe–S distances perpendicular to the same axis. As an example, Fig. 20 shows schematic representations

TABLE 8

Redox potentials (in volts) of the redox processes of the $[Fe_4S_4]^{2+}$ core in $[Fe_4S_4(SR)_4]^z$ clusters

R	z	$[Fe_4S_4]^{3+/2+}$	$[Fe_4S_4]^{2+/1+}$	$[Fe_4S_4]^{1+/0}$	Solvent	Ref.
CH_3	2−	–	−1.60	−2.33	DMF	41
CH_2CH_3	2−	–	−1.64	−2.35	DMF	41
CH_2CH_3	2−	–	−1.80	−2.44	TMU	45
$CH_2CH_2CH_3$	2−	–	−1.65	–	DMF	41
$CH(CH_3)_2$	2−	–	−1.69	−2.41	DMF	41
$CH_2CH(CH_3)_2$	2−	–	−1.58	–	MeOH	46
$C(CH_3)_3$	2−	−0.17	−1.73	−2.47	DMF	40, 41
$C(CH_3)_3$	2−	–	−1.82	–	NMP	47
$CH_2C_6H_{11}$	2−	–	−1.71	−2.44	DMF	41
1,1-$C_6H_{10}CH_3$	2−	–	−1.79	−2.51	DMF	40
C_6H_5	2−	–	−1.35	−2.06	DMF	41
C_6H_5	2−	–	−1.45	–	DMF	49
C_6H_5	2−	–	−1.23	−1.99	DMSO	41
C_6H_5	2−	–	−1.25	−1.97	AN	39
C_6H_5	2−	–	−1.31	–	AN	49
C_6H_5	2−	–	−1.44	−2.15	NMP	47
C_6H_5	2−	–	−1.45	−2.08	NMP	48
C_6Cl_5	2−	–	−1.09	–	DMF	41
C_6F_5	2−	–	−1.10	–	DMF	41
$CH_2C_6H_5$	2−	–	−1.56	−2.27	DMF	41
$CH_2C_6H_5$	2−	–	−1.65	−2.35	NMP	47
$CH(CH_3)C_6H_5$	2−	–	−1.57	−2.29	DMF	40
m-$C_6H_4(CH_2)_2$	2−	–	−1.70	−2.34	DMF	41
m-$C_6H_4(CH_2)_2$	2−	–	−1.60	−2.36	DMSO	41
p-$C_6H_4CH_3$	2−	–	−1.40	−2.07	DMF	41
m-$C_6H_4CH_3$	2−	–	−1.38	−2.04	DMF	51
o-$C_6H_4CH_3$	2−	–	−1.36	−2.05	DMF	51
p-$C_6H_4CF_3$	2−	–	−1.14	−1.87	DMF	52
m-$C_6H_4CF_3$	2−	–	−1.19	−2.04 [d]	DMF	52
p-C_6H_4Cl	2−	–	−1.26	−1.94	DMF	42
p-C_6H_4Br	2−	–	−1.24	−1.95	DMF	55
p-$C_6H_4NO_2$	2−	–	−1.00	–	DMF	41
p-C_6H_4–n-C_4H_9	2−	–	−0.79	–	H_2O [a]	60
p-C_6H_4–n-C_8H_{17}	2−	–	−0.79	–	H_2O [a]	60
p-C_6H_4–n-C_8H_{17}	2−	–	−1.55	–	DMSO	60
p-C_6H_4–n-C_8H_{17}	2−	–	−1.55	–	DMF	61
p-C_6H_4–n-$C_{12}H_{25}$	2−	–	−0.82	–	H_2O [a]	60

TABLE 8 (continued)

R	z	$[Fe_4S_4]^{3+/2+}$	$[Fe_4S_4]^{2+/1+}$	$[Fe_4S_4]^{1+/0}$	Solvent	Ref.
2,4,6-$(CH_3)_3$-C_6H_2	2−	−0.43		–	DMF	58
2,4.6-(CH-$(CH_3)_2)_3C_6H_2$	2−	−0.75		–	DMF	58
2,4,6-(CH-$(CH_3)_2)_3C_6H_2$	2−	−0.61	−1.69	–	CH_2Cl_2	59
2,3,5,6-$(CH_3)_4C_6H$	2−	−0.54	−1.59	–	CH_2Cl_2	59
CH_2CH_2OH	2−	–	−1.46	–	DMSO [b]	43
CH_2CH_2OH	2−	–	−0.92	–	H_2O [c]	43
CH_2CH_2OH	2−	–	−0.98	–	H_2O [c]	56
$C(CH_3)_2CH_2OH$	2−	−0.52	−1.54	−2.29	DMF	40
$C(CH_3)_2CH_2OH$	2−	–	−1.0	–	H_2O [c]	40
$C(CH_3)_2CH_2$-NHC_6H_5	2−	−0.44	−1.53	−2.23	DMF	40
$CH_2CH_2COO^-$	6−	–	−1.58	–	MeOH	49
$CH_2CH_2COO^-$	6−	–	−1.0	–	H_2O [c]	49
$CH_2CH_2COO^-$	6−	–	−0.97	−1.36	H_2O [c]	53
$CH_2CH_2COO^-$	6−	–	−0.71	−1.11	H_2O [c]	56
$CH_2CH_2CH_2$-COO^-	6−	–	−1.58	–	MeOH	49
$CH_2CH_2CH_2$-COO^-	6−	–	−0.9	–	H_2O [c]	49
o-C_6H_4OH	2−	–	−1.19	−1.82 [d]	DMF	54
o-$C_6H_4OCH_3$	2−	–	−1.46	−2.09 [d]	DMF	54
o-$C_6H_4NH_2$	2−	–	−1.38	−2.00 [d]	DMF	54
o-$C_6H_4SCH_3$	2−	–	−1.31	−2.01 [d]	DMF	54
p-C_6H_4OH	2−	–	−1.43	−2.17 [d]	DMF	54
p-$C_6H_4OCH_3$	2−	–	−1.40	−2.13 [d]	DMF	54
p-$C_6H_4NH_2$	2−	–	−1.51	−2.17 [d]	DMF	54
p-$C_6H_4NH_2$	2−	–	−1.57	−2.19 [d]	DMF	57
p-$C_6H_4N(CH_3)_2$	2−	–	−1.45	−2.10	DMF	41
p-$C_6H_4N(CH_3)_3$	2−	–	−1.10	−1.67	DMF	41, 42
$(CH_2)_3Si(OMe)_3$	2−	–	−1.81	–	DMF	50
Ac-(*S*)Cys-$NHCH_3$	2−	–	−1.40	−1.97	DMF	41
Ac-(*S*)Cys-$NHCH_3$	2−	–	−1.29	−2.02	DMSO [b]	41, 43, 44
Ac-(*RS*)Cys-$NHCH_3$	2−	–	−1.27	–	DMSO [b]	43
Ac-(*RS*)Cys-$NHCH_3$	2−	–	−0.90	–	H_2O [c]	43

[a] Aqueous micellar solution at pH 7.00. [b] Redox potentials in DMSO/H_2O mixtures also reported. [c] pH 8–10. [d] Irreversible charge transfer.

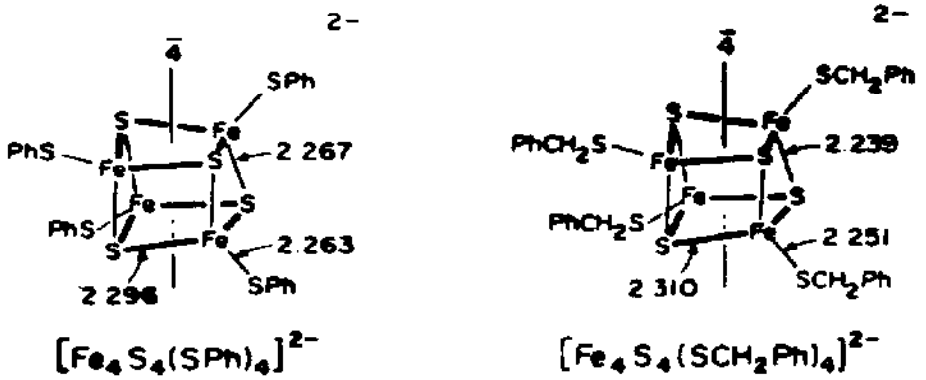

Fig. 20. Schematic representation of the molecular structure of two $[Fe_4S_4(SR)_4]^{2-}$ dianions in the solid state (from ref. 63).

of two such structures. The structural assignment of the one-electron reduced $[Fe_4S_4(SR)_4]^{3-}$ trianions appears more ambiguous. In fact, in the solid state these cores range from elongated tetragonal to more or less rhombic (non-tetragonal) structures. In this connection, Fig. 21 shows the structural features of the trianions $[Fe_4S_4(SPh)_4]^{3-}$ and $[Fe_4S_4(SCH_2Ph)_4]^{3-}$, congeners of the dianions illustrated in Fig. 20.

In the core of $[Fe_4S_4(SPh)_4]^{3-}$ there are four long Fe–S bonds parallel to the $\bar{4}$ axis, and eight shorter Fe–S bonds perpendicular to this axis, giving to the core an elongated tetragonal geometry of idealized D_{2d} symmetry. In the core of $[Fe_4S_4(SCH_2Ph)_4]^{3-}$ there are six long and six short Fe–S bonds, providing a less regular configuration with idealized C_{2v} symmetry.

A more complete set of structural parameters for the $2-/3-$ redox couple of some tetrathiolate complexes is reported in Table 9.

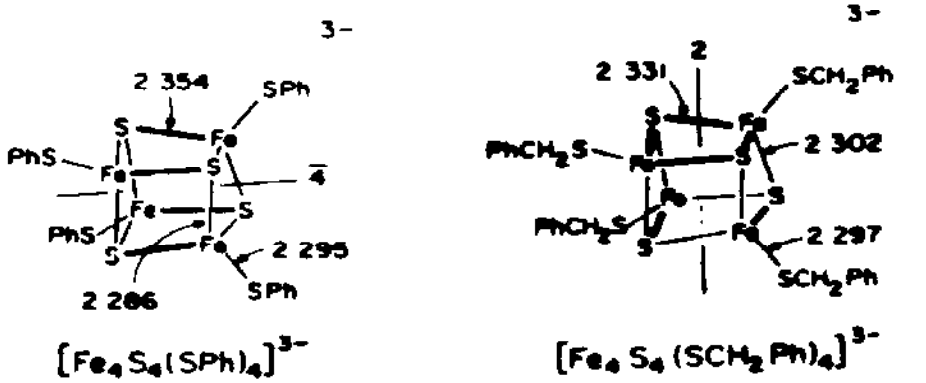

Fig. 21. Schematic representation of the molecular structure of two $[Fe_4S_4(SR)_4]^{3-}$ trianions (from ref. 63).

TABLE 9

Selected structural parameters for $[Fe_4S_4(SR)_4]^{2-/3-}$ species (from refs. 40, 64)

Cluster	Distance (Å)		Volume (Å^3)		
	Fe–S	Fe–SR	Fe_4	S_4	Fe_4S_4
$[Fe_4S_4(S\text{-}t\text{-}Bu)_4]^{2-}$ [a]	4 at 2.252 (8) 8 at 2.315 (5)	2.261 (5)	2.45	5.55	9.68
$[Fe_4S_4(S\text{-}t\text{-}Bu)_4]^{2-}$ [b]	4 at 2.274 (3) 8 at 2.294 (2)	2.254 (3)	2.47	5.53	9.69
$[Fe_4S_4(S\text{-}t\text{-}Bu)_4]^{3-}$ [b,c]	4 at 2.297 (6) 8 at 2.330 (7)	2.300 (4)	2.50	5.79	9.93
$[Fe_4S_4(SPh)_4]^{2-}$	4 at 2.267 (9) 8 at 2.296 (12)	2.263 (7)	2.41	5.54	9.55
$[Fe_4S_4(SPh)_4]^{3-}$ [d,e]	4 at 2.351 (9) 8 at 2.288 (15)	2.295 (7)	2.43	5.76	9.73
$[Fe_4S_4(SCH_2Ph)_4]^{2-}$	4 at 2.239 (7) 8 at 2.310 (8)	2.251 (5)	2.44	5.52	9.61
$[Fe_4S_4(SCH_2Ph)_4]^{3-}$ [b]	6 at 2.302 (4) 6 at 2.332 (5)	2.297 (12)	2.48	5.80	9.86

[a] $(Me_3NCH_2Ph)^+$ salt. [b] $(Et_4N)^+$ salt. [c] Acetonitrile monosolvate. [d] $(Et_3MeN)^+$ salt. [e] Average values of two inequivalent anions.

Notwithstanding the non-uniformity of the crystal structures of $[Fe_4S_4(SR)_4]^{3-}$, a body of evidence indicates that in solution all the trianions assume an elongated D_{2d} structure [55,63,64]. Departures from this geometry in the solid state are attributed to environmental constraints imposed by crystal packing forces. In conclusion, it is assumed that the intrinsic core structural change following the one-electron redox change $[Fe_4S_4]^{2+} \underset{-e^-}{\overset{+e^-}{\rightleftharpoons}} [Fe_4S_4]^{+}$ may be written [63]:

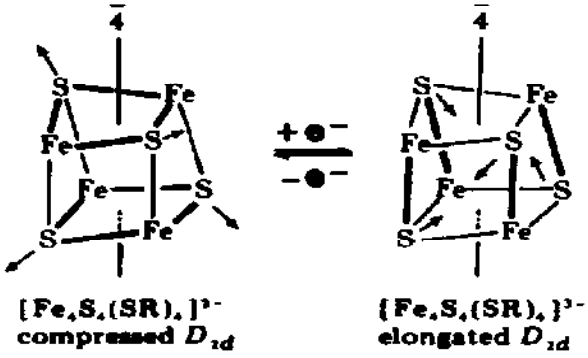

$[Fe_4S_4(SR)_4]^{3-}$ compressed D_{2d} $[Fe_4S_4(SR)_4]^{3-}$ elongated D_{2d}

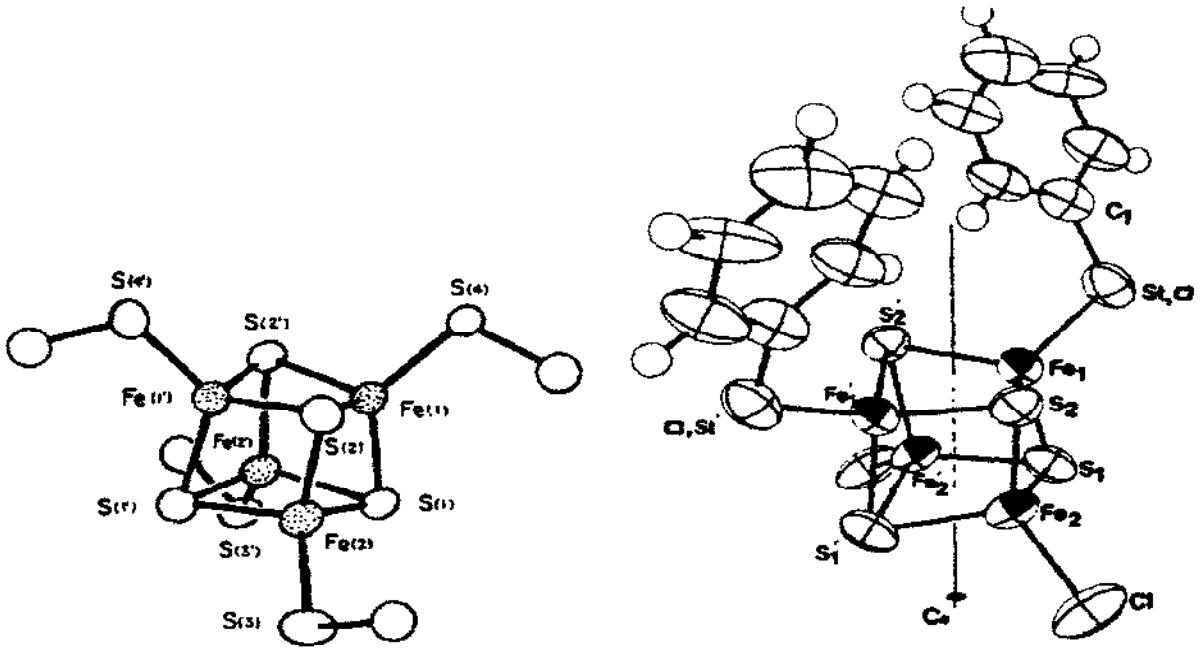

Fig. 22. Molecular structure of $[Fe_4S_4(S\text{-}2,4,6\text{-}(CH(CH_3)_2)_3C_6H_2)_4]^-$ (from ref. 59).

Fig. 23. Molecular structure of $[Fe_4S_4(SC_6H_5)_2Cl_2]^{2-}$ (from ref. 49).

A further step towards completion of the knowledge concerning the structural changes accompanying redox changes in these tetrametal clusters comes from the X-ray study of the monoanion $[Fe_4S_4(S\text{-}2,4,6\text{-}(CH(CH_3)_2)_3C_6H_2)_4]^-$ (Fig. 22).

The $[Fe_4S_4]^{3+}$ core, which has a tetragonally compressed structure of approximate D_{2d} symmetry, contains four short Fe–S bonds parallel to the $\bar{4}$ axis and eight long Fe–S bonds perpendicular to this axis [59]. Both the two sets of Fe–S distances average 0.02 Å shorter than the corresponding ones in various $[Fe_4S_4]^{2+}$ cores. Even if this is, for the present, the only reported structure of an $[Fe_4S_4]^{3+}$ core, it seems that in the core redox change $[Fe_4S_4]^{3+} \overset{+e^-}{\underset{-e^-}{\rightleftarrows}} [Fe_4S_4]^{2+}$ the only structural consequence is a simple reversible expansion $(+e^-)$/contraction $(-e^-)$, without drastic configurational reorganizations.

Electronic structural calculations on [4Fe–4S] models are becoming progressively more refined [65–68], but are still too incomplete to account for the distortions accompanying the redox changes cited.

(f) Fe_4S_4–mixed thiolate–nonthiolate derivatives

In some Fe–S proteins it has been ascertained that the iron atoms in the $[Fe_4S_4]^{2+}$ core are not precisely equivalent. Such an inequivalence may be

TABLE 10

Standard potentials (in volts) for the redox processes observed in solutions of $[Fe_4S_4(SR)_{4-n}X_n]^{2-}$

R	X	Redox change	n					Solvent	Ref.
			0	1	2	3	4		
$C(CH_3)_3$	Cl	2−/3−	−1.82	−1.72	−1.58	−1.40	−1.25	NMP	47
$C(CH_3)_3$	OAc	2−/3−	−1.82	−1.69	−1.56	−1.45	−1.33	NMP	47
$CH_2C_6H_5$	Cl	2−/3−	−1.65	−1.56	−1.47	−1.38	−1.28	NMP	47
$CH_2C_6H_5$	OAc	2−/3−	−1.65	−1.57	−1.49	−1.40	−1.32	NMP	47
$CH_2C_6H_5$	OAc	3−/4−	−2.35	−2.24	−2.16	−2.07	−2.02	NMP	47
C_6H_5	CF_3CO_2	2−/3−	−1.44	−1.34	–	–	–	NMP	47
C_6H_5	CF_3SO_3	2−/3−	−1.44	−1.33	–	–	–	NMP	47
C_6H_5	Cl	2−/3−	−1.31	–	−1.17	–	−1.10	AN	49, 69
C_6H_5	Cl	2−/3−	−1.45	–	−1.33	–	−1.25	DMF	49, 69
C_6H_5	Br	2−/3−	−1.31	–	−1.21	–	−1.06	AN	49
C_6H_5	Br	2−/3−	−1.45	–	−1.29	–	−1.22	DMF	49
C_6H_5	OC_6H_5	2−/3−	−1.31	–	−1.43	–	–	AN	49
C_6H_5	OC_6H_5	2−/3−	−1.45	–	−1.55	–	–	DMF	49
C_6H_5	$(C_2H_5)_2$-NCS_2 [a]	2−/3−	−1.45	–	−1.65 [b,c]	–	–	DMF	70, 71
C_6H_5	$(C_2H_5)_2$-NCS_2 [a]	2−/1−	–	–	−0.52 [d]	–	–	DMF	70, 71

[a] $(C_2H_5)NCS_2^{2-}$ = ethyldithiocarbamate ion. [b] Peak potential value for an irreversible process. [c] Complicated by (likely) complex equilibria among statistical mixtures. [d] Stable only in the short time of cyclic voltammetry (~100 ms).

attributed to different coordination environments between the four iron centres.

On this basis a series of cubane Fe_4S_4 derivatives containing mixed terminal ligands has been prepared and characterized. These compounds, of general formula $[Fe_4S_4(SR)_{4-n}X_n]^{2-}$, display electrochemical behaviour qualitatively similar to that of the parent compounds $[Fe_4S_4(SR)_4]^{2-}$ described in Section (e) above in that they undergo two consecutive one-electron reductions, and, rarely, a one-electron oxidation.

Table 10 summarizes this redox behaviour.

Except for the ethyldithiocarbamate ligand, the sequential substitution of thiolate groups with the cited ligands facilitates the reduction processes, indicating their electron withdrawing character with respect to the thiolate ligands.

Probably because of the closeness of the standard potentials for the 2−/3− couple in the different sequentially substituted species, no $[Fe_4S_4(SR)_{4-n}]^{3-}$ ($n \neq 0,4$) species has been isolated either as chemical or

electrochemical processes. This prevents any analysis of the structural rearrangements following the redox changes. However, an interesting aspect of these mixed-ligated Fe_4S_4 derivatives lies in the fact that the $[Fe_4S_4]^{2+}$ core of these mixed thiolate–non-thiolate tetramers does not show the compressed D_{2d} geometry, typical of all tetrathiolate complexes. In this connection Fig. 23 illustrates the crystal structure of $[Fe_4S_4(SC_6H_5)_2Cl_2]^{2-}$ [49].

Contrary to the compressed D_{2d} distortion from T_d symmetry, which divides the Fe–S bonds in the tetrathiolate $[Fe_4S_4]^{2+}$ cores into two sets of four short and eight longer distances, in the present case the Fe–S distances are roughly nearly all equivalent, giving rise to an essentially undistorted Fe_4S_4 core of maximum idealized C_{2v} symmetry; this structure is unlikely to be attributable to unusual crystal packing forces.

Also, the $[Fe_4S_4]^{2+}$ core of $[Fe_4S_4(SPh)_2((C_2H_5)_2NCS_2)_2]^{2-}$ departs from the compressed D_{2d} symmetry, Fig. 24. Its cubic geometry is highly distorted, and at best it possesses C_2 symmetry. The main reason for the distortion arises from the Fe–Fe distance between the iron atoms (Fe(2)) coordinated to the bidentate $(C_2H_5)_2NCS_2$ ligand, which is noticeably longer (3.05 Å) than the Fe–Fe distance between the iron atoms [Fe(1)] coordinated to the monodentate PhS ligand (2.73 Å). However, the Fe–S distances make the core assume a compressed geometry along the 2-fold

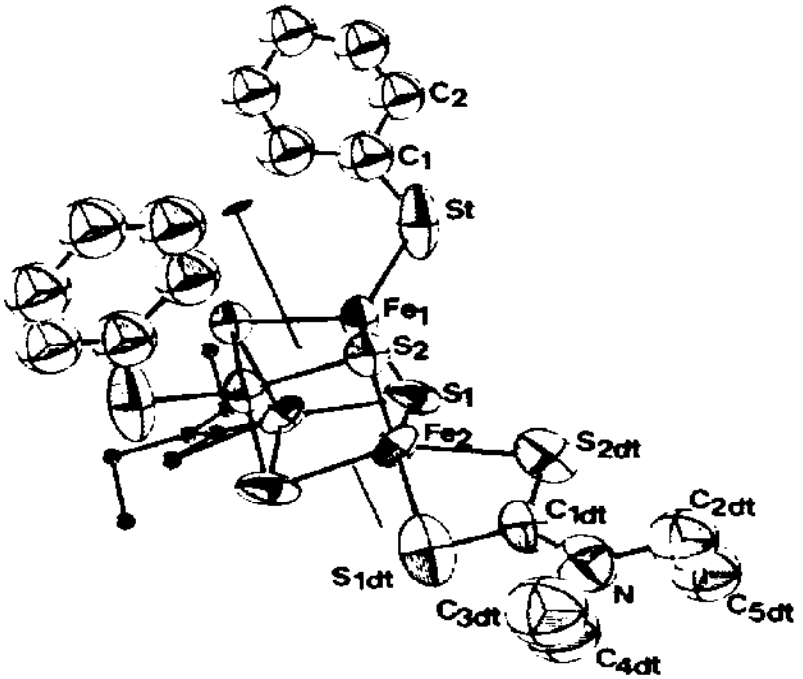

Fig. 24. Crystal structure of $[Fe_4S_4(SC_6H_5)_2((C_2H_5)_2NCS_2)_2]^{2-}$ (from ref. 70).

axis. In this molecule there are two different iron sites: a tetrahedral FeS_4 site having a PhS terminal ligand and a distorted square-pyramidal FeS_5 site having a terminal $(C_2H_5)_2NCS_2$ chelating ligand [70,71].

(g) Fe_4S_4–halide derivatives

In the course of study of the reactivity of tetrathiolate $[Fe_4S_4(SR)_4]^{2-}$ complexes, Holm and co-workers isolated the tetrahalide species $[Fe_4S_4X_4]^{2-}$ (X = Cl, Br, I) [72]. As shown in Fig. 25 for $[Fe_4S_4Cl_4]^{2-}$, the $[Fe_4S_4]^{2+}$ core in these derivatives maintains D_{2d} geometry compressed along the $\bar{4}$ axis, typical of the tetrathiolate dianions, which are precursors in the synthesis of the present halide species.

Figure 26 illustrates the cyclic voltammetric behaviour of $[Fe_4S_4Cl_4]^{2-}$ in acetonitrile solution [72].

Comparison with the redox behaviour of the tetrathiolate complexes reported in Fig. 19a shows that the most striking feature is the marked irreversibility of the 3 − /4 − charge transfer.

Table 11 reports the redox potentials for the charge transfers of the tetrahalide species.

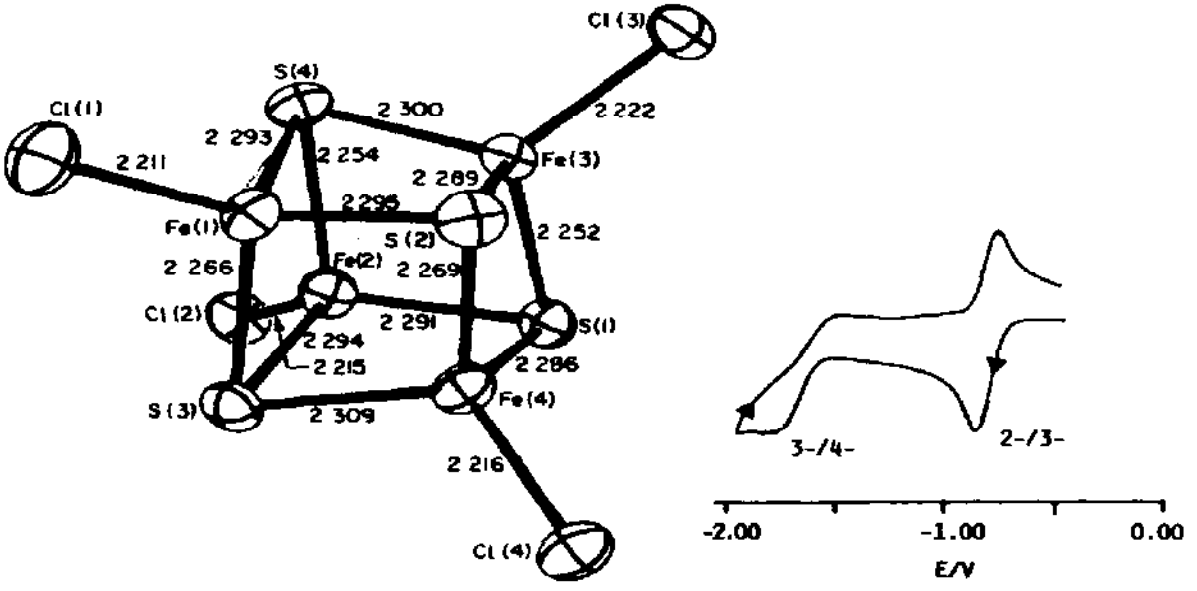

Fig. 25. Crystal structure of the dianion $[Fe_4S_4Cl_4]^{2-}$ (from ref. 73).

Fig. 26. Cyclic voltammetric response of $[Fe_4S_4Cl_4]^{2-}$ in acetonitrile solution. Potential values vs. S.C.E.

TABLE 11

Standard potentials (in volts) for the redox processes of the $[Fe_4S_4X_4]^{2-}$ species (X = halide)

X	Redox changes		Solvent	Ref.
	2−/3−	3−/4−		
Cl	−1.04	−1.99 [a]	AN	72
Cl	−1.10	–	AN	49
Cl	−1.25	–	NMP	47
Cl	−1.25	–	DMF	49
Br	−0.99	−1.91 [a]	AN	72
Br	−1.06	–	AN	49
Br	−1.22	–	DMF	49
I	−0.98 [a]	–	AN	72

[a] Peak potential value for irreversible processes.

The reduction potentials of the core change $[Fe_4S_4]^{2+}/[Fe_4S_4]^{1+}$ shift towards less-negative potential values when substituting the terminal thiolate ligands with halide ligands.

Attempts to obtain the trianions $[Fe_4S_4X_4]^{3-}$ by chemical reduction failed [72]; it is hence impossible to evaluate if the core structural rearrangement $D_{2d\ \text{compressed}} \underset{-e^-}{\overset{+e^-}{\rightleftarrows}} D_{2d\ \text{elongated}}$ accompanies the 2− /3− redox change of tetrahalide species.

(h) Fe_4S_4–phenoxide derivatives

In order to mimic Fe_4S_4 centres coordinated to a protein through tyrosinate ligands rather than cysteine ligands, the phenolato complexes $[Fe_4S_4(OAr)_4]^{2-}$ (Ar = C_6H_5, C_6H_4-*p*-CH_3) have been prepared [48,74]. Also in this case, the $[Fe_4S_4]^{2+}$ core has the usual cubane shape of D_{2d} symmetry compressed along the $\bar{4}$ axis (Fig. 27).

Like tetrathiolate analogues, the dianions $[Fe_4S_4(OAr)_4]^{2-}$ undergo two quasi-reversible one-electron reduction processes, corresponding to the subsequent 2− /3− and 3− /4− charge transfers. The relevant potential values are reported in Table 12.

Comparison with the corresponding thiolate shows the reduction potentials of phenolate to be slightly more cathodic (~ 100 mV). The fact that phenoxide ligands are unexpectedly more electron donating than thiophenoxide ligands has been attributed to a relatively covalent Fe–O interaction [48], as proven by the unusually short Fe–O distances.

No attempts have been made to obtain, by chemical or electrochemical reduction of $[Fe_4S_4(OAr)_4]^{2-}$, the reduced congeners, probably because of the difficulty of manipulating these labile phenoxide-ligated derivatives.

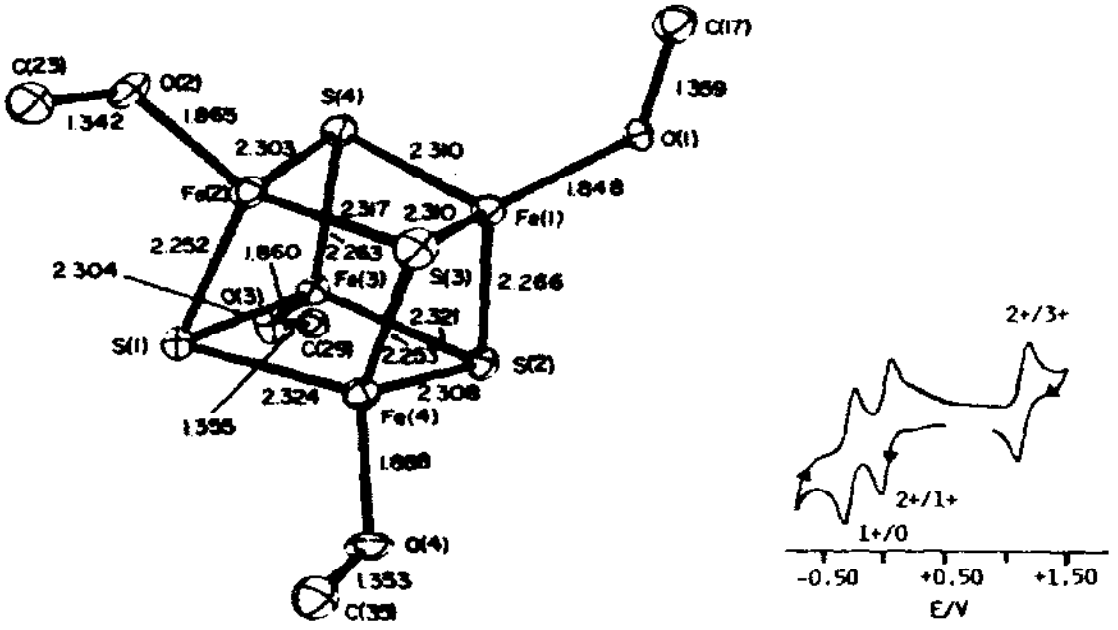

Fig. 27. Stereoscopic view of $[Fe_4S_4(OC_6H_5)_4]^{2-}$, and interatomic distances of the inner core (from ref. 48).

Fig. 28. Cyclic voltammogram of $[(C_5H_5)_4Fe_4S_5]^{2+}$ in acetonitrile solvent. Potential values vs. S.C.E.

(i) Fe_4S_4–mixed phenoxide–halide derivatives

Only the species $[Fe_4S_4(OC_6H_5)_2Cl_2]^{2-}$ having a mixed phenoxide–halide terminal ligand coordinated to an Fe_4S_4 core, has been characterized [49]. This species is isostructural with the dianion $[Fe_4S_4(SC_6H_5)_2Cl_2]^{2-}$, the structure of which is reported in Fig. 23. This species displays an $[Fe_4S_4]^{2+}$ core which departs from the usual compressed D_{2d} geometry.

$[Fe_4S_4(OC_6H_5)_2Cl_2]^{2-}$ undergoes a one-electron quasi-reversible cathodic process at $E^{0\prime} = -1.39$ V in DMF, and $E^{0\prime} = -1.25$ V in AN [49].

TABLE 12

Standard electrode potentials (in volts) for the redox processes of $[Fe_4S_4(OAr)_4]^{2-}$

Ar	Redox processes		Solvent	Ref.
	2−/3−	3−/4−		
C_6H_5	−1.55	−2.20	NMP	48
C_6H_5	−1.46	−2.18	AN	48, 74
C_6H_4–*p*-CH_3	−1.59	−2.23	NMP	48
C_6H_4–*p*-CH_3	−1.51	−2.19	AN	48

TABLE 13

Redox potentials (in volts) for the two subsequent one-electron cathodic processes for $[Fe_4S_4(SeC_6H_5)_4]^{2-}$

Couple	$E^{0\prime}$	Solvent
2−/3−	−1.23	AN
2−/3−	−1.35	DMF
3−/4−	−1.91	AN
3−/4−	−2.03	DMF

The 2−/3− charge transfer seems complicated, however, by following chemical reactions ($i_{pa}/i_{pc} < 1$), which probably make the corresponding trianion unstable.

(j) Fe_4S_4–selenolate derivatives

Since selenium is a component of certain proteins, the dianion $[Fe_4S_4(SeC_6H_5)_4]^{2-}$, isostructural with the thiolate $[Fe_4S_4(SC_6H_5)_4]^{2-}$, has been prepared [75]. In non-aqueous solvent it undergoes a quasi-reversible 2−/3− reduction step together with a further one-electron 3−/4− reduction step, complicated by following chemical reactions. Table 13 reports the relevant redox potentials [75].

There is no significant difference with respect to the corresponding thiolate, as far as the electron-transfer ability is concerned.

The trianion $[Fe_4S_4(SeC_6H_5)_4]^{3-}$ has been electrochemically generated and its EPR spectrum testifies to the similarity, also structural, with $[Fe_4S_4(SC_6H_5)_4]^{3-}$ [75].

(k) Fe_4S_4–biological fragment ligated derivatives

A series of derivatives containing an Fe_4S_4 core ligated to biologically significant molecules has been characterized electrochemically. Table 14 briefly summarizes the electrode potentials of the redox changes in these clusters. The reader is referred to the specific references as far as the biological abbreviations are concerned.

The incorporation of these fragments makes the redox potentials of the relevant cubane tetramers approach those of natural ferredoxins (~ -0.8 vs. Fc^+/Fc). In addition, both the serum albumin and insulin derivatives stabilize the clusters towards aerobic oxidation [56].

(v) Fe_4S_5 core

In the continuing effort to prepare iron–sulfur tetramers having different coordination geometries, the $(C_5H_5)_4Fe_4S_5$ assembly is assuming increasing interest.

TABLE 14

Redox potentials (in volts) for the redox processes of biologically significant synthetic Fe_4S_4 clusters, $[Fe_4S_4-fragment]^{2-}$

Fragment	1−/2−	2−/3−	3−/4−	Solvent	Ref.
(t-BOC–Gly–Cys–Gly_2–Cys–Gly_2–Cys–Gly–NH_2)(S–$C(CH_3)_3$)	–	−1.06	–	20% H_2O/80% DMSO	44
(t-BOC–Gly–Cys–Gly_2–Cys–Gly_2–Cys–Gly–NH_2)(S–Cys(Ac)NHMe)	–	−1.02	–	20% H_2O/80% DMSO	44
(t-BOC–Gly–Cys–Gly_2–Cys–Gly_2–Cys–Gly_2–Cys–Gly–NH_2)	–	−1.00	–	20% H_2O/80% DMSO	44
(Ac–Gly_2–Cys–Gly_2–Cys–Gly_2NH_2)$_2$	–	−1.15	–	20% H_2O/80% DMSO	76
(Bovine serum albumin)	–	−0.61	−0.97 [a]	H_2O [b]	56
(Bovine insulin)	–	−0.58	–	H_2O [b]	56
($PhCH_2O_2C$–Cys–Ile–Ala–OMe)$_4$	−0.33	–		DMF	58

[a] Irreversible process. [b] Mercaptide buffer at pH 9.2.

Figure 28 shows the redox behaviour of $[(C_5H_5)_4Fe_4S_5]^{2+}$ as probed by cyclic voltammetry [77].

This type of cluster gives rise to the four-membered chemically reversible electron-transfer sequence

$$(C_5H_5)_4Fe_4S_5 \underset{+e^-}{\overset{-e^-}{\rightleftarrows}} [(C_5H_5)_4Fe_4S_5]^+ \rightleftarrows$$
$$E^{0\prime} = -0.66\ \text{V}$$

$$\underset{+e^-}{\overset{-e^-}{\rightleftarrows}} [(C_5H_5)_4Fe_4S_5]^{2+} \quad \underset{+e^-}{\overset{-e^-}{\rightleftarrows}} [(C_5H_5)_4Fe_4S_5]^{3+}$$
$$E^{0\prime} = -0.36\ \text{V} \qquad E^{0\prime} = +0.76\ \text{V}$$

The species with charge 0, 1 + , 2 + have been isolated [77–79]. Figure 29 shows an ORTEP drawing of the Fe_4S_5 cores of $[Fe_4(\mu_3\text{-}S)_3(\mu_3\text{-}S_2)(C_5H_5)_4]^{2+,1+}$ cations.

In both the assemblies there are three triply bridging S atoms and one triply bridging S_2 group "side-on", bonded to one iron atom (Fe(3)). This unusual sulfur ligation leads to three different types of iron atom: (i) Fe(3), bonded to four sulfur atoms, is not involved in Fe–Fe bonds; (ii) Fe(1) and Fe(4), each bonded to three sulfur atoms, are involved in one Fe–Fe bond; (iii) Fe(2), bonded to three sulfur atoms, is involved in two Fe–Fe bonds. In summary, the Fe–Fe bond lengths divide into four sets: two bonding

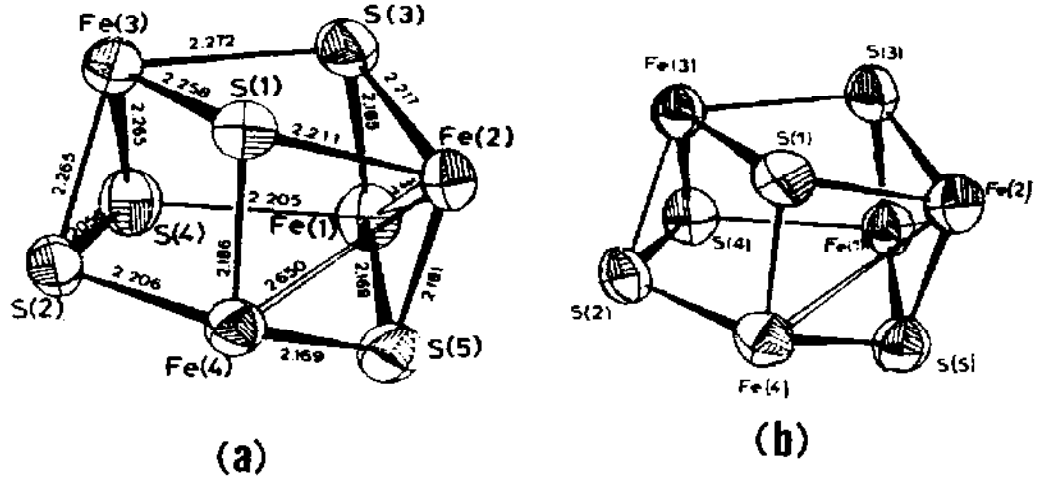

Fig. 29. Structures of the inner core of: (a) $[Fe_4S_5(C_5H_5)_4]^{2+}$; (b) $[Fe_4S_4(C_5H_5)_4]^{+}$ (from refs. 78, 79).

distances (mean value 2.65 Å in the dication, and 2.79 Å in the monocation); two non-bonding distances (Fe(1)–Fe(3) and Fe(4)–Fe(3)) having a mean value of 3.38 Å in both the dication and monocation; one non-bonding distance (Fe(1)–Fe(4)) at 3.64 Å in the dication, and 3.72 Å in the monocation; finally one further non-bonding distance (Fe(2)–Fe(3)) at a mean value of 3.41 Å in both compounds.

In a similar manner the 13 Fe–S bonds divide into two sets: nine short bonds (involving the Fe(1), Fe(2), Fe(4) atoms) ranging from 2.17 to 2.22 Å in the dication, and from 2.19 to 2.24 Å in the monocation; four long bonds (centred on Fe(3)) ranging from 2.26 to 2.27 Å in the dication, and from 2.27 to 2.28 Å in the monocation.

All these data, together with some EXAFS (Extended X-ray Absorption Fine Structure) evidence on the neutral congeners, testify that the redox changes do not afford substantial structural modifications, except for reversible core contractions or expansion as a result of removing or adding electrons. The relative variations of the metal–metal distances are interpreted on the basis that upon reduction the extra electrons go into non-bonding or anti-bonding tetrametal orbitals which are essentially centred on the Fe(1), Fe(2), Fe(4) atoms [79].

(vi) Fe_4S_6 core

The field of cyclopentadienyl–tetra-iron–sulfur clusters also includes $(C_5H_5)_4Fe_4S_6$. As with the case of the less sulfur-rich complexes $(C_5H_5)_4Fe_4S_4$ and $(C_5H_5)_4Fe_4S_5$, discussed above, this compound under-

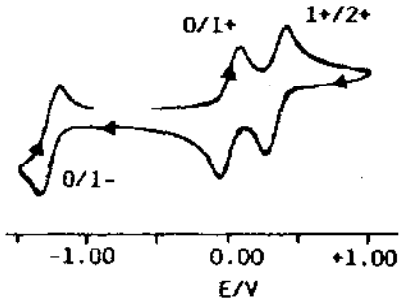

Fig. 30. Cyclic voltammetric response of $(C_5H_5)_4Fe_4S_6$ in dichloromethane solution. Potential values vs. S.C.E.

goes the redox series shown in Fig. 30 [77]. This sequence of reversible one-electron charge-transfers can be written:

$$[(C_5H_5)_4Fe_4S_6]^- \underset{+e^-}{\overset{-e^-}{\rightleftarrows}} (C_5H_5)_4Fe_4S_6 \rightleftharpoons$$
$$E^{0\prime} = -1.81 \text{ V}$$

$$\underset{+e^-}{\overset{-e^-}{\rightleftarrows}} [(C_5H_5)_4Fe_4S_6]^+ \quad \underset{+e^-}{\overset{-e^-}{\rightleftarrows}} [(C_5H_5)_4Fe_4S_6]^{2+}$$
$$E^{0\prime} = -0.43 \text{ V} \qquad E^{0\prime} = -0.12 \text{ V}$$

The 1 + /2 + step is followed, however, by a slow loss of sulfur according to the reaction:

$$|(C_5H_5)_4Fe_4S_6|^{2+} \overset{-S}{\rightarrow} |(C_5H_5)_4Fe_4S_5|^{2+}$$

The molecular structure of $(C_5H_5)_4Fe_4S_6$ is illustrated in Fig. 31 [80]. The Fe_4S_6 core possesses a C_2 axis. The iron atoms are paired by two metal–metal bonds (Fe(1)–Fe(2) and Fe(1)′–Fe(2)′ = 2.64 Å), and two non-bonding distances (Fe(2)–Fe(2)′ = 3.41 Å; Fe(1)–Fe(1)′ = 4.34 Å).

Attempts to prepare the monocation $[(C_5H_5)_4Fe_4S_6]^+$ by chemical oxidation with silver salts surprisingly afforded the trication $[\{(C_5H_5)_4Fe_4S_6)\}_2 Ag]^{3+}$, in which two monocations are ligated to a silver(I) ion, as shown in Fig. 32 [80]. Assuming that ligation to the silver(I) ion does not substantially affect the intimate geometry of the monocation core, note that the removal of one electron causes a slight distortion of the Fe_4S_6 core. In fact, while the two bonding Fe–Fe distances lengthen to 2.66 Å and the non-bonding Fe(1)–Fe(1)′ distance increases to 4.38 Å, the Fe(2)–Fe(2)′ non-bonding distance shortens to 3.00 Å. This significant shortening of one metal–metal distance with respect to the slight expansion of the others, has been interpreted in the sense that the HOMO of the neutral cluster has metal–metal antibonding character [80].

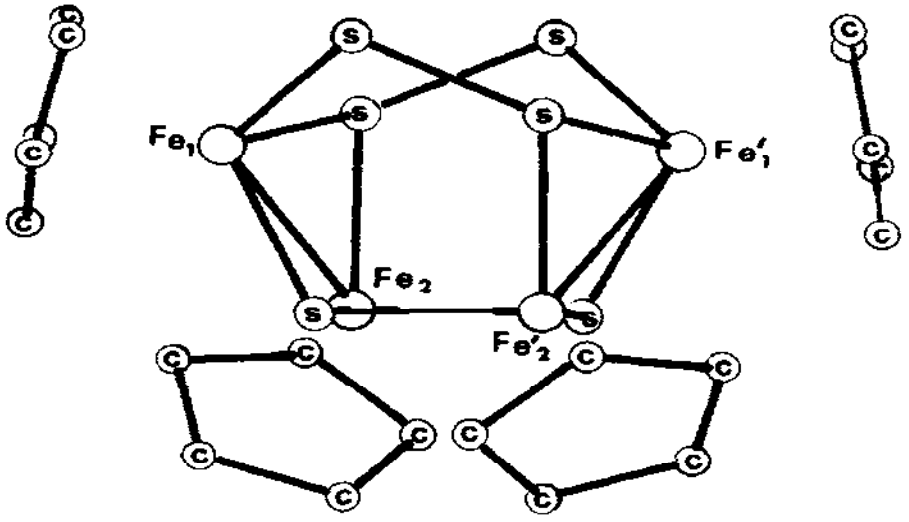

Fig. 31. Molecular structure of $(C_5H_5)_4Fe_4S_6$ (from ref. 80).

Another interesting aspect of the Fe_4S_6 core is the structural geometry it assumes in thiolate clusters. The structural chemistry of the metal thiolate has been reviewed recently [81]. In the thiolate dianions $[Fe_4(SR)_{10}]^{2-}$ (R = Ph [82,83], Et [84]), as well as in the mixed-ligand dianion $[Fe_4(SPh)_6Cl_4]^{2-}$ [69], the $Fe_4(\mu\text{-}S)_6$ core assumes an adamantane-like stereochemistry (Fig. 33) (composed of a nearly regular Fe_4 tetrahedron and a distorted S_6 octahedron) which results in distortion from ideal cubic T_d symmetry.

Surprisingly, in these reports no information is given concerning the redox behaviour. Possibly this adamantane geometry cannot support the addition/removal of electrons without breakage. This, in fact, happens in

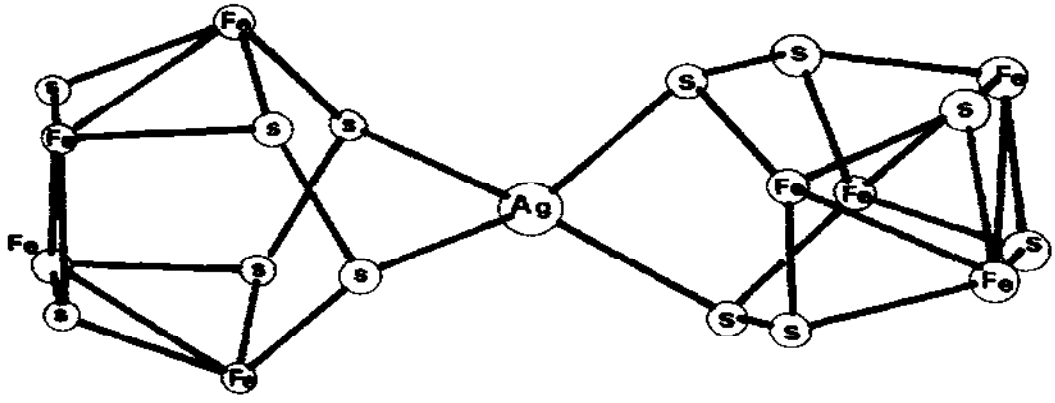

Fig. 32. Inner core of the trication $[(Fe_4S_6\{C_5H_5\}_4)_2Ag]^{3+}$ (from ref. 80).

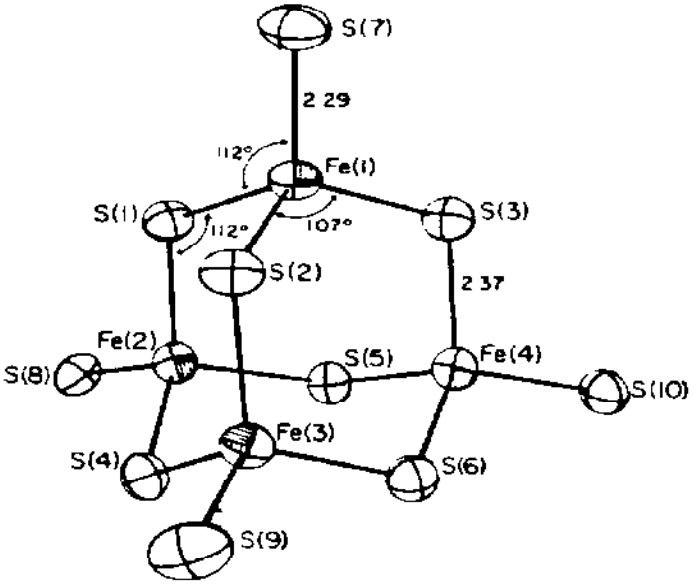

Fig. 33. Molecular structure of the Fe_4S_6 core in $[Fe_4(SPh)_{10}]^{2-}$ (from ref. 82).

$[Mn_4(SPh)_{10}]^{2-}$, which undergoes an irreversible cathodic process in acetonitrile at about -1.9 V [85].

(vii) Fe_6S_6 cores

A series of hexanuclear complexes $[Fe_6S_6X_6]^{n-}$ has recently been prepared, with X = halide, phenolate, arylthiolate [86–92]. In some cases their crystal structure has been also determined (namely: X = I, $n = 2$ [86]; X = Cl, $n = 2$ [90]; X = Cl, $n = 3$ [87,88]; X = Br, $n = 3$ [89]; X = OC_6H_4-*p*-CH_3, $n = 3$ [89,92]. These complexes undergo sequential one-electron charge transfers. Generally the $2-/3-$ step is electrochemically quasi-reversible, but chemically reversible, even if the choice of the solvent plays an important role in stabilizing the relevant products. On the other hand the $3-/4-$ step is generally complicated by subsequent chemical reactions, which make unstable the $4-$ complex. Table 15 summarizes the redox potentials for the series of charge transfer reactions of these clusters.

An evaluation of the structural consequences accompanying the redox changes can easily be performed through the structures of the two congeners $[Fe_6S_6Cl_6]^{2-,3-}$. Figure 34 shows the molecular shape of $[Fe_6S_6Cl_6]^{3-}$.

The $[Fe_6(\mu\text{-}S)_6]^{3+}$ core of the trianion can be described as a hexagonal prism (from which the term "prismane") with alternating Fe and S atoms of idealized D_{3d} symmetry, of which two identical cyclohexane-chair Fe_3S_3 units form the bases. Two types of parameter are of interest: those within

TABLE 15

Redox potentials (in volts) for the charge transfers of $[Fe_6S_6X_6]^{n-}$

X	Redox processes				Solvent	Ref.
	2−/3−	3−/4−	4−/5−	5−/6−		
Cl	−0.08 [a]	−1.13			AN	88
Cl	−0.25	−1.19			DCM	88, 89
Br	−0.22	−1.19			DCM	88
OC_6H_4-*p*-Cl		−1.50	−2.11 [a]	−2.42 [a]	AN	91
OC_6H_4-*p*-CH_3		−1.57	−2.11 [a]	−2.37 [a]	AN	91
OC_6H_4-*p*-CH_3	−0.49 [a]				AN	88
OC_6H_4-*p*-CH_3	−0.68				DCM	88, 89
OC_6H_4-*p*-C_2H_5	−0.69	−1.65			DCM	89
SC_6H_4-*p*-CH_3	−0.60	−1.41			AN	88
SC_6H_4-*p*-CH_3	−0.65	−1.59 [a]			DCM	88, 89
$SCH_2C_6H_5$	−0.73	−1.66			DCM	89

[a] Peak potential value for irreversible processes.

the "cyclohexane" Fe_3S_3 fragments (Fe–Fe, 3.79 Å; Fe–S, 2.28 Å; S–Fe–S, 113.7°; Fe–S–Fe, 113.2°); those within the "rhombic" Fe_2S_2 fragments (Fe–Fe, 2.76 Å; Fe–S, 2.27 Å; S–Fe–S, 105.2°; Fe–S–Fe, 74.8°).

The $[Fe_6(\mu\text{-}S)_6]^{4+}$ core of the dianion $[Fe_6S_6Cl_6]^{2-}$ possesses substantially the same hexagonal prismatic geometry as the trianion. With respect to the trianion, within the Fe_3S_3 unit the Fe–Fe distances (3.79 Å) remain unaltered; slight variations occur in the Fe–S distances (2.27 Å) and angles (S–Fe–S, 112.0°; Fe–S–Fe, 114.5°). Within the Fe_2S_2 fragment once again the Fe–Fe distances are invariant (2.76 Å), while the Fe–S distances (2.25

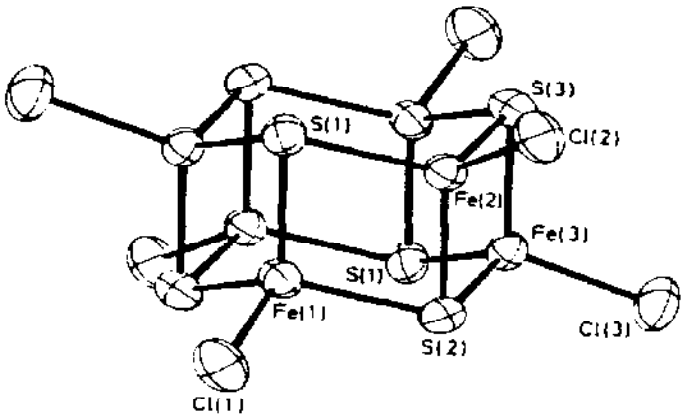

Fig. 34. Crystal structure of $[Fe_6S_6Cl_6]^{3-}$ (from ref. 87).

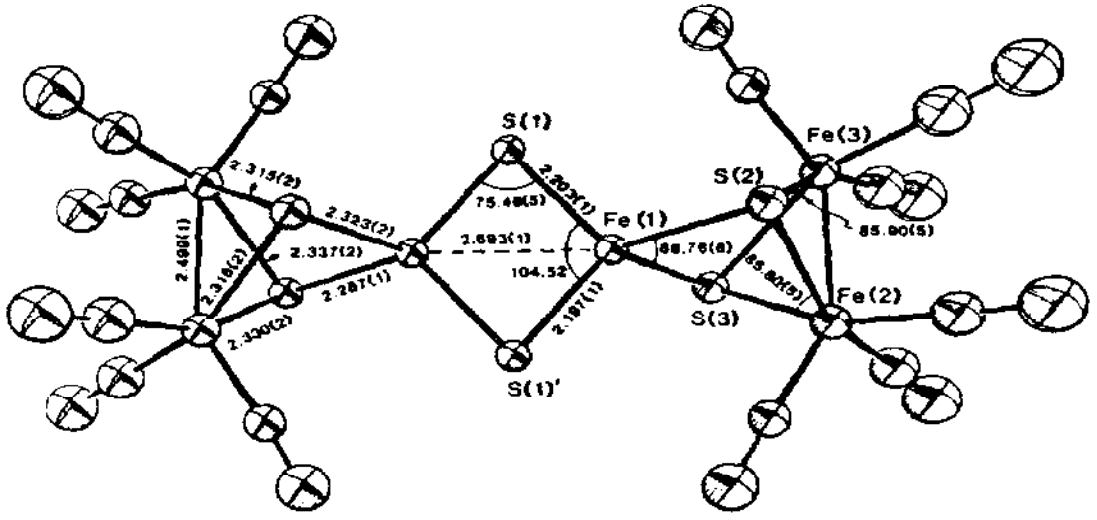

Fig. 35. Molecular structure of $[Fe_6S_6(CO)_{12}]^{2-}$ (from ref. 93).

Å) are slightly shorter. The angles remain nearly equal (S–Fe–S, 104.8°; Fe–S–Fe, 75.1°).

In conclusion, the removal of one electron from the $[Fe_6S_3]^{3+}$ core simply causes the shortening (by about 0.02 Å) of all the Fe–S bonds, indicating that the HOMO of the trianion (or the LUMO of the dianion) essentially has antibonding metal–sulfur character.

A quite different structural Fe_6S_6 core is contained in the dianion $[Fe_6S_6(CO)_{12}]^{2-}$ [93]. As shown in Fig. 35, it consists of a central $[Fe_2S_2]^{2+}$ unit, in which each Fe is ligated to a $[Fe_2S_2(CO)_6]^{2-}$ fragment. Within this latter unit the Fe–Fe distance is indicative of a bonding interaction.

$[Fe_6S_6(CO)_{12}]^{2-}$ in acetonitrile undergoes two subsequent quasi-reversible one-electron cathodic processes located at $E°'$ values of -1.51 V and -2.11 V, respectively [93]. The electrogenerable trianion $[Fe_6S_6(CO)_{12}]^{3-}$ could be a stable product.

(viii) Fe_6S_8 core

The dication $[Fe_6(\mu_3\text{-}S)_8(PEt_3)_6]^{2+}$ is another member of the hexanuclear metal–sulfur clusters [94,95]. This complex, containing six unpaired electrons ($\mu_{eff} = 6.04\ \mu_B$), should be a powerful agent for multiple electron-transfer processes. Its electrochemical behaviour supports this assertion [96].

As shown in Fig. 36, in dichloromethane this iron–sulfur assembly exhibits the five-membered sequence

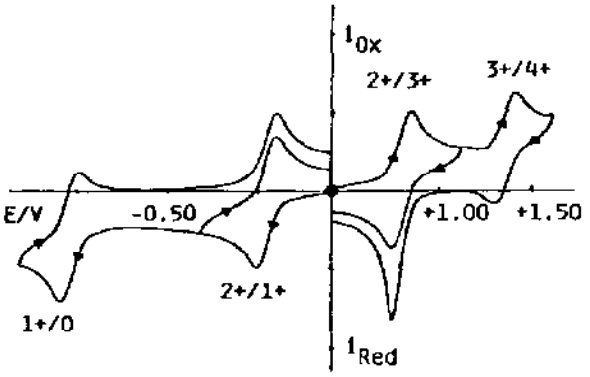

Fig. 36. Cyclic voltammogram of $[Fe_6S_8(PEt_3)_6]^{2+}$ in dichloromethane solution. Potential values vs. S.C.E.

$$[Fe_6S_8]^{4+} \underset{-e^-}{\overset{+e^-}{\rightleftarrows}} [Fe_6S_8]^{3+} \underset{-e^-}{\overset{+e^-}{\rightleftarrows}} [Fe_6S_8]^{2+} \underset{-e^-}{\overset{+e^-}{\rightleftarrows}} [Fe_6S_8]^{+} \underset{-e^-}{\overset{+e^-}{\rightleftarrows}} [Fe_6S_8]^{0}$$

$$E^{0\prime} = +0.87\ \text{V} \qquad E^{0\prime} = +0.31\ \text{V} \qquad E^{0\prime} = -0.43\ \text{V} \qquad E^{0\prime} = -1.52\ \text{V}$$

Macroelectrolysis experiments, however, showed both the species $[Fe_6S_8(PEt_3)_6]^{4+}$ (which causes electrode poisoning phenomena) and $Fe_6S_8(PEt_3)_6$ to be stable only in the short times of cyclic voltammetry.

Figure 37 shows a perspective view of the Fe_6S_8 core in $[Fe_6(\mu_3\text{-}S)_8(PEt_3)_6]^{2+}$. It consists of a nearly regular Fe_6 octahedron with all the faces symmetrically capped by triply bridging sulfur atoms. Alternatively, it may be described as a slightly distorted cube of sulfur atoms with the iron atoms occupying the face-centered sites. The Fe–Fe distance has a mean value of 2.62 Å; the Fe–S distance has a mean value of 2.25 Å; the Fe–P distance has a mean value of 2.29 Å. Explanations of the bonding pattern in this cluster are not yet unequivocal [95,97–99]. While attempts to isolate the stable trication $[Fe_6S_8(PEt_3)_6]^{3+}$ failed, the monocation $[Fe_6S_8(PEt_3)_6]^{+}$ was successfully crystallized [96]. It is isostructural with the dication.

The addition of one electron induces an elongation of the Fe–Fe distance (0.02 Å) as well as a shortening of the Fe–P distance (0.03 Å), while leaving almost unchanged the Fe–S distance (+0.004 Å).

The magnetic moment (7.4 μ_B) of the monocation indicates the presence of seven unpaired electrons. This result agrees with the proposed very-crowded distribution of valence electron orbitals around the HOMO–LUMO levels, which, because of the interelectronic repulsions, favours high spin multiplicities [95].

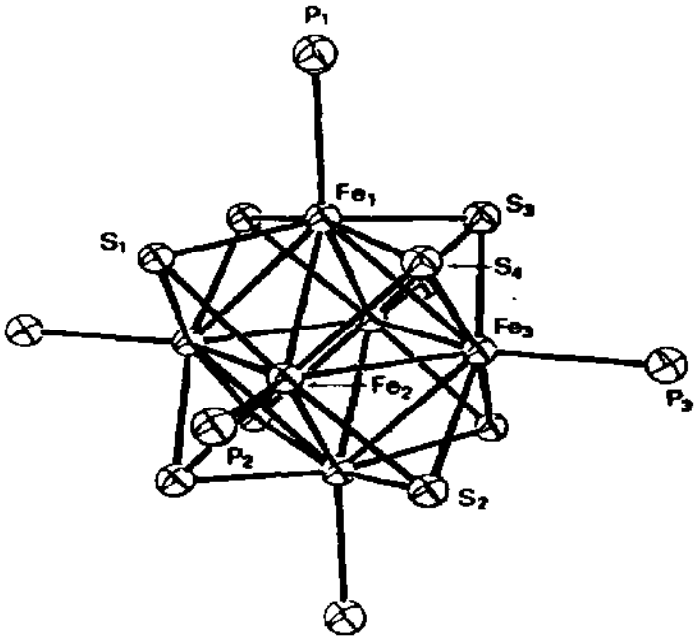

Fig. 37. Molecular structure of the Fe_6S_8 core in the dication $[Fe_6S_8(PEt_3)_6]^{2+}$ (from ref. 95).

We underline the structural flexibility of the present iron–sulfur core, which allows it to support the gradual expansion accompanying the variation of the number of valence electrons from 88 ($[Fe_6S_8]^{4+}$) to 92 ($[Fe_6S_8]^{0}$).

(ix) Fe_6S_9 core

The last electrochemically active member of the hexanuclear iron–sulfur derivatives contains the Fe_6S_9 core. A series of thiolate derivatives of formula $[Fe_6S_9(SR)_2]^{4-}$ has been characterized (R = C_2H_5 [24], t-C_4H_9 [100,101], $CH_2C_6H_5$ [102]). These clusters generally undergo both an uncomplicated quasi-reversible one-electron reduction and an uncomplicated quasi-reversible one-electron oxidation. Table 16 reports the redox

TABLE 16

Standard electrode potentials (in volts) for the redox processes of $[Fe_6S_9(SR)_2]^{4-}$

R	Redox processes		Solvent	Ref.
	3−/4−	4−/5−		
C_2H_5	−0.88	−2.00	AN	24
$C(CH_3)_3$	−0.92	−2.01	DMSO	101
$CH_2C_6H_5$	−0.78	−1.03	AN	102

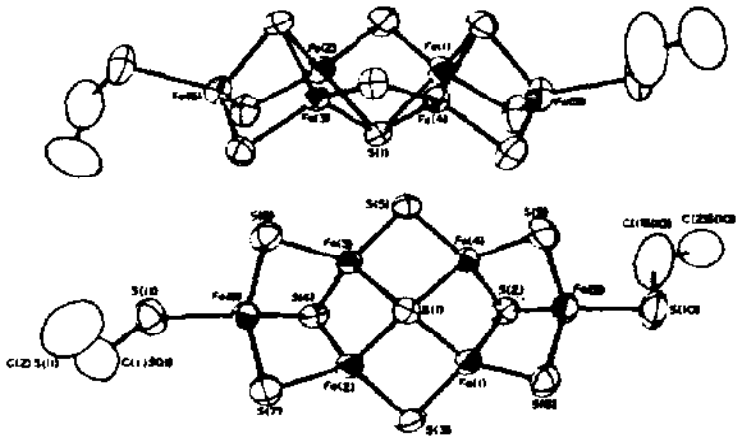

Fig. 38. Structure of the tetraanion $[Fe_6S_9(SC_2H_5)_2]^{4-}$. Bottom: view along the idealized C_2 axis passing through S(1) and perpendicular to the Fe(1–4) plane (from ref. 24).

potentials of these charge transfers.

The typical molecular structure of these complexes is shown in Fig. 38, which refers to $[Fe_6S_9(SC_2H_5)_2]^{4-}$ [24]. All six iron atoms are coplanar, and give rise to two triangles participating in a central square; each iron atom has an approximately tetrahedral coordination. The sulfur atoms involve four distinct coordination modes: two terminally bound thiolato Fe–S bonds (mean length 2.29 Å); twelve Fe–μ_2S bonds, which divide in three equivalent sets (Fe(1)–S(6), Fe(2)–S(7), Fe(3)–S(8), Fe(4)–S(9), mean distance 2.22 Å; Fe(1)–S(3), Fe(2)–S(3), Fe(3)–S(5), Fe(4)–S(5), mean distance 2.23 Å; Fe(5)–S(6), Fe(5)–S(9), Fe(6)–S(7), Fe(6)–S(8), mean distance 2.25 Å); six Fe–μ_3S bonds, which divide into two sets (Fe(1)–S(2), Fe(2)–S(4), Fe(3)–S(4), Fe(4)–S(2), mean distance 2.32 Å; Fe(5)–S(2), Fe(6)–S(4), mean distance 2.27 Å); finally four Fe–μ_4S bonds (Fe(1)–S(1), Fe(2)–S(1), Fe(3)–S(1), Fe(4)–S(1), mean distance 2.34 Å).

Unfortunately, attempts to isolate the one-electron oxidized trianion $[Fe_6S_9(SR)_2]^{3-}$ failed, because of its instability, and no attempt to obtain the one-electron reduced pentaanion $[Fe_6S_9(SR)_2]^{5-}$ has been made.

C. COBALT–SULFUR CLUSTERS

(i) Co_3S core

The simplest Co_3S core is present in the carbonyl derivative $Co_3(\mu_3\text{-}S)(CO)_9$. The structure of this complex is shown in Fig. 39 [103]. In this trigonally capped molecule of C_{3v} symmetry, the cobalt–cobalt bonding distance in the closed trimetal triangle is 2.64 Å, and the cobalt–sulfur

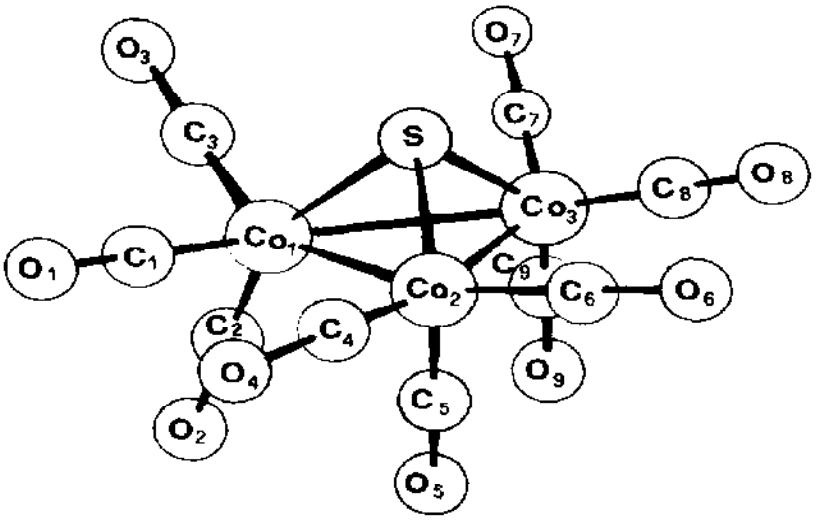

Fig. 39. Idealized molecular structure of $Co_3S(CO)_9$ (from ref. 103).

bonding distance is 2.14 Å. Interestingly, this species possesses one electron in excess of the closed-shell electronic configuration for each cobalt atom.

In dichloroethane, $Co_3S(CO)_9$ undergoes a near reversible one-electron oxidation ($E^{0\prime} = +0.04$ V), and an irreversible two-electron reduction ($E^{irr}_{1/2} = -1.1$ V) [12]. The expectedly stable monocation $[Co_3S(CO)_9]^+$ is indeed only stable in solution [104]. To evaluate the stereochemical consequence of the 0/1 + redox change, one may compare the crystal structure of $Co_3S(CO)_9$ with that of $FeCo_2S(CO)_9$, which is isoelectronic with $[Co_3S(CO)_9]^+$; the covalent radii for the two metals also being virtually identical [105].

$FeCo_2S(CO)_9$ is isomorphous with $Co_3S(CO)_9$. The removal of one electron from the tricobalt complex simply seems to cause a significant shortening of the metal–metal bond (about 0.09 Å), accompanied by a minor lengthening (~ 0.02 Å) of the metal–sulfur distance. This information has been assumed to provide evidence that in $Co_3S(CO)_9$ the electron in excess resides in an antibonding tricobalt orbital [106].

A series of tricobalt carbonyl complexes capped by a triply bridging sulfur atom, but with a bridging bidentate ligand substituting two CO molecules (Chart 1) have been characterized [107–109].

Since these derivatives can be considered to arise from $Co_3S(CO)_9$ by the substitution of two two-electron-donating carbonyl ligands with one three-electron bidentate ligand, they possess a closed shell electronic configuration for each cobalt atom. Something similar happens in each $Co_3S(CO)_7$ moiety of $[Co_3S(CO)_7]_2S_2$ [110]. In both cases the stereochemical differences with respect to $Co_3S(CO)_9$ are very similar (the trimetallic triangle is no longer equilateral because of the constraints imposed by the chelating ligand, and

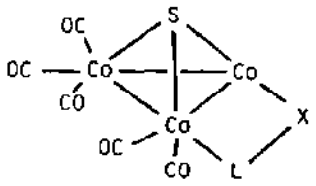

CHART I

Ia L–X = μ-1,2-η^2-C(CH_3)N(C_6H_{11})

Ib L–X = μ-1,2-η^2-C(C_6H_5)N(C_6H_{11})

Ic L–X = μ-1,2-η^2-SC[N(CH_3)$_2$]

Id L–X = μ-1,3-η^2-N(H)C(CH_3)S

Ie L–X = μ-1,3-η^2-N(H)C(C_6H_5)S

the Co–Co distances are notably shorter because of the lack of the unpaired electron in an antibonding orbital). It is hence expected that compounds **Ia–Ie** are able to lodge one electron in an antibonding trimetal orbital. In non-aqueous solvents they undergo a near reversible one-electron reduction at the potentials reported in Table 17. The relevant monoanions seem stable at least on the cyclic voltammetric time scale [109].

The usual trigonal pyramidal $Co_3(\mu_3$-S) core is also present in $Co_3(\eta^5$-$C_5H_5)_3(\mu_3$-S)(μ_3-CS) [111], which is isostructural with $Co_3(\eta^5$-$C_5H_5)_3(\mu_3$-S)(μ_3-CO) [112]. A schematic representation of these molecules is shown in Fig. 40.

The electrode behaviour of the thiocarbonyl substituted species in benzonitrile solvent is reported in Fig. 41 [13].

TABLE 17

Redox potentials (in volts) for the one-electron reduction step of (μ_3-S)$Co_3(CO)_7$(LX) derivatives [109]

Complex	$E^{0\prime}$	Solvent
Ia	−1.12	DMF
Ib	−1.08	DMF
Ib	−1.29	DCM
Ic	−1.12	DMF
Ic	−1.31	DCM
Id	−0.89	DMF
Id	−1.01	DCM
Ie	−0.98	DCM

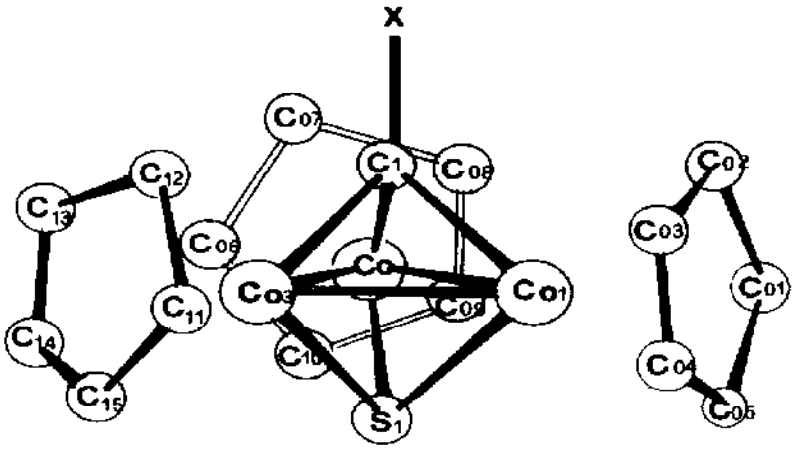

Fig. 40. Schematic structure of $Co_3(C_5H_5)_3(S)(CX)$ where X = O, S.

The derivative displays a chemically reversible one-electron reduction step, and a declustering one-electron oxidation step, according to the sequence

$$[(C_5H_5)_3Co_3S(CS)]^+ \xleftarrow[E_p = +0.02\ V]{-e^-} (C_5H_5)_3Co_3S(CS) \overset{+e^-}{\underset{-e^-}{\rightleftharpoons}} [(C_5H_5)_3Co_3S(CS)]^-$$

$$\downarrow \text{fast decomposition} \qquad E^{0\prime} = -1.55\ V$$

unidentified products

If we speculate that the MO diagram for $(C_5H_5)_3Co_3(S)(CS)$ is likely substantially similar to the one for $(C_5H_5)_3Co_3(S)(CO)$, reported in Fig. 42

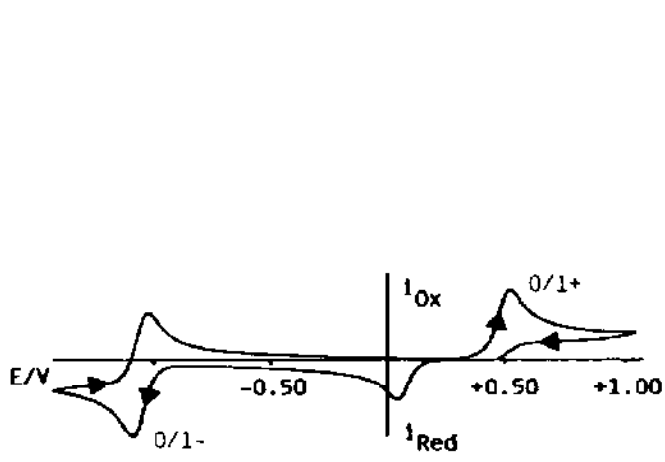

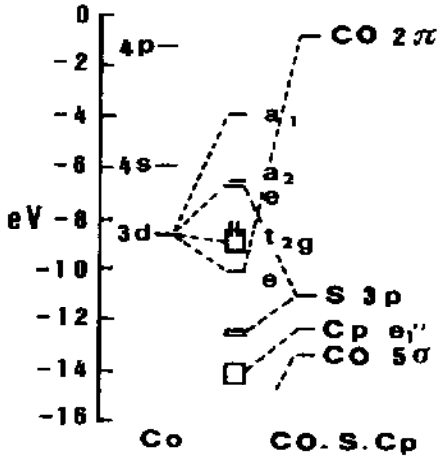

Fig. 41. Cyclic voltammetric response recorded for a benzonitrile solution of $Co_3(C_5H_5)_3(S)(CS)$. Potential values vs. Ag/AgCl.

Fig. 42. MO diagram for $(C_5H_5)_3Co_3(S)(CO)$.

[16], this result is not unexpected. In fact, at variance with $Fe_3(CO)_9(S)(CO)$ (see Section B(i)), the LUMO *e* is not highly destabilized, so that the addition of one electron does not lead to an energetically unfavoured monoanion. On the contrary, in this case the removal of one electron from the stabilized *e* orbital, i.e. from the electron-poor M–(μ_3-CS) bonds, causes destruction of the molecular framework.

Finally, the pyramidal $Co_3(\mu_3\text{-}S)$ core is present in the electroactive dianion $[Co_3S(1,2\text{-}(SCH_2)_2C_6H_4)_3]^{2-}$ [17]. This compound, isostructural with the Fe(II) analog (see Section B(i)), undergoes a single one-electron reversible reduction in acetonitrile [17] at $E^{0\prime} = -2.11$ V. This notably negative potential value prevented straightforward isolation and characterization of the trianion $[Co_3S(1,2\text{-}(SCH_2)_2C_6H_4)_3]^{3-}$.

(ii) Co_3S_2 core

The compound $Co_3(\eta^5\text{-}C_5H_5)_3(\mu_3\text{-}S)_2$ contains a Co_3S_2 core, in which the cobalt and sulfur atoms form a regular trigonal bipyramid, as schematized in Fig. 43. The molecule possesses D_{3h} geometry with three equivalent Co–Co distances of 2.69 Å [112].

Figure 44 shows the redox behaviour of this cluster in benzonitrile solution, as probed by cyclic voltammetry [13]. Two subsequent reversible one-electron oxidation steps as well as a reversible one-electron reduction step are displayed, according to the four-membered sequence

$$[Co_3(C_5H_5)_3S_2]^{2+} \underset{-e^-}{\overset{+e^-}{\rightleftarrows}} [Co_3(C_5H_5)_3S_2]^{+} \rightleftarrows$$

$$\underset{E^{0\prime} = -0.62\text{ V}}{\overset{+e^-}{\underset{-e^-}{\rightleftarrows}} [Co(C_5H_5)_3S_2]^{0}} \qquad \underset{E^{0\prime} = -1.65\text{ V}}{\overset{+e^-}{\underset{-e^-}{\rightleftarrows}} [Co_3(C_5H_5)_3S_2]^{-}}$$

$E^{0\prime} = +0.16$ V

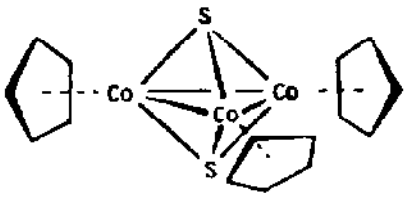

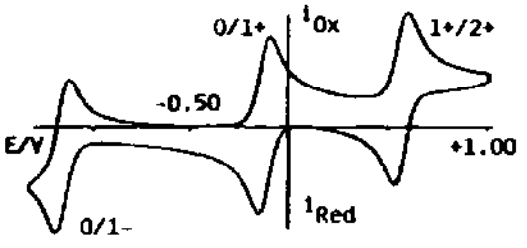

Fig. 43. Schematic representation of the molecular structure of $Co_3S_2(C_5H_5)_3$.

Fig. 44. Cyclic voltammogram recorded in a benzonitrile solution of $Co_3S_2(C_5H_5)_3$. Potential values vs. Ag/AgCl.

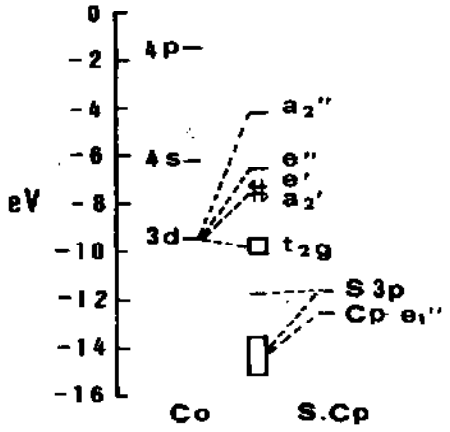

Fig. 45. MO diagram for $Co_3S_2(C_5H_5)_3$.

Considering the MO diagram reported in Fig. 45 [16], these reversible redox changes correspond both to the removal of the two electrons residing in the destabilized $a_2'e'$ orbitals, and to the addition of one electron probably in the metal–metal bonding e' level.

Although there is the potential stability of the whole family $[Co_3(C_5H_5)_3S_2]^{1-,0,1+,2+}$, only the monocation species has been obtained by chemical oxidation of the neutral parent. This complex, shown in Fig. 46, is deformed to C_{2v} geometry, with respect to the neutral precursor, with one short Co–Co distance of 2.47 Å and two long Co–Co distances of 2.65 Å [112]. The shortening of the Co–Co distances, in particular one of them, indicates that in the oxidation process the antibonding a_2' electron is removed with consequent Jahn–Teller distortion.

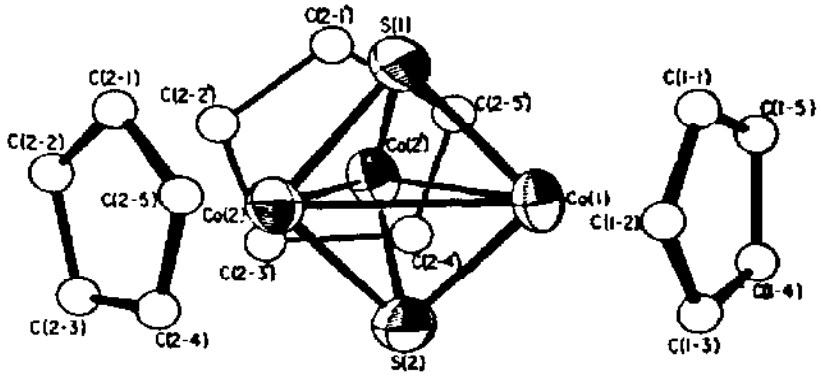

Fig. 46. The molecular structure of $[Co_3(C_5H_5)_3S_2]^+$ (from ref. 112).

(iii) Co_4S_4 core

Two cubane-like cobalt–sulfur clusters of the family $[Co_4(\eta^5\text{-}C_5H_5)_4S_4]^n$ have been isolated ($n = 0, 1+$) [113]. Even if of unknown electrochemistry, we briefly illustrate their structures. Figure 47a shows the crystal structure of the neutral species, and Fig. 47b illustrates selected distances of both Co_4S_4 cores. The neutral parent possesses an almost undistorted cubic geometry (some slight distortion lowering the symmetry from T_d to C_2 is attributed to crystal packing forces) with Co–Co non-bonding distances of average length 3.29 Å, and Co–S bonding distances of average length 2.23 Å.

Removal of one electron causes a regular tetragonal deformation of the Co_4S_4 core from idealized T_d geometry to an approximate D_{2d} geometry. The Co–Co distances occur in four shortened distances (mean value 3.17 Å) and two slightly elongated distances (mean value 3.30 Å). On the other hand the tetragonal distortion divides the Co–S distances into two sets: four equivalent distances of 2.21 Å, and eight equivalent distances of 2.22 Å. It is evident that the Co–S distances are only very slightly affected by one-electron oxidation.

Dahl and co-workers explain this tetragonal deformation of the starting regular cubic framework on the basis of their bonding description based on tetrametal orbital interactions, previously mentioned (see Section B(iv)(b)). In the neutral molecule the 24 valence electrons (from a formal Co(III) configuration) fully occupy both the six bonding orbitals ($a_1 + e + t_2$) and the six antibonding orbitals ($t_1 + t_2$) (zero order Co–Co bond). Removing one electron from one of the antibonding t levels would produce an orbital degeneracy of the ground state causing both a deformation via a Jahn–Teller vibration, and a shortening of the metal–metal distances. An interpretation based on slightly different orbital levels has been also proposed [97].

(iv) Co_6S_8 core

We have recently reported on the redox properties of the cation $[Co_6(\mu_3\text{-}S)_8(PEt_3)_6]^+$ [114]. As shown in Fig. 48, this polynuclear derivative undergoes a series of reversible or near reversible one-electron charge transfers in non-aqueous solvents, namely two anodic and one cathodic steps, according to the sequence

$$Co_6S_8(PEt_3)_6 \underset{+e^-}{\overset{-e^-}{\rightleftarrows}} [Co_6S_8(PEt_3)_6]^+ \underset{+e^-}{\overset{-e^-}{\rightleftarrows}} [Co_6S_8(PEt_3)_6]^{2+} \underset{+e^-}{\overset{-e^-}{\rightleftarrows}} [Co_6S_8(PEt_3)_6]^{3+}$$

AN	$E_{p0} = -0.89$ V	$E^{0\prime} = -0.13$ V	$E^{0\prime} = +0.57$ V
DCM	$E^{0\prime} = -0.97$ V	$E^{0\prime} = -0.12$ V	$E^{0\prime} = +0.64$ V

Controlled potential coulometric experiments showed, however, that the trication is stable only for a short time (half life of about 5 s). This provides

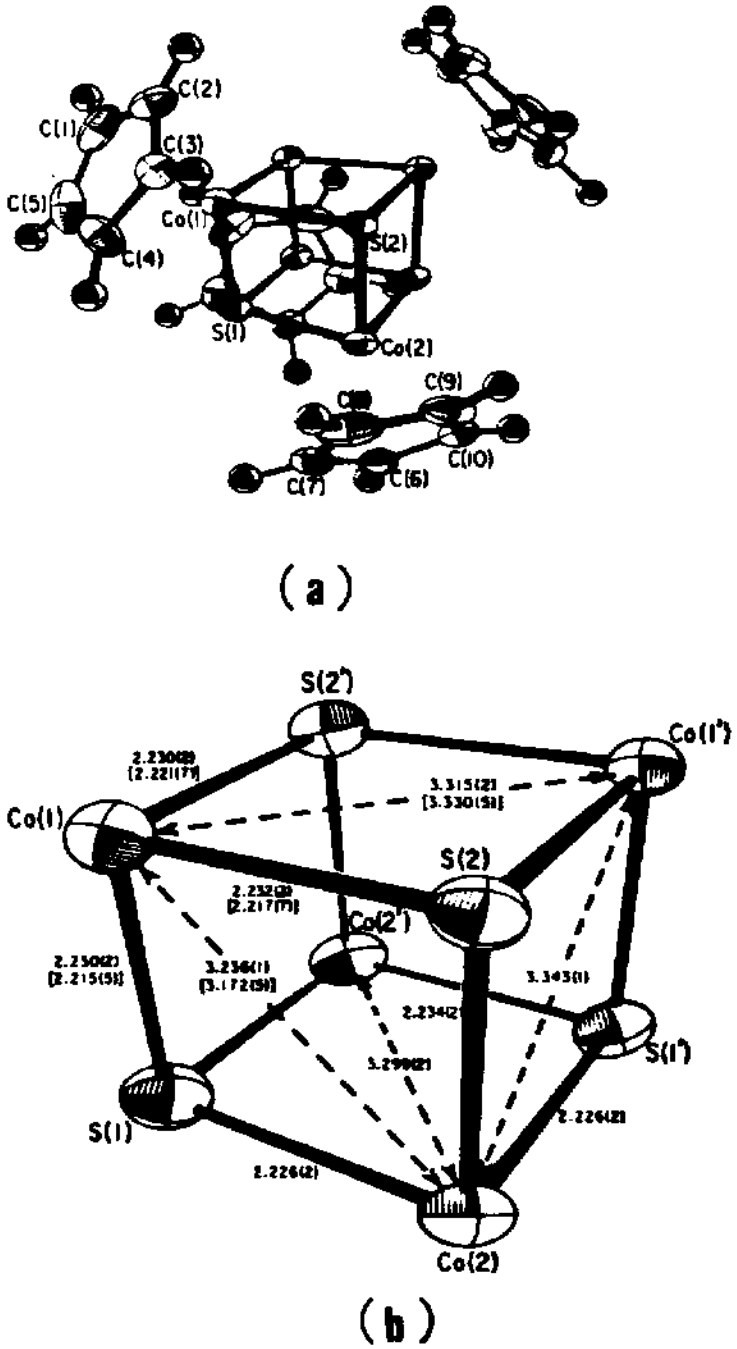

Fig. 47. (a) Molecular structure of $Co_4(C_5H_5)_4S_4$; (b) selected distances in $[Co_4(C_5H_5)_4S_4]^{0,1+}$; those reported in brackets refer to the monocation (from ref. 113).

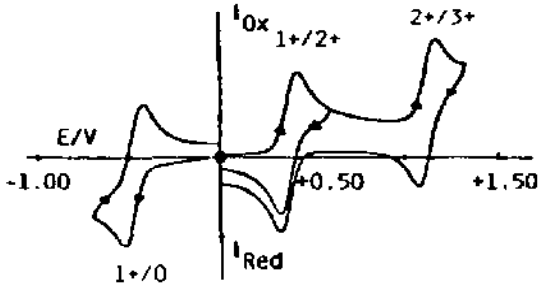

Fig. 48. Cyclic voltammetric response recorded on a dichloromethane solution of $[Co_6S_8(PEt_3)_6]^+$. Potential values vs. S.C.E.

evidence for the ability of this metal–sulfur assembly to maintain its framework, at least for short times, with gradual variation of the valence electron number from 98 to 95.

Although $[Co_6S_8(PEt_3)_6]^{2+}$ is stable, we were unable to obtain it in a crystalline form suitable for X-ray investigation. However, the neutral species $Co_6S_8(PEt_3)_6$ has been prepared by chemical reduction and structurally characterized [114,115].

Fig. 49 shows a perspective view of the inner core of $[Co_6S_8(PEt_3)_6]^+$ [114,116]. The cation, which is isostructural with $[Fe_6(\mu_3\text{-}S)_8(PEt_3)_6]^{2+}$ (see

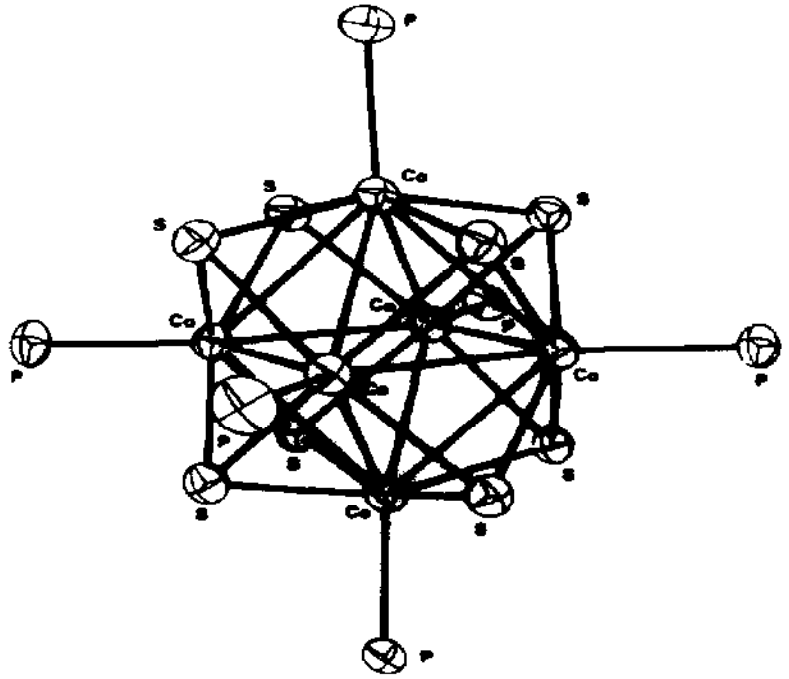

Fig. 49. Inner core of $[Co_6(\mu_3\text{-}S)_8(PEt_3)_6]^+$ (from ref. 116).

Section B(viii)), consists of a nearly regular octahedron of cobalt atoms with all the faces symmetrically capped by triply bridging sulfur atoms. The average Co–Co distance is 2.79 Å; the average Co–S distance is 2.23 Å; the average Co–P distance is 2.16 Å.

The neutral species $Co_6(\mu_3\text{-}S)(PEt_3)_6$ possesses the same octahedral face-capped geometry of the parent monocation species. Addition of one electron simply causes elongation (of about 0.02 Å) of the Co–Co distance as well as shortening of the Co–P distance (of about 0.02 Å), while leaving the Co–S distance unchanged. This trend, which is the same observed for the redox change $[Fe_6(\mu_3\text{-}S)_8(PEt_3)_6]^{2+/+}$, leads us to conclude that only the metal–sulfur bonds are the stabilizing factors on which the high flexibility of these clusters is centred.

(v) Co_8S_6 core

The high-nuclearity metal–sulfur cluster $[Co_8S_6(SPh)_8]^{4-}$ is the last member of the electroactive cobalt–sulfur derivatives described here. Figure 50 shows the redox changes occurring in an acetonitrile solution of this tetra anion [117,118]. Both an uncomplicated quasi-reversible one-electron oxidation and an uncomplicated quasi-reversible one-electron reduction are displayed, testifying to the chemically reversible electron-transfer sequence

$$[Co_8S_6(SPh)_8]^{5-} \underset{+e^-}{\overset{-e^-}{\rightleftarrows}} [Co_8S_6(SPh)_8]^{4-} \underset{+e^-}{\overset{-e^-}{\rightleftarrows}} [Co_8S_6(SPh)_8]^{3-}$$

$$E^{0\prime} = -1.37\ \text{V} \qquad E^{0\prime} = -0.77\ \text{V}$$

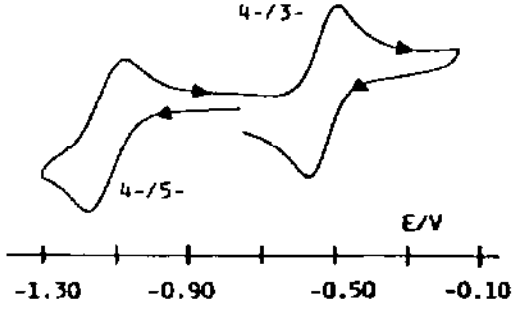

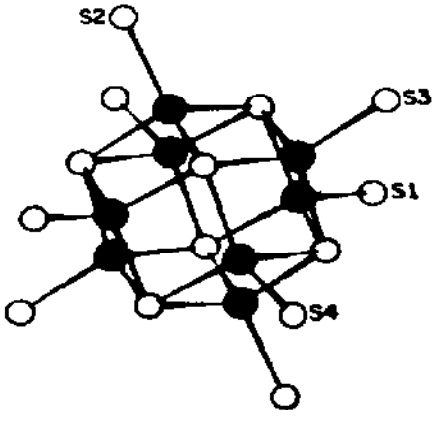

Fig. 50. Cyclic voltammetric response recorded in an acetonitrile solution of $[Co_8S_6(SPh)_8]^{4-}$. Potential values vs. S.C.E.

Fig. 51. Perspective view of the inner core of $[Co_8S_6(SPh)_8]^{4-}$ (from ref. 118).

While no attempt has been made to isolate the stable one-electron oxidized product, the one-electron reduced species $[Co_8S_6(SPh)_8]^{5-}$ was successfully obtained by chemical reduction.

Figure 51 shows the molecular structure of the tetra-anion $[Co_8S_6(SPh)_8]^{4-}$. The anion is composed of concentric Co_8 cubes and S_6 octahedra forming a rhombic dodecahedral $[Co_8(\mu_4\text{-}S)_6]^{4+}$ core, of idealized O_h cubic symmetry. Interestingly, this assembly is simply reversed with respect to the previously described $[Co_6S_8(PEt_3)_6]^{1+,0}$ as far as the positions of the cobalt and sulfur atoms are concerned. The mean Co–Co non-bonding distance is 2.66 Å, the bonding $Co–S_{(bridging)}$ distance is 2.23 Å, and the bonding $Co–S_{(thiolate)}$ distance is 2.24 Å.

Addition of one electron leads to a $[Co_8(\mu_4\text{-}S)_6]^{3+}$ core of the same geometry. The expected expansion is very limited, in that the Co–Co distance elongates 0.01 Å and the $Co–S_{(bridging)}$ distance remains practically unaltered. The $Co–S_{(thiolate)}$ distance increases by 0.04 Å. It is argued that the LUMO of the tetra-anion has detectable cobalt character [118].

D. NICKEL–SULFUR CLUSTERS

There are indeed few reports dealing with the electrochemistry of polynuclear nickel–sulfur derivatives.

(i) Ni_3S_2 cores

The first isolated and crystallographically characterized Ni_3S_2-core-containing derivative is the cyclopentadienyl complex $(\eta^5\text{-}C_5H_5)_3Ni_3(\mu_3\text{-}S)_2$ [119]. As shown in Fig. 52, the molecule is a triangle of nickel atoms capped above and below by triply bridging sulfur atoms, so forming a regular trigonal bipyramid. The Ni–Ni distance is 2.80 Å, indicative of a weak

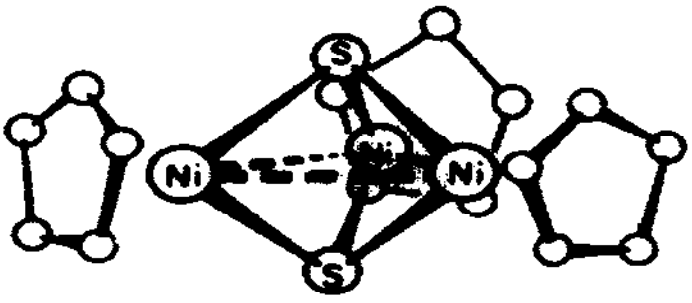

Fig. 52. Molecular configuration of $Ni_3S_2(C_5H_5)_3$ (from ref. 119).

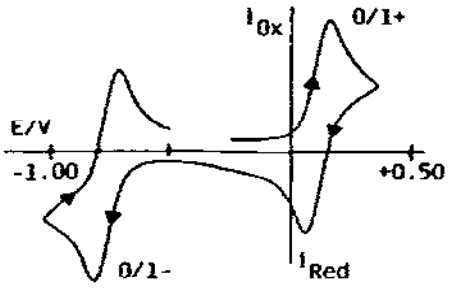

Fig. 53. Cyclic voltammogram recorded for a benzonitrile solution of $(C_5H_5)_3Ni_3S_2$. Potential values vs. Ag/AgCl.

TABLE 18

Standard potentials (in volts) for the redox processes of derivatives containing a Ni_3S_2 core

Complex	Redox processes			Solvent	Ref.
	2+/1+	1+/0	0/1−		
$(C_5H_5)_3Ni_3S_2$	–	−0.38	−1.25	BN	13
$[Ni_3S_2(PEt_3)_6]^{2+}$	−1.57	−1.71 [a]	–	AN	122

[a] Peak potential value for irreversible processes.

metal–metal interaction. The Ni–S distance is 2.17 Å, and the S–S non-bonding distance is 2.90 Å.

The electrode behavior of $(C_5H_5)_3Ni_3S_2$ is illustrated in Fig. 53 [13]. Two reversible one-electron charge transfers are displayed, corresponding to both a cathodic and an anodic step. The relevant standard potentials are summarized in Table 18.

The apparent stability of both the monoanion and the monocation could be interpreted, on the basis of the MO diagram shown in Fig. 54 [16], as being a consequence of the filling of the metal–metal bonding e' orbital and removal of one electron from the metal–metal antibonding a_2' orbital, respectively.

No attempts seem to have been made to isolate $[(C_5H_5)_3Ni_3S_2]^+$ and $[(C_5H_5)_3Ni_3S_2]^-$.

Another derivative containing a Ni_3S_2 core is the dication $[Ni_3(\mu_3\text{-}S)_2(PEt_3)_6]^{2+}$, the structure of which is reported in Fig. 55 [120,121]. In this

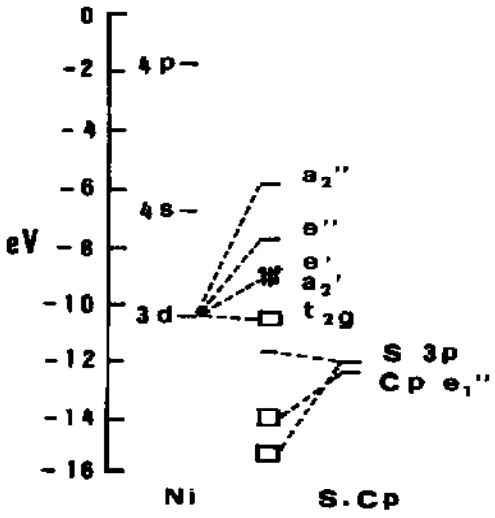

Fig. 54. MO diagram of $(C_5H_5)_3Ni_3S_2$.

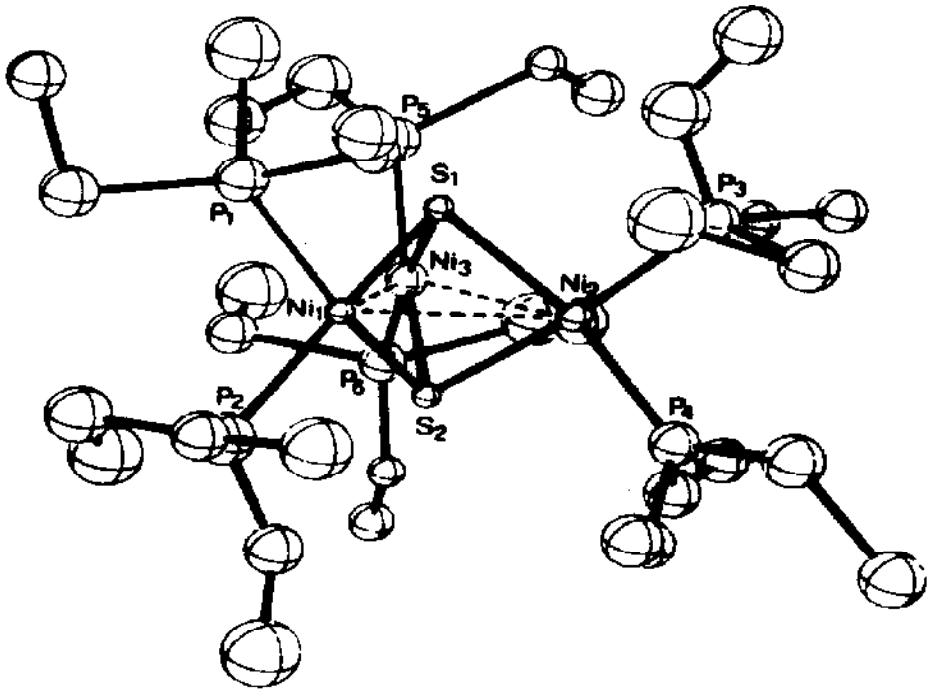

Fig. 55. Perspective view of $[Ni_3S_2(PEt_3)_6]^{2+}$ (from ref. 120).

case the Ni_3S_2 core is composed of a substantially regular trigonal bipyramid. The Ni–Ni distance of 2.91 Å is longer than in the preceding case, indicating no significant metal–metal interaction. The Ni–S distance is 2.15 Å, and the S–S distance is 2.70 Å. This latter distance is indicative of a higher extent of axial compression of the trigonal bipyramid with respect to the preceding one.

Figure 56 shows the redox behaviour in cyclic voltammetry of $[Ni_3S_2(PEt_3)_6]^{2+}$ [122]. The trinickel cation undergoes a series of cathodic processes, of which only the first displays some features of reversibility followed, however, by chemical complications ($i_{pa}/i_{pc} < 1$). In conclusion, the following electrode mechanism holds:

$$[Ni_3S_2(PEt_3)_6]^{2+} \underset{-e^-}{\overset{+e^-}{\rightleftarrows}} [Ni_3S_2(PEt_3)_6]^{+} \qquad \underset{-e^-}{\overset{+e^-}{\rightleftarrows}} Ni_3S_2(PEt_3)_6$$

$$\downarrow \text{slow} \qquad\qquad \downarrow \text{fast}$$

decomposition products decomposition products

The relevant redox potentials are reported in Table 18.

It is evident that the Ni_3S_2 core of $[Ni_3S_2(PEt_3)_6]^{2+}$ is much less flexible than that of $(C_5H_5)_3Ni_3S_2$, in view of its easy breakage following the redox changes.

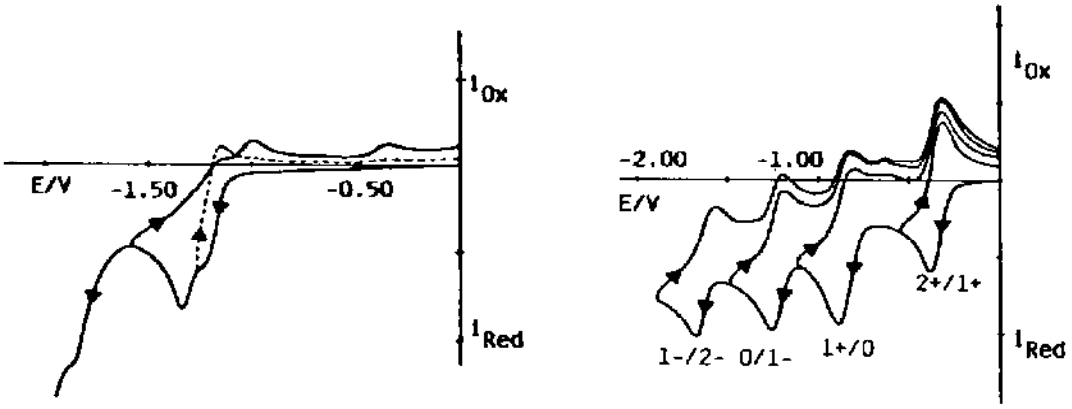

Fig. 56. Cyclic voltammetric response recorded for an acetonitrile solution of $[Ni_3S_2(PEt_3)_6]^{2+}$. Potential values vs. S.C.E.

Fig. 57. Cyclic voltammetric response of $[Ni_9S_9(PEt_3)_6]^{2+}$ in acetonitrile solution. Potential values vs. SCE.

(ii) Ni_9S_9 core

The enneanickel compound $[Ni_9(\mu_4\text{-}S)_3(\mu_3\text{-}S)_6(PEt_3)_6]^{2+}$ shows an unusually rich redox chemistry [122]. Figure 57 reports the cyclic voltammogram recorded on an acetonitrile solution of this dication.

The ability of this derivative to undergo multiple redox changes, non-declustering at least in the short term is in evidence by the overall redox series

$$\begin{array}{lcll} & E^{0\prime} = -0.67\ V & & E^{0\prime} = -1.16\ V \\ [Ni_9S_9(PEt_3)_6]^{2+} & \overset{+e^-}{\underset{-e^-}{\rightleftarrows}} [Ni_9S_9(PEt_3)_6]^{+} & \overset{+e^-}{\underset{-e^-}{\rightleftarrows}} & Ni_9S_9(PEt_3)_6 \rightleftarrows \\ & \overset{+e^-}{\underset{-e^-}{\rightleftarrows}} [Ni_9S_9(PEt_3)_6]^{-} & \overset{+e^-}{\underset{-e^+}{\rightleftarrows}} & [Ni_9S_9(PEt_3)_6]^{2-} \\ & E^{0\prime} = -1.54\ V & & E^{0\prime} = -1.90\ V \end{array}$$

However, among the different congeners of the starting dication only the monocation $[Ni_9S_9(PEt_3)_6]^{+}$ gave stable products over the long times of macroelectrolysis tests.

The structure of $[Ni_9S_9(PEt_3)_6]^{2+}$ is shown in Fig. 58 [121,123]. The Ni_9S_9 core, of idealized D_{3h} symmetry, is composed of a Ni_9 cofacial bi-octahedron, in which three parallel Ni_3 triangles are connected to three coplanar S_3 triangles. The sulfur ligands are divided in six triply bridging atoms (outer triangles) and three quadruply bridging atoms (inner triangle), respectively. The Ni–Ni distance in the basal triangles is 2.95 Å, while in the equatorial triangle it is 2.87 Å. The interlayer Ni–Ni distance is 2.69 Å. The average value of Ni–(μ_3-S) bonds (2.17 Å) is shorter than the one for

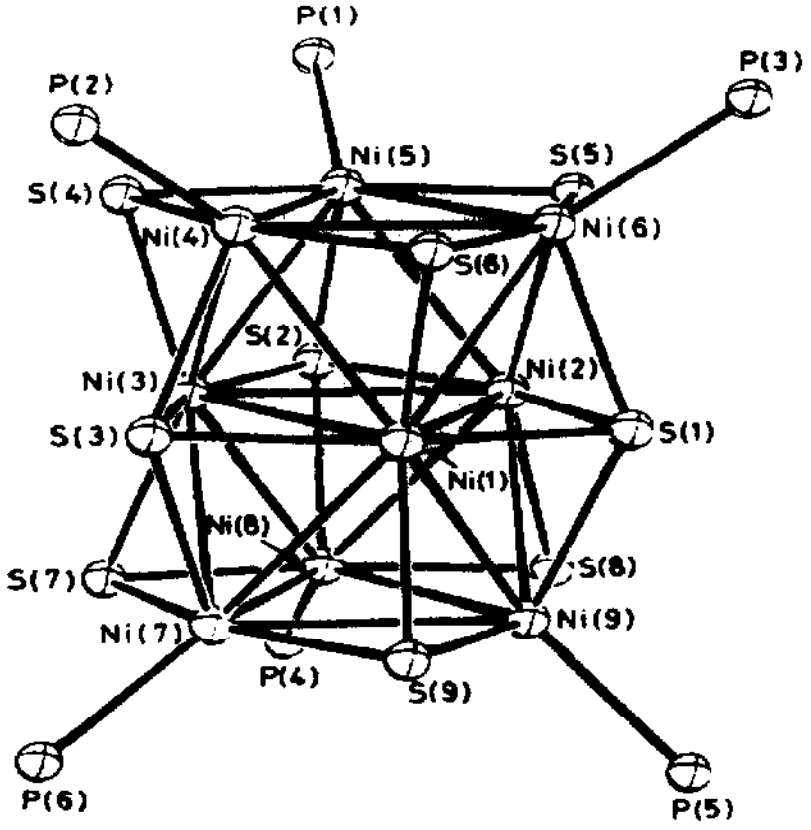

Fig. 58. Perspective view of the inner core of the dication $[Ni_9S_9(PEt_3)_6]^{2+}$ (from ref. 123).

Ni–(μ_4-S) bonds (2.23 Å). In addition, for both types of sulfur atoms the Ni–S interlayer distances are longer than the Ni–S intralayer distances.

The high flexibility of the Ni_9S_9 core allows it to support, at least for short times, the stereochemical reorganization following the step-by-step variation of the number of valence electrons from 70 (for the dicationic form) to 74 (for the dianionic form).

In order to evaluate accurately, even if only partially, these structural changes, work is in progress to obtain crystals suitable for an X-ray investigation of the monocation $[Ni_9S_9(PEt_3)_6]^{+}$.

E. MOLYBDENUM-SULFUR CLUSTERS

In recent years, the interest in the chemistry of molybdenum–sulfur complexes has been growing rapidly, mainly because of their involvement in important biological functions, such as nitrogenases (as we shall examine in Part II of this review, dealing with heterometallic clusters), and in the catalysis of hydrodesulfurization processes [124].

(i) $Mo_3O_nS_{4-n}$ cores

The complete series of triangular metal–metal bonded oxo/sulfido bridged molybdenum complexes (Chart II) has been synthesized [125]. These cores are commonly defined as having an "incomplete cubane-type structure". Isomerism between (μ_3-S) and (μ_3-O) forms can occur.

Examination of the redox properties of the $[Mo_3O_4]^{4+}$ ion is outside the range of this review, and is covered in refs. 126 and 127.

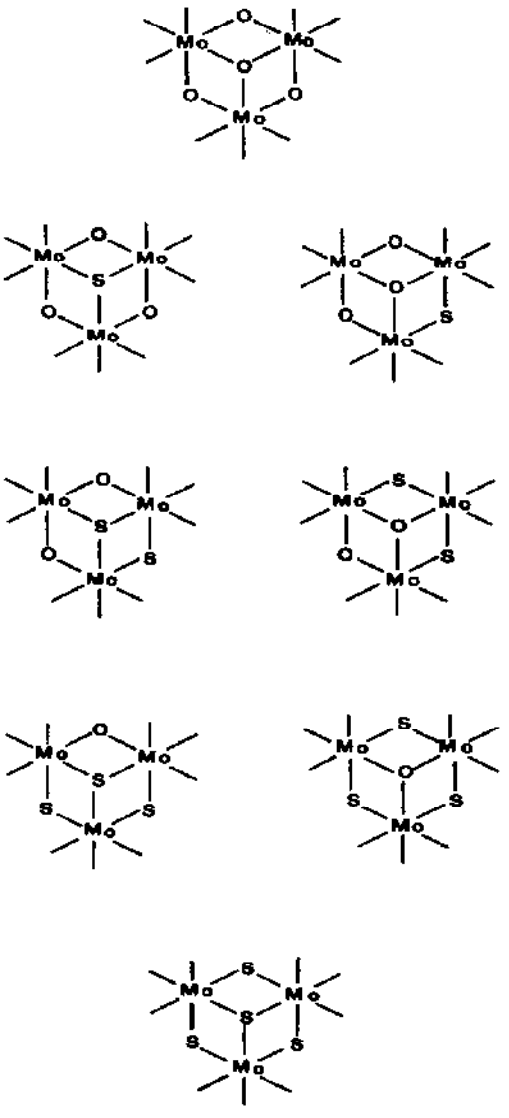

Chart II

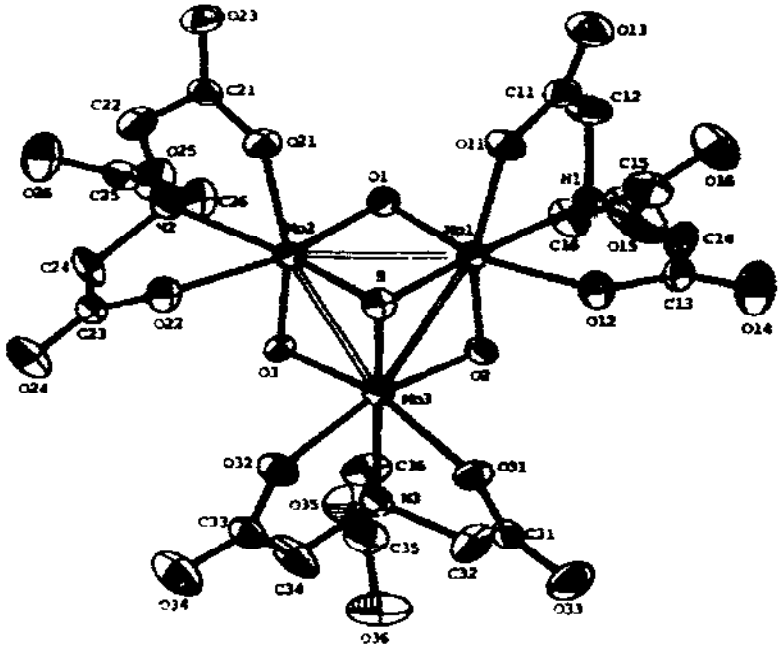

Fig. 59. Molecular structure of $[Mo_3O_3S\{HN(CH_2CO_2)_3\}_3]^{2-}$. Average distances for core: Mo–Mo 2.59 Å, Mo–S 2.36 Å, Mo–O 1.92 Å (from ref. 129).

The μ_3-S aqua ion $[Mo_3O_3S]^{4+}$ undergoes a near reversible cathodic reduction in 2 M *p*-toluenesulfonic acid at $E^{0\prime} = -0.57$ V. Controlled potential coulometric tests indicate this step to involve three electrons per molecule, suggesting that the Mo_3^{IV}/Mo_3^{III} reduction occurs in a single step, without the formation of stable mixed-valent intermediates [128].

While the molecular structure of the ion $[Mo_3O_3S]^{4+}$ is proven by that of $[Mo_3O_3S\{HN(CH_2CO_2)_3\}_3]^{2-}$ [129], reported in Fig. 59, no structural data are available for the three-electron reduced species.

The μ_3-S aqua ion $[Mo_3O_2S_2]^{4+}$ undergoes a two-step cathodic reduction in 2 M *p*-toluenesulfonic acid [130]:

$$Mo_3^{IV} \overset{+2e^-}{\rightleftarrows} Mo_2^{III}Mo^{IV} \overset{+e^-}{\rightleftarrows} Mo_3^{III}$$

$$E^{0\prime} = -0.57 \text{ V} \qquad E^{0\prime} = -0.63 \text{ V}$$

As in the previous case, only the molecular structure of the starting aqua ion is known, through the form $[Mo_3O_2S_2(NCS)_9]^{5-}$ [130] (Fig. 60).

The μ_3-S aqua ion $[Mo_3OS_3]^{4+}$ undergoes a single-stepped quasi-reversible three-electron reduction in 2 M *p*-toluenesulfonic acid at $E^{0\prime} = -0.53$ V [128]. Again no intermediate mixed-valent species appears stable in the overall Mo_3^{IV}/Mo_3^{III} reduction pathway.

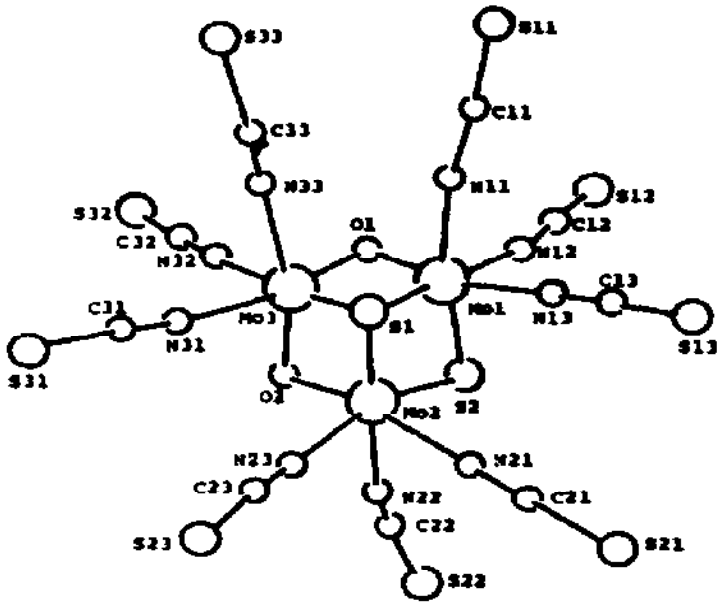

Fig. 60. Perspective view of $[Mo_3O_2S_2(NCS)_9]^{5-}$. Average distances for core: Mo–Mo 2.66 Å (two sets of distances depending upon μ_2-O or μ_2-S), Mo–μ_3-S 2.32 Å, Mo–μ_2-O 1.94 Å, Mo–μ_2-S 2.25 Å (from ref. 130).

The structure of the $[Mo_3OS_3]^{4+}$ ion is given by the X-ray analysis of $[Mo_3OS_3\{HN(CH_2CO_2)_2\}_3]^{2-}$ reported in Fig. 61 [131].

A relatively large series of papers have appeared devoted to species containing the Mo_3S_4 core.

The electrode behaviour of the aqua ion $[Mo_3S_4]^{4+}$ has not yet unequivocally been determined, in that both a single-step (Mo_3^{IV}/Mo_3^{III}, $E^{0\prime} = -0.52$ V) [128] and a two-step ($Mo_3^{IV}/Mo_2^{III}Mo^{IV}/Mo_3^{III}$) [132] three-electron reduction have been reported to occur at mercury electrodes in 2 M *p*-toluenesulfonic acid; it has also been reported that adsorption phenomena occur at mercury electrodes (in 0.1 M KCl), while no reduction process occurs at a glassy carbon electrode [133].

The electrochemical behavior of the coordination compounds of the $[Mo_3S_4]^{4+}$ ion appears more defined. The general structure of the Mo_3S_4 core is shown in Fig. 62. A trimetallic plane capped by a triply bridging sulfur atom forms a pyramid linked below by three doubly bridging sulfur atoms.

Figure 63(b) shows the redox changes occurring in an aqueous solution of $[Mo_3S_4\{HN(CH_2CO_2)_2\}_3]^{2-}$, the crystal structure of which is reported in Fig. 63(a) [133].

Three subsequent steps can easily be observed, the first two being near

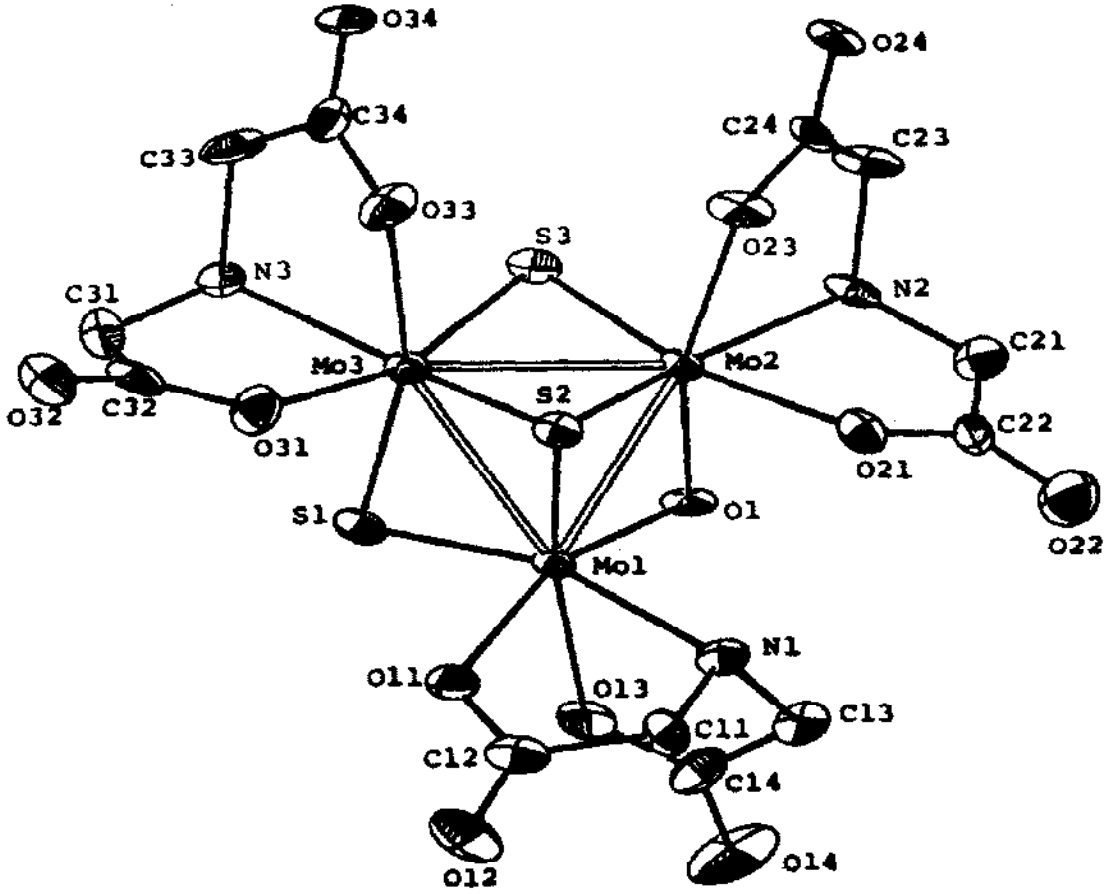

Fig. 61. Perspective view of $[Mo_3OS_3\{HN(CH_2CO_2)_2\}_3]^{2-}$. Average distances for core: μ-O bridged Mo–Mo 2.61 Å, μ-S bridged Mo–Mo 2.72 Å, Mo–μ_3-S 2.35 Å, Mo–μ-O 1.94 Å, Mo–μ-S 2.31 Å (from ref. 131).

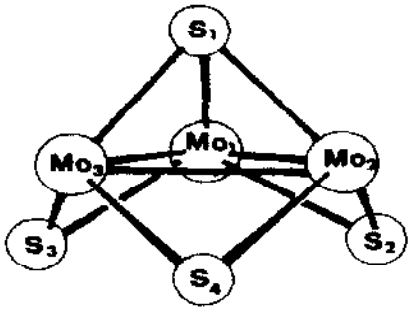

Fig. 62. Representation of the structure of the Mo_3S_4 core.

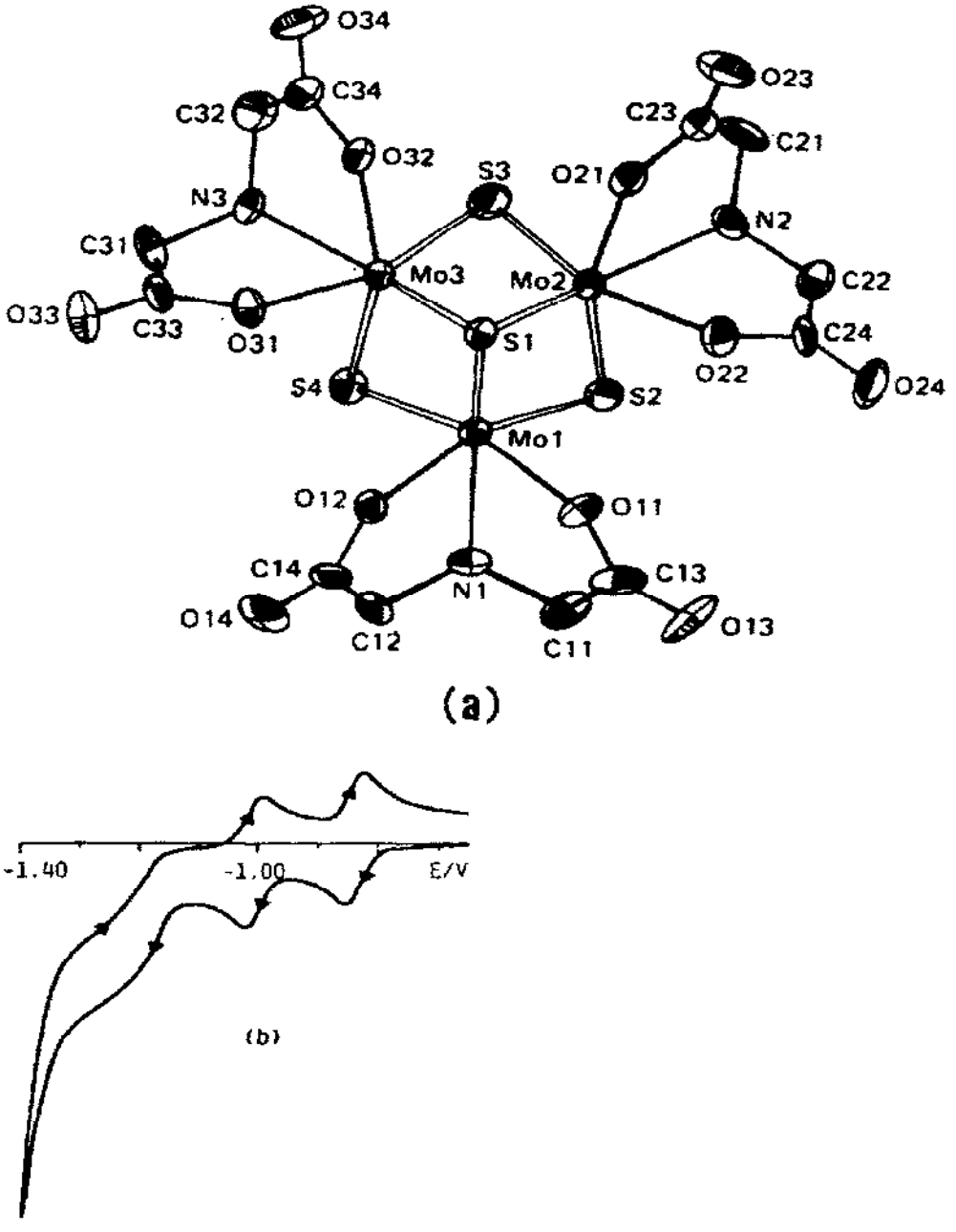

Fig. 63. (a) Crystal structure of $[Mo_3S_4\{HN(CH_2CO_2)_2\}_3]^{2-}$. Average distances for core: Mo–Mo 2.75 Å, Mo–μ_3-S 2.35 Å, Mo–μ_2-S 2.29 Å. (b) Cyclic voltammogram of $[Mo_3S_4\{HN(CH_2CO_2)_2\}_3]^{2-}$ in 0.1 M KCl solution. Glassy carbon working electrode. Potential values vs. S.C.E. (from ref. 133).

reversible. At least in the short times of cyclic voltammetry the following electron transfer series holds:

$$Mo_3^{IV} \underset{-e^-}{\overset{+e^-}{\rightleftarrows}} Mo_2^{IV}Mo^{III} \underset{-e^-}{\overset{+e^-}{\rightleftarrows}} Mo^{IV}Mo_2^{III} \overset{-e^-}{\rightleftarrows} Mo_3^{III}$$

$$E^{0\prime} = -0.83 \text{ V} \qquad E^{0\prime} = -1.17 \text{ V} \quad E^{0\prime} = -1.36 \text{ V}$$

No data are available concerning various reduction products.

The crystal structure of $[Mo_3S_4(CN)_9]^{5-}$ [134,135] is reported in Fig. 64. While it has been established that this compound undergoes a quasi-reversible one-electron anodic oxidation in dimethylsulfoxide solvent, $Mo_3^{IV}/Mo_2^{IV}Mo^{V}$, ($E^{0\prime} = +0.06$ V) [135–137], some discrepancies exist as to its reduction behavior. In fact, it is reported to undergo a single three-electron irreversible step, Mo_3^{IV}/Mo_3^{III}, ($E_p = -2.4$ V) [135], as well as a quasi-reversible (supposed) one-electron step, $Mo_3^{IV}/Mo_2^{IV}Mo^{III}$, ($E^{0\prime} = -1.9$ V) [136,137].

Finally, the cation $[Mo_3S_4(\eta^5\text{-}C_5H_5)_3]^+$, whose structure is reported in Fig. 65 [138], undergoes a one-electron cathodic reduction ($E^{0\prime} = -1.04$ V) in dichloromethane solvent [138]. This agrees with the MO calculation of the

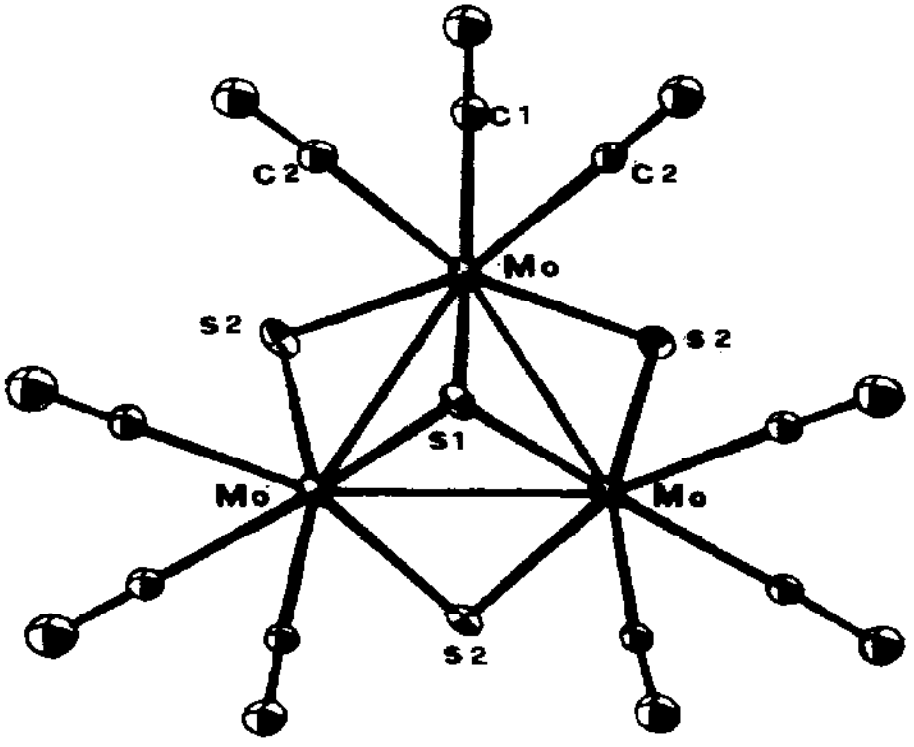

Fig. 64. Perspective view of $[Mo_3S_4(CN)_9]^{5-}$. Average distances for core: Mo–Mo 2.76 Å, Mo–μ_3-S 2.36 Å, Mo–μ_2-S 2.31 Å (from ref. 135).

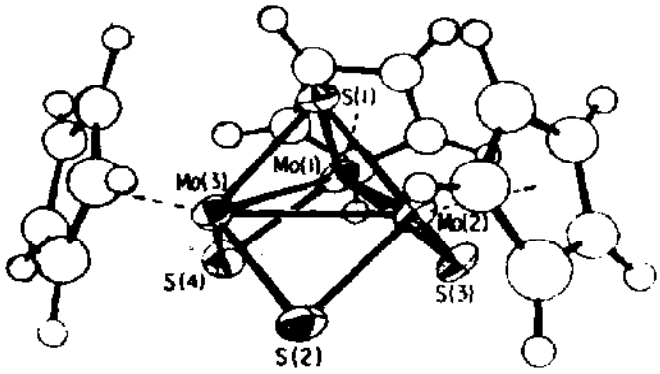

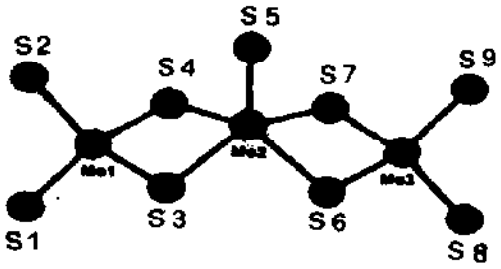

Fig. 65. Perspective view of $[Mo_3S_4(C_5H_5)_3]^+$. Average distances for core: Mo–Mo 2.81 Å, Mo–μ_3-S 2.31 Å, Mo–μ_2-S 2.29 Å (from ref. 138).

Fig. 66. Perspective view of $[Mo_3S_9]^{2-}$. Selected mean distances: Mo–Mo 2.95 Å, $Mo_1-S_{(bridging)}$ 2.23 Å, $Mo_2-S_{(bridging)}$ 2.39 Å, Mo_2-S_5 2.09 Å, $Mo_1-Mo_2-Mo_3$ angle 155° (from ref. 142).

same authors who predict that in the monocation only six electrons occupy the four bonding metal symmetry orbitals ($2a_1 + e$). Hence, the electrogenerable neutral species would possess shorter Mo–Mo distances. Indeed, $Mo_3S_4(\eta^5\text{-}C_5H_5)_3$ has been chemically prepared [139], but the relevant structural parameters are not available.

Structural comparisons among Mo_3S_4 species reported above and other Mo_3S_4 derivatives of unknown electrochemistry can be found [133,140].

(ii) Mo_3S_9 core

The dianion $[Mo_3S_9]^{2-}$ has been recently obtained [141], and its structure is reported in Fig. 66. The molecule, of idealized C_{2v} symmetry, can be viewed as being formed by two tetrathiomolybdate(VI) units bridged through a five-coordinated Mo(IV) in a square-pyramidal arrangement. In dimethylformamide this dianion undergoes a quasi-reversible one-electron reduction ($E^{0\prime} = -1.60$ V), followed by two other irreversible cathodic processes. No attempt to electrogenerate the apparently stable trianion $[Mo_3S_9]^{3-}$ has been made.

(iii) Mo_3S_{13} core

The structure of the dianion $[Mo_3(\mu_3\text{-}S)(\mu_2\text{-}S_2)_3(S_2)_3]^{2-}$ is shown in Fig. 67 [143]. The pyramidal fragment Mo_3S is linked both to three bridging S_2^{2-} ligands and to three terminal S_2^{2-} ligands, lying above and below the trimetallic plane.

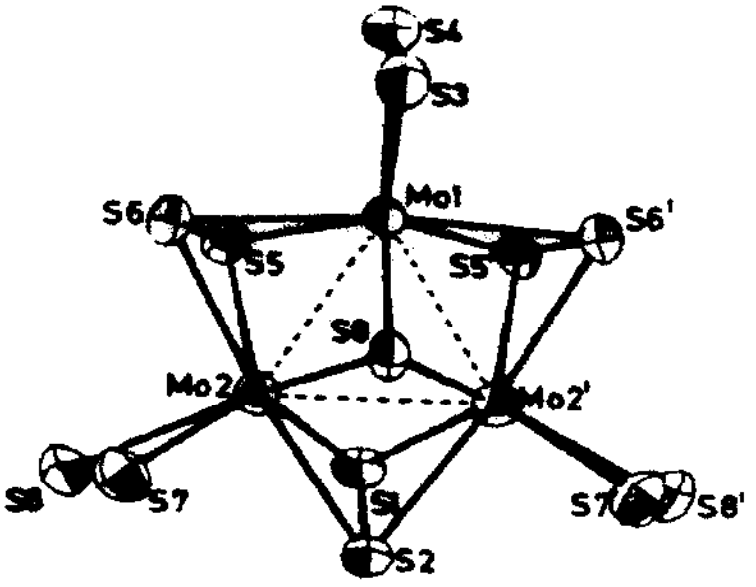

Fig. 67. Perspective view of the dianion $[Mo_3S_{13}]^{2-}$. Mean distances: Mo–Mo 2.72 Å, Mo–μ_3-S 2.35 Å, Mo–$S_{terminal}$ 2.43 Å, Mo–$S_{bridging}$ 2.45 Å (from ref. 143).

In accordance with the MO diagram reported in Fig. 68, $[Mo_3S_{13}]^{2-}$ undergoes (in dimethylformamide solvent?) two irreversible (likely decluster-ing) reduction processes at $E_p = -1.29$ V and -1.54 V, respectively [144]. In fact, the added electrons can only enter antibonding orbitals, destabiliz-ing the single metal–metal bonds.

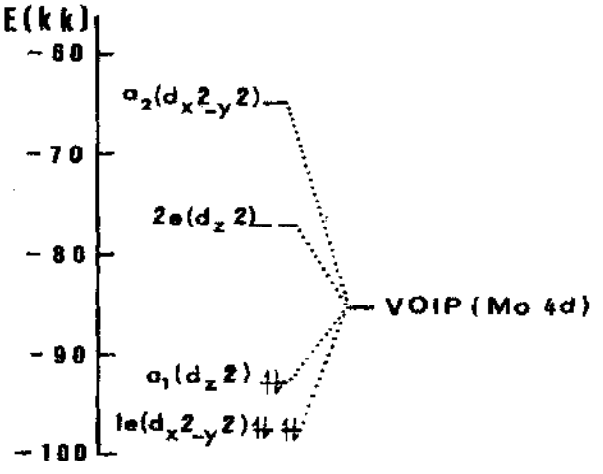

Fig. 68. MO diagram for $[Mo_3S_{13}]^{2-}$ (from ref. 144).

(iv) Mo_4S_4 cores

A variety of cubane-type Mo_4S_4 derivatives have been structurally characterized [145–153], but only in a few cases have the electrochemical properties been tested.

Figure 69 shows a perspective view of the anion $[Mo_4S_4(CN)_{12}]^{8-}$.

The cubane unit Mo_4S_4, in which the interpenetrating tetrahedra Mo_4 and S_4 are almost regular, gives rise to a slight distortion from the idealized cubic geometry towards a tetragonal D_{2d} symmetry [145].

As shown in Fig. 70 [136] this Mo_4^{III} anion is capable of undergoing two distinct anodic quasi-reversible one-electron steps in aqueous solution, according to the sequence [136,137]:

$$[Mo_4S_4(CN)_{12}]^{8-} \underset{+e^-}{\overset{-e^-}{\rightleftarrows}} [Mo_4S_4(CN)_{12}]^{7-} \underset{+e^-}{\overset{-e^-}{\rightleftarrows}} [Mo_4S_4(CN)_{12}]^{6-}$$
$$E^{0\prime} = -0.59\ \text{V} \qquad E^{0\prime} = +0.07\ \text{V}$$

The resulting mixed valent species ($Mo_3^{III}Mo^{IV}$ and $Mo_2^{III}Mo_2^{IV}$, respectively) have not been isolated.

As illustrated in Fig. 71, $[Mo_4(\mu_3\text{-}S)_4(edta)_2]^{3-}$ (edta = tetraanion of ethylenediaminetetraacetic acid) undergoes in 0.1 M perchloric acid both a

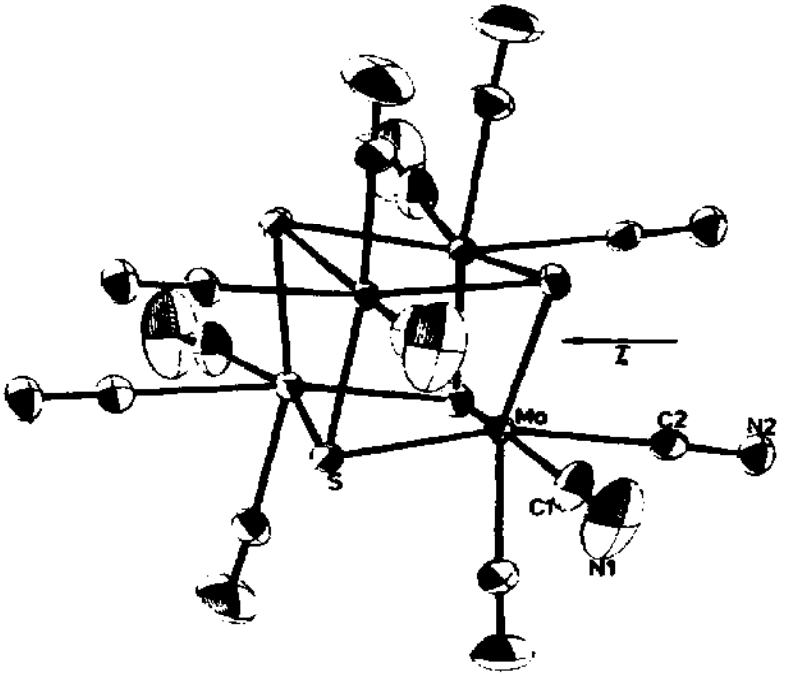

Fig. 69. Molecular structure of the anion $[Mo_4S_4(CN)_{12}]^{8-}$. Average distances for core: Mo–Mo 2.85 Å; Mo–S 2.38 Å (from ref. 145).

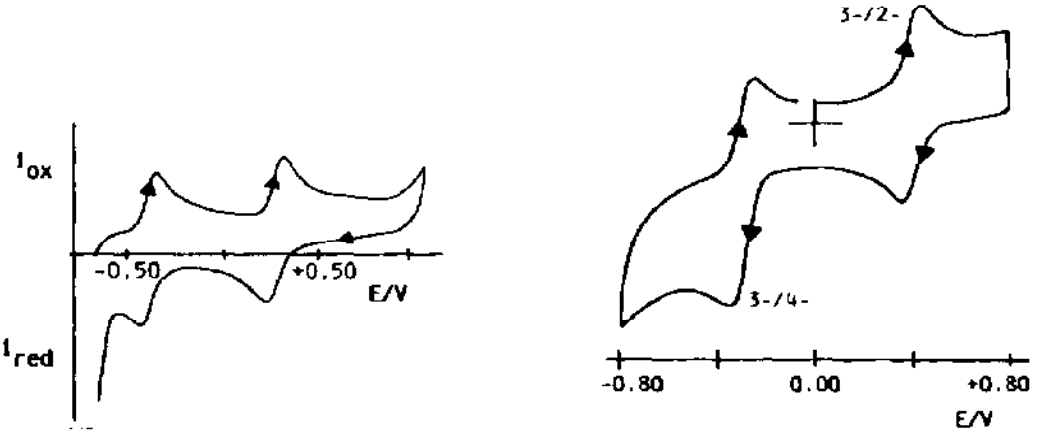

Fig. 70. Cyclic voltammetric behavior of $[Mo_4S_4(CN)_{12}]^{8-}$ in aqueous solution (KCl 0.1 M). Potential values vs. NHE.

Fig. 71. Cyclic voltammetric response of $[Mo_4S_4(edta)_2]^{3-}$ in 0.1 M $HClO_4$. Potential values vs. SCE.

non-complicated, near reversible, one-electron anodic oxidation and a non-complicated near reversible, cathodic reduction [149], according to the sequence:

$$[Mo_4S_4(edta)_2]^{2-} \underset{-e^-}{\overset{+e^-}{\rightleftarrows}} [Mo_4S_4(edta)_2]^{3-} \underset{-e^-}{\overset{+e^-}{\rightleftarrows}} [Mo_4S_4(edta)_2]^{4-}$$
$$E^{0\prime} = +0.24\ \text{V} \qquad E^{0\prime} = -0.46\ \text{V}$$

The crystal structure of $[Mo_4S_4(edta)_2]^{3-}$ is shown in Fig. 72.

In the cubane-type $[Mo_4S_4]^{5+}$ core, the four molybdenum atoms form an approximately regular tetrahedron with each face triply bridged by one sulfur atom.

Both the congeners $[Mo_4S_4(edta)_2]^{2-}$ and $[Mo_4S_4(edta)_2]^{4-}$ have been prepared chemically or electrochemically [149]. These two species, which contain an $[Mo_4S_4]^{6+}$ and an $[Mo_4S_4]^{4+}$ core, respectively, are isostructural with the trianion; some significant structural parameters for these derivatives are reported in Table 19 [150].

The fact that both the addition of one electron to the trianion, as well as the removal of one electron, does not result in significant changes in the Mo–S bond lengths, while at the same time it affects the Mo–Mo distances, clearly indicates that the HOMO and LUMO of $[Mo_4S_4(edta)_2]^{3-}$ are essentially tetrametal based. The lengthening ($-e^-$) and the shortening ($+e^-$) of the Mo–Mo distances as a consequence of the redox changes on $[Mo_4S_4(edta)_2]^{3-}$ have been explained [150] on the basis that, according to Dahl's model [28], the 11 ($4d$) electrons of the trianion ($Mo_3^{III}Mo^{IV}$) are

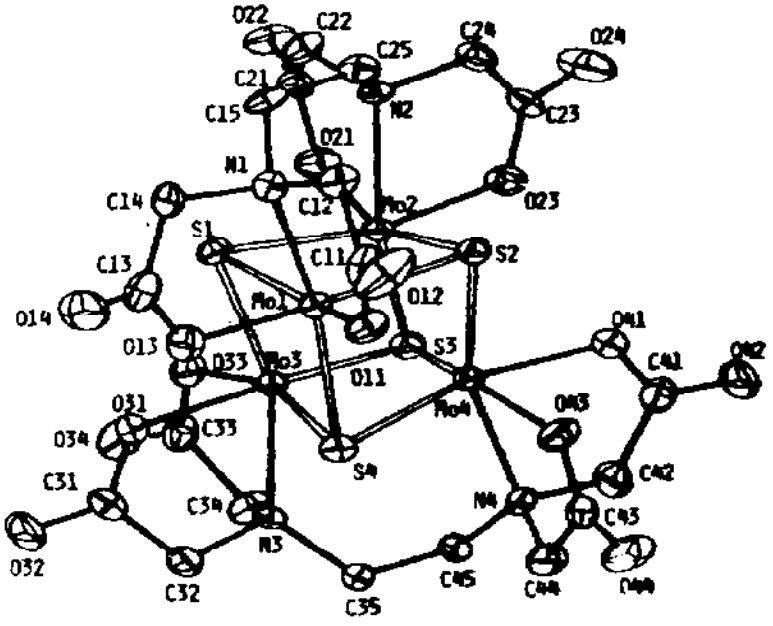

Fig. 72. Molecular structure of $[Mo_4S_4(edta)_2]^{3-}$ (from ref. 149).

distributed in the six bonding tetrametal symmetry orbitals ($a_1 + e + t_2$) normally available for the six Mo–Mo bonds.

A few electrochemically active cyclopentadienyl–Mo_4S_4 derivatives have been characterized, namely $Mo_4S_4(C_5H_4\text{-}i\text{-}Pr)_4$ [151], $Mo_4S_4(C_5H_4Me)_4$ [152] and $Mo_4S_4(C_5H_5)_2(C_5Me_5)_2$ [154]. In non-aqueous solvents these clusters undergo two subsequent reversible one-electron anodic processes according to the sequence:

$$Mo_4S_4(Cp')_4 \underset{+e^-}{\overset{-e^-}{\rightleftarrows}} [Mo_4S_4(Cp')_4]^+ \underset{+e^-}{\overset{-e^-}{\rightleftarrows}} [Mo_4S_4(Cp')_4]^{2+}$$

(Cp′ = cyclopentadienyl-type ligand)

The standard potentials for these redox changes are summarized in Table 20.

TABLE 19

Selected structural parameters for the cores of the congeners $[Mo_4S_4(edta)_2]^{2-,3-,4-}$

Complex	Molybdenum oxidation state	Volume (Å^3)		Mean distance (Å)	
		Mo_4	Mo_4S_4	Mo–Mo	Mo–S
$[Mo_4S_4(edta)_2]^{2-}$	$Mo_2^{III}Mo_2^{IV}$	2.65	10.97	2.83	2.35
$[Mo_4S_4(edta)_2]^{3-}$	$Mo_3^{III}Mo^{IV}$	2.60	10.87	2.81	2.35
$[Mo_4S_4(edta)_2]^{4-}$	Mo_4^{III}	2.54	10.78	2.78	2.35

TABLE 20

Standard electrode potentials (in volts) for the redox changes of some cyclopentadienyl–Mo_4S_4 clusters

Derivatives	Redox changes		Solvent	Ref.
	0/1+	1+/2+		
$Mo_4S_4(C_5H_4\text{-i-Pr})_4$	−0.76	−0.11	DMF	151
$Mo_4S_4(C_5H_4Me)_4$	−0.89	−0.19	MeCN	152
$Mo_4S_4(C_5H_5)_2(C_5Me_5)_2$	−1.01 [a]	−0.27	MeCN	154

[a] In ref. 154 this step has probably erroneously been assigned to the redox change 0/1− [152].

The crystal structure of the neutral derivative $Mo_4S_4(C_5H_4\text{-i-Pr})_4$ is shown in Fig. 73.

The products resulting from the removal of one or two electrons, $[Mo_4S_4(C_5H_4\text{-i-Pr})_4]^{n+}$ ($n = 1, 2$), have been chemically produced; they are

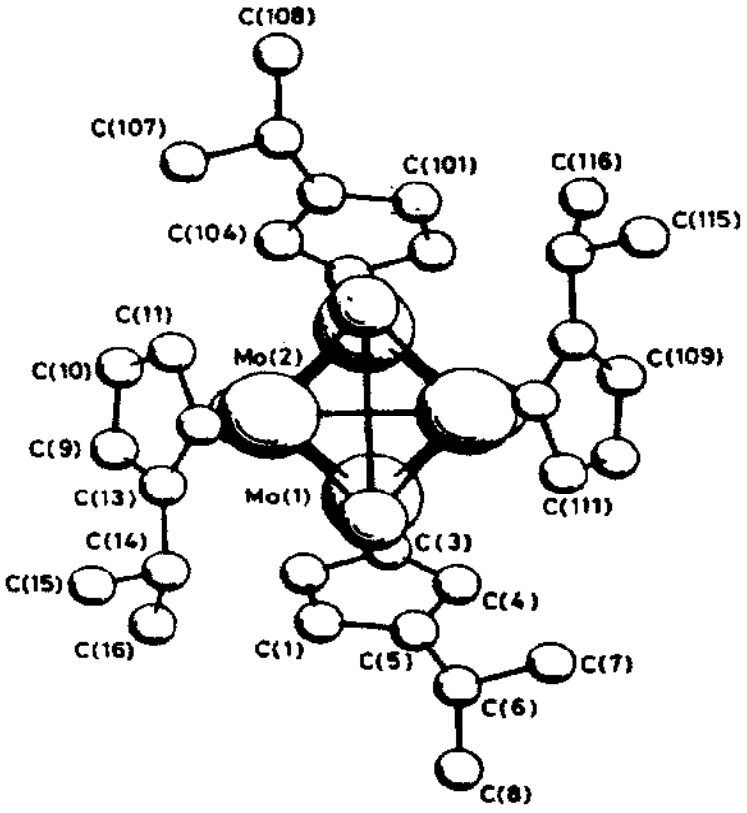

Fig. 73. Molecular structure of $Mo_4S_4(C_5H_4\text{-i-Pr})_4$ (from ref. 151).

TABLE 21

Selected structural parameters for the cores of the congeners $[Mo_4S_4(C_5H_4\text{-i-Pr})_4]^{0,1+,2+}$

Complex	Mo_4 volume (Å^3)	Mean distance (Å)	
		Mo–Mo	Mo–S
$Mo_4S_4(C_5H_5\text{-i-Pr})_4$	2.89	2.90	2.34
$[Mo_4S_4(C_5H_5\text{-i-Pr})_4]^+$	2.86	2.89	2.34
$[Mo_4S_4(C_5H_5\text{-i-Pr})_4]^{2+}$	2.75	2.86	2.34

isostructural with the parent neutral compound. Table 21 reports some selected structural parameters for the three congeners [151].

As in the case of the family $[Mo_4S_4(edta)_2]^{n-}$, the redox changes only slightly affect the metal–metal bonding distances (even if now the structural effect seems reversed, in that the removal of an electron causes shortening of the Mo–Mo bonds). Also in this case, the Dahl bonding description has been invoked, assigning to the 12-($4d$) electron $Mo_4S_4(C_5H_4\text{-i-Pr})_4$ a ground state configuration ($a^2e^4t^6$). The removal of the electrons seems centred on t_2 orbitals [151]. The validity of the Dahl model for the description of bonding in these clusters has been noted [152].

The stereochemical changes accompanying the electron-transfer sequences in the two fully characterized families cited here do not seem to support the Cotton et al. hypothesis [147] that the $12e^- \rightarrow 10e^-$ step would involve pronounced Jahn–Teller distortions in these clusters.

As a final consideration we note that, in agreement with the redox behavior of the Mo_4S_4 derivatives above, the $[Mo_4S_4]^{5+}$ aqua ion is electroactive and in 2 M *p*-toluenesulfonic acid undergoes both the one-electron oxidation $[Mo_4S_4]^{5+}/[Mo_4S_4]^{6+}$ and the one-electron reduction $[Mo_4S_4]^{5+}/[Mo_4S_4]^{4+}$ [132,150]. Some discrepancies hold as far as the redox potentials of the two steps and the stability of the $[Mo_4S_4]^{6+}$ ion are concerned.

F. TUNGSTEN–SULFUR DERIVATIVES

(i) W_3S_4 core

Contrast to the $[Mo_3S_4]^{4+}$ ion, the $[W_3S_4]^{4+}$ ion does not undergo electrode redox processes in 2 M *p*-toluenesulphonic acid in the potential range from +0.55 to −0.85 V [155]. Further electrochemical investigations in solvents of wider useful potentials are required in order to evaluate from a thermodynamic viewpoint the chemical evidence of a redox chemistry for this ion, whose incomplete cubane-type structure, derived from $(bpyH)_5[W_3S_4(NCS)_9]$ (bpy = 2,2′-bipyridine), is shown in Fig. 74. The bond distances decidedly parallel those of $[Mo_3S_4]^{4+}$.

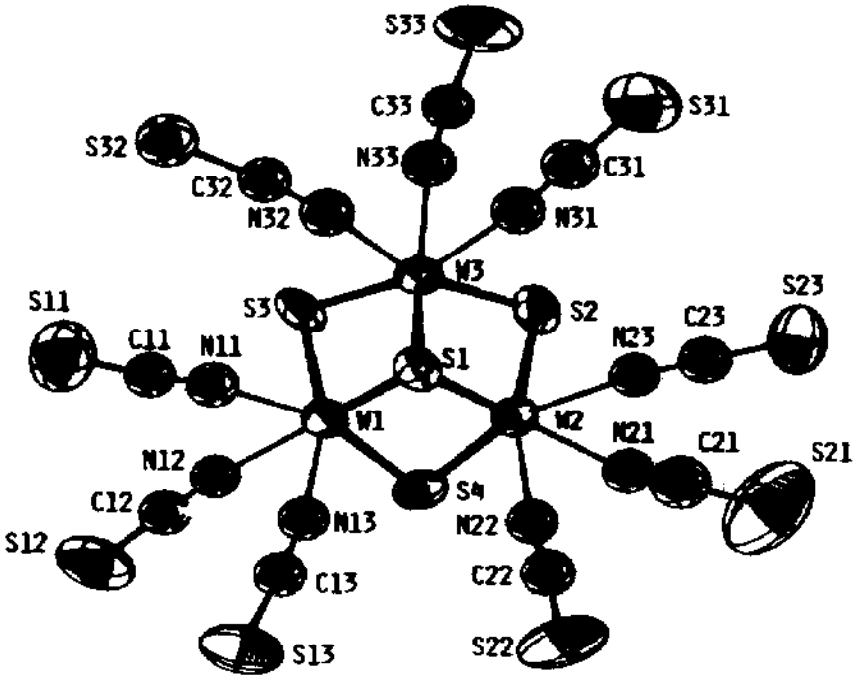

Fig. 74. Molecular structure of $[W_3S_4(NCS)_9]^{5-}$. Average distances for core: W–W 2.76 Å, W–μ_3–S 2.36 Å, W–μ_2–S 2.31 Å (from ref. 155).

(ii) W_3S_8 core

The preparation of the dianion $[W_3S_8]^{2-}$ has recently been reported [156]; its crystal structure is shown in Fig. 75. The central W atom is essentially planar, whereas the terminal W atoms possess tetrahedral coordination. In

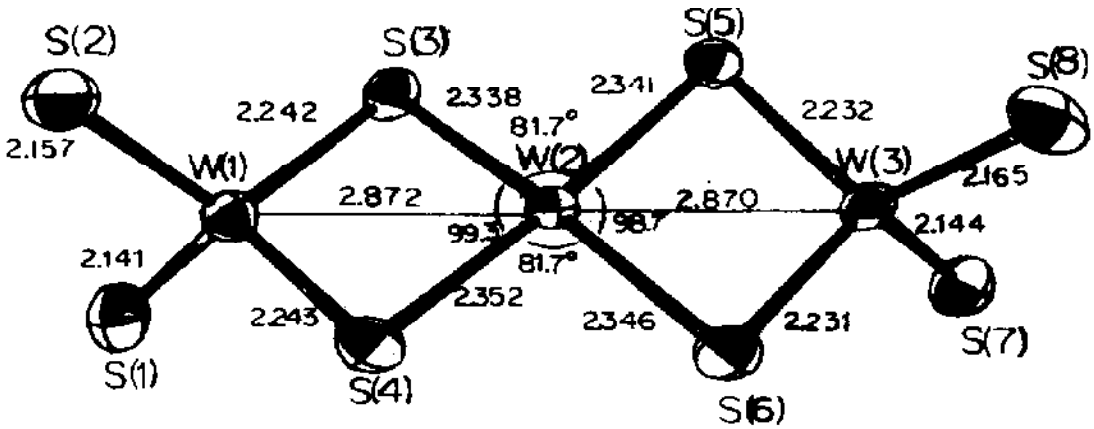

Fig. 75. X-ray structure of the dianion $[W_3S_8]^{2-}$ (from ref. 156).

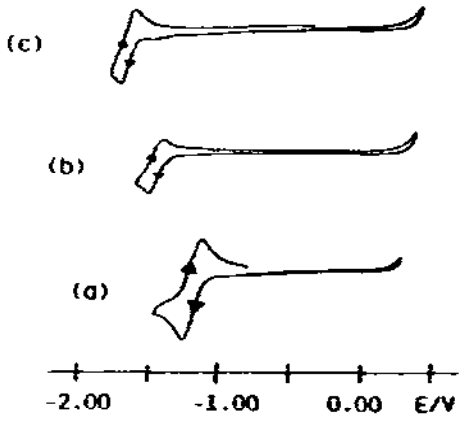

Fig. 76. Cyclic voltammograms recorded in dimethylformamide solutions of: (a) $[Mo_3S_9]^{2-}$; (b) $[W_3S_9]^{2-}$; (c) $[W_3OS_8]^{2-}$.

acetonitrile solution this species is completely unable to undergo chemically reversible redox processes [156].

(iii) $W_3O_nS_{9-n}$ *cores*

The electrochemical behavior of the dianions $[W_3S_9]^{2-}$ and $[W_3OS_8]^{2-}$ has been studied, also in comparison with that of the homologue $[Mo_3S_9]^{2-}$

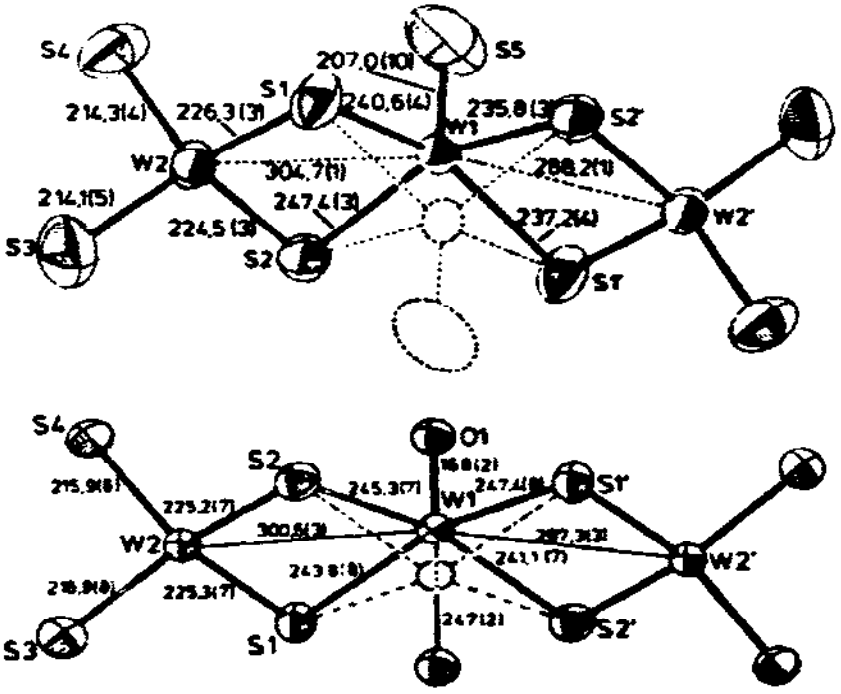

Fig. 77. Molecular structure of: (a) $[W_3S_9]^{2-}$; (b) $[W_3OS_8]^{2-}$ (distances in pm) (from ref. 161).

[141]. Like $[Mo_3S_9]^{2-}$, these tritungsten complexes undergo, in dimethylformamide solution, a quasi-reversible one-electron reduction step ($E^{0\prime}_{[W_3S_9]^{2-}} = -1.87$ V; $E^{0\prime}_{[W_3OS_8]^{2-}} = -2.13$ V), followed by further irreversible processes. As shown in Fig. 76, $[Mo_3S_9]^{2-}$ is more easily reducible than $[W_3S_9]^{2-}$, which in its turn is more easily reducible than $[W_3OS_8]^{2-}$ [141].

Figure 77 shows the molecular structure of the dianions $[W_3S_9]^{2-}$ and $[W_3OS_8]^{2-}$ [157–161] both isostructural with $[Mo_3S_9]^{2-}$, previously discussed, and $[Mo_3OS_8]^{2-}$ [162] of which we do not know the electrochemical behaviour.

Nothing is known about the stability of the species $[W_3S_9]^{3-}$ and $[W_3OS_8]^{3-}$, respectively.

G. CONCLUDING REMAKRS

In the examination of the structural effects following the redox changes in metal–sulfur clusters, we have pointed out the occurrence of stereochemical reorganization ranging from totally declustering processes to quite-slight core expansions/contractions, through intermediate effects causing more or less pronounced distortions in the starting core geometry.

Since the study of structural–redox relationships can greatly help a theoretical approach to the bonding description in such polynuclear compounds, we expect more attention to be paid to this aspect of the chemistry of metal–sulfur clusters in the future.

However, we note that at the present stage, most of the electrochemical investigations are limited to the simple, even if useful, thermodynamic characterization of the redox processes (i.e. the determination of redox potentials); the full potential of electrochemistry (which encompasses, for instance, the study of the heterogeneous charge transfer as well as of kinetic complications often following a redox change, an experimental measure of the HOMO–LUMO energies of the metal–sulfur derivatives, and the guided synthesis of congeners not readily chemically obtainable) is largely unexplored.

REFERENCES

1 J.M. Berg and R.H. Holm, in T.G. Spiro (Ed.), Iron-Sulfur Proteins, Vol. IV, Wiley, New York, 1982.
2 B.A. Averill, Struct. Bonding (Berlin), 53 (1983) 59.
3 A. Müller, Polyhedron, 5 (1986) 323, and references therein.
4 S. Kuwabata, K. Tanaka, and T. Tanaka, Inorg. Chem., 25 (1986) 1691, and references therein.
5 T. Hughbanks and R. Hoffmann, J. Am. Chem. Soc., 105 (1983) 1150.
6 R.G. Wooley, Inorg. Chem., 24 (1985) 3519.

7 R. Chevrel, M. Hirrien, and M. Sergent, Polyhedron, 5 (1986) 87.
8 J.A. Ibers and R.H. Holm, Science, 209 (1980) 223.
9 G. Gritzner and J. Kuta, Pure Appl. Chem., 56 (1984) 461.
10 A.J. Bard and L.R. Faulkner, in Electrochemical Methods: Fundamental and Applications, Wiley, New York, 1980, p. 52.
11 L. Markó, J. Takaks, S. Papp, and B. Markó-Monostory, Inorg. Chim. Acta, 45 (1980) L189.
12 U. Honrath and H. Vahrenkamp, Z. Naturforsch., Teil B, 39 (1984) 545.
13 T. Madach and H. Vahrenkamp, Chem. Ber., 114 (1981) 505.
14 L. Markó, T. Madach, and H. Vahrenkamp, J. Organomet. Chem., 190 (1980) C67.
15 L. Markó, B. Markó-Monostory, T. Madach, and H. Vahrenkamp, Angew. Chem. Int. Ed. Engl., 19 (1980) 226.
16 A.R. Rives, Y. Xiao-Zeng, and R.F. Fenske, Inorg. Chem., 21 (1982) 2286.
17 K.S. Hagen, G. Christou, and R.H. Holm, Inorg. Chem., 22 (1983) 309.
18 A.L. Balch, J. Am. Chem. Soc., 91 (1969) 6962.
19 A. Darchen, C. Mahé, and H. Patin, J. Chem. Soc., Chem. Commun., (1982) 243.
20 C.H. Wey and L.F. Dahl, Inorg. Chem., 4 (1965) 493.
21 R.J. Haines, J.A. De Beer, and R. Greatrex, J. Organomet. Chem., 55 (1973) C30.
22 R.J. Haines, J.A. De Beer, and R. Greatrex, J. Organomet. Chem., 85 (1975) 89.
23 K.S. Hagen and R.H. Holm, J. Am. Chem. Soc., 104 (1982) 5496.
24 K.S. Hagen, A.D. Watson, and R.H. Holm, J. Am. Chem. Soc., 105 (1983) 3905.
25 G.N. Schrauzer, V.P. Mayweg, H.W. Finck, and W. Henrich, J. Am. Chem. Soc., 88 (1966) 4604.
26 I. Bernal, B.R. Davis, M.L. Good and S. Chandra, J. Coord. Chem., 2 (1972) 61.
27 T.H. Lemmen, J.A. Kocal, F.Y.-K. Lo, M.W. Chen, and L.F. Dahl, J. Am. Chem. Soc., 103 (1981) 1932.
28 T. Toan, B.K. Teo, J.A. Ferguson, T.J. Meyer, and L.F. Dahl, J. Am. Chem. Soc., 99 (1977) 408.
29 J.A. Ferguson and T.J. Meyer, Chem. Commun., (1971) 623.
30 R.A. Schunn, C.J. Fritchie, Jr., and C.T. Prewitt, Inorg. Chem., 5 (1966) 892.
31 C.H. Wey, G.R. Wilkes, P.M. Treichel, and L.F. Dahl, Inorg. Chem., 5 (1966) 900.
32 T. Toan, W.P. Fehlhammer, and L.F. Dahl, J. Am. Chem. Soc., 99 (1977) 402.
33 B. Tulyathan and W.E. Geiger, J. Am. Chem. Soc., 107 (1985) 5960, and references therein.
34 C.T.-W. Chu, F.Y.-K. Lo, and L.F. Dahl, J. Am. Chem. Soc., 104 (1982) 3409.
35 R.S. Gall, C.T.-W. Chu, and L.F. Dahl, J. Am. Chem. Soc., 96 (1974) 4019.
36 C.T.-W. Chu, R.S. Gall, and L.F. Dahl, J. Am. Chem. Soc., 104 (1982) 737.
37 L.L. Nelson, F.Y.-K. Lo, A.D. Rae, and L.F. Dahl, J. Organomet. Chem., 225 (1982) 309.
38 K.S. Bose, E. Sinn, and B.A. Averill, Organometallics, 3 (1984) 1126.
39 J. Cambray, R.W. Lane, A.G. Wedd, R.W. Johnson, and R.H. Holm, Inorg. Chem., 16 (1977) 2565.
40 P.K. Mascharak, K.S. Hagen, J.T. Spence, and R.H. Holm, Inorg. Chim. Acta, 80 (1983) 157.
41 B.V. DePamphilis, B.A. Averill, T. Herskovitz, L. Que, Jr., and R.H. Holm, J. Am. Chem. Soc., 96 (1974) 4159.
42 J.J. Mayerle, S.E. Denmark, B.V. DePamphilis, T.A. Ibers, and R.H. Holm, J. Am. Chem. Soc., 97 (1975) 1032.
43 C.L. Hill, J. Renaud, R.H. Holm, and L.E. Mortenson, J. Am. Chem. Soc., 99 (1977) 2549.

44 L. Que, Jr., J.R. Anglin, M.A. Bobrik, A. Davison, and R.H. Holm, J. Am. Chem. Soc., 96 (1974) 6042.
45 A. Schwartz and E.E. van Tamelen, J. Am. Chem. Soc., 99 (1977) 3189.
46 R. Maskiewicz and T.C. Bruice, J. Chem. Soc., Chem. Commun., (1978) 703.
47 R.W. Johnson and R.H. Holm, J. Am. Chem. Soc., 100 (1978) 5338.
48 W.E. Cleland, D.A. Holtman, M. Sabat, J.A. Ibers, G.C. De Fotis, and B.A. Averill, J. Am. Chem. Soc., 105 (1983) 6021.
49 M.G. Kanatzidis, N.C. Baenziger, D. Coucouvanis, A. Simopoulos, and A. Kostikas, J. Am. Chem. Soc., 106 (1984) 4500.
50 R.J. Burt, G.J. Leigh, and C.J. Pickett, J. Chem. Soc., Chem. Commun., (1976) 940.
51 J.G. Reynolds, E.J. Laskowski, and R.H. Holm, J. Am. Chem. Soc., 100 (1978) 5315.
52 G.B. Wong, D.M. Kurtz Jr., R.H. Holm, L.E. Mortenson, and R.G. Upchurch, J. Am. Chem. Soc., 101 (1979) 3078.
53 R.H. Henderson and A.G. Sykes, Inorg. Chem., 19 (1980) 3103.
54 R.E. Johnson, G.C. Papaefthymiou, R.B. Frankel, and R.H. Holm, J. Am. Chem. Soc., 105 (1983) 7280.
55 D.W. Stephan, G.C. Papaefthymiou, R.B. Frankel, and R.H. Holm, Inorg. Chem., 22 (1983) 1550.
56 B. Odell and P.J. Geary, J. Chem. Soc., Dalton Trans., (1984) 29.
57 T.J. Ollerenshaw, C.D. Garner, B. Odell, and W. Clegg, J. Chem. Soc., Dalton Trans., (1985) 2161.
58 N. Ueyama, T. Terakawa, T. Sugawara, M. Fugi, and A. Nakamura, Chem. Lett., (1984) 1287.
59 T. O'Sullivan and M.M. Millar, J. Am. Chem. Soc., 107 (1985) 4096.
60 K. Tanaka, T. Tanaka and I. Kawafune, Inorg. Chem., 23 (1984) 516.
61 K. Tanaka, M. Moriya, and T. Tanaka, Inorg. Chem., 25 (1986) 835.
62 R.J. Kassner and W. Yang, J. Am. Chem. Soc., 99 (1977) 4351, and references therein.
63 J.M. Berg, K.O. Hodgson, and R.H. Holm, J. Am. Chem. Soc., 101 (1979) 4586.
64 K.S. Hagen, A.D. Watson, and R.H. Holm, Inorg. Chem., 23 (1984) 2984.
65 C.Y. Yang, K.H. Johnson, R.H. Holm, and J.G. Norman, Jr., J. Am. Chem. Soc., 97 (1975) 6596.
66 A.J. Thomson, J. Chem. Soc., Dalton Trans., (1981) 1180.
67 A. Aizman and D.A. Case, J. Am. Chem. Soc., 104 (1982) 3269.
68 L. Noodleman, J.G. Norman, Jr., J.H. Osborne, A. Aizman, and D.A. Case, J. Am. Chem. Soc., 107 (1985) 3418.
69 D. Coucouvanis, M. Kanatzidis, E. Simhon, and N.C. Baenziger, J. Am. Chem. Soc., 104 (1982) 1874.
70 M.G. Kanatzidis, M. Ryan, D. Coucouvanis, A. Simopoulos, and A. Kostikas, Inorg. Chem., 22 (1983) 179.
71 M.G. Kanatzidis, D. Coucouvanis, A. Simopoulos, A. Kostikas, and V. Papaefthyniou, J. Am. Chem. Soc., 107 (1985) 4925.
72 G.B. Wong, M.A. Bobrik, and R.H. Holm, Inorg. Chem., 17 (1978) 578.
73 M.A. Bobrik, K.O. Hodgson, and R.H. Holm, Inorg. Chem., 16 (1977) 1851.
74 W.E. Cleland and B.A. Averill, Inorg. Chim. Acta, 56 (1981) L9.
75 M.A. Bobrik, E.J. Laskowski, R.W. Johnson, W.O. Gillum, J.M. Berg, K.O. Hodgson, and R. Holm, Inorg. Chem., 17 (1978) 1402.
76 M.W.W. Adams, S.G. Reeves, D.O. Hall, G. Christou, B. Ridge, and H.N. Rydon, Biochem. Biophys. Res. Commun., 79 (1977) 1184.
77 G.J. Kubas and P.J. Vergamini, Inorg. Chem., 20 (1981) 2667.

78 N. Dupré, H.M.J. Hendriks, J. Jordanov, J. Gallard, and P. Auric, Organometallics, 3 (1984) 800.
79 N. Dupré, P. Auric, H.M.J. Hendriks, and J. Jordanov, Inorg. Chem., 25 (1986) 1391.
80 P.J. Vergamini and G.J. Kubas, Prog. Inorg. Chem., 21 (1976) 261.
81 I.G. Dance, Polyhedron, 5 (1986) 1037.
82 K.S. Hagen, J.M. Berg, and R.H. Holm, Inorg. Chim. Acta, 45 (1980) L17.
83 K.S. Hagen, D.W. Stephan, and R.H. Holm, Inorg. Chem., 21 (1982) 3928.
84 K.S. Hagen and R.H. Holm, Inorg. Chem., 23 (1984) 418.
85 T. Costa, J.R. Dorfman, K.S. Hagen, and R.H. Holm, Inorg. Chem., 22 (1983) 4091.
86 W. Saak, G. Henkel, and S. Pohl, Angew. Chem. Int. Ed. Engl., 23 (1984) 150.
87 M.G. Kanatzidis, W.R. Dunham, W.R. Hagen and D. Coucouvanis, J. Chem. Soc., Chem. Commun., (1984) 356.
88 M.G. Kanatzidis, W.R. Hagen, W.R. Dunham, R.K. Lester, and D. Coucouvanis, J. Am. Chem. Soc., 107 (1985) 953.
89 M.G. Kanatzidis, A. Salifoglou, and D. Coucouvanis, Inorg. Chem., 25 (1986) 2460.
90 D. Coucouvanis, M.G. Kanatzidis, W.R. Dunham, and W.R. Hagen, J. Am. Chem. Soc., 106 (1984) 7998.
91 W.E. Cleland, Jr., and B.A. Averill, Inorg. Chim. Acta, 106 (1985) L17.
92 M.G. Kanatzidis, A. Salifoglou, and D. Coucouvanis, J. Am. Chem. Soc., 107 (1985) 3358.
93 G.L. Lilley, E. Sinn, and B.A. Averill, Inorg. Chem., 25 (1986) 1073.
94 F. Cecconi, C.A. Ghilardi, and S. Midollini, J. Chem. Soc., Chem. Commun., (1981) 640.
95 A. Agresti, M. Bacci, F. Cecconi, C.A. Ghilardi, and S. Midollini, Inorg. Chem., 24 (1985) 689.
96 F. Cecconi, C.A. Ghilardi, S. Midollini, A. Orlandini, and P. Zanello, J. Chem. Soc., Dalton Trans., (1987) 831.
97 F. Bottomley and F. Grein, Inorg. Chem., 21 (1982) 4170.
98 A. Celeumans and P.W. Fowler, Inorg. Chim. Acta, 105 (1985) 75.
99 R.G. Woolley, Inorg. Chem., 24 (1985) 3519.
100 G. Christou, R.H. Holm, M. Sabat, and J.A. Ibers, J. Am. Chem. Soc., 103 (1981) 6269.
101 G. Christou, M. Sabat, J.A. Ibers, and R.H. Holm, Inorg. Chem., 21 (1982) 3518.
102 H. Strasdeit,, B. Krebs, and G. Henkel, Inorg. Chem., 23 (1984) 1816, and references therein.
103 C.H. Wey and L.F. Dahl, Inorg. Chem., 6 (1967) 1229.
104 U. Honrath and H. Vahrenkamp, Z. Naturforsch., Teil B, 39 (1984) 555.
105 D.S. Stevenson, C.H. Wey, and L.F. Dahl, J. Am. Chem. Soc., 93 (1971) 6027.
106 C.E. Strouse and L.F. Dahl, J. Am. Chem. Soc., 93 (1971) 6032.
107 H. Patin, G. Mignani, C. Mahé, J.Y. Le Marouille, A. Benoit, D. Grandieau, and G. Levesque, J. Organomet. Chem., 208 (1981) C39.
108 C. Mahé, H. Patin, A. Benoit, and Y.J. Le Marouille, J. Organomet. Chem., 216 (1981) C15.
109 A. Benoit, A. Darchen, J.Y. Le Marouille, C. Mahé, and H. Patin, Organometallics, 2 (1983) 555.
110 D.E. Stevenson, V.R. Magnuson, and L.F. Dahl, J. Am. Chem. Soc., 89 (1967) 3727.
111 H. Werner, K. Leonhard, O. Kolb, E. Rottinger, and H. Vahrenkamp, Chem. Ber., 113 (1980) 1654.
112 P.D. Frisch and L.F. Dahl, J. Am. Chem. Soc., 94 (1972) 5082.
113 G.L. Simon and L.F. Dahl, J. Am. Chem. Soc., 95 (1973) 2164.
114 F. Cecconi, C.A. Ghilardi, S. Midollini, A. Orlandini, and P. Zanello, Polyhedron, 5 (1986) 2021.

115 F. Cecconi, C.A. Ghilardi, S. Midollini, and A. Orlandini, Inorg. Chim. Acta, 76 (1983) L183.
116 F. Cecconi, C.A. Ghilardi, and S. Midollini, Inorg. Chim. Acta, 64 (1981) L47.
117 G. Christou, K.S. Hagen, and R.H. Holm, J. Am. Chem. Soc., 104 (1982) 1744.
118 G. Christou, K.S. Hagen, J.K. Bashkin, and R.H. Holm, Inorg. Chem., 24 (1985) 1010.
119 H. Vahrenkamp, V.A. Uchtman, and L.F. Dahl, J. Am. Chem. Soc., 90 (1968) 3272.
120 C.A. Ghilardi, S. Midollini, and L. Sacconi, Inorg. Chim. Acta, 31 (1978) L431.
121 F. Cecconi, C.A. Ghilardi, and S. Midollini, Inorg. Chem., 22 (1983) 3802.
122 F. Cecconi, C.A. Ghilardi, S. Midollini, A. Orlandini, and P. Zanello, work in progress.
123 C.A. Ghilardi, S. Midollini, and L. Sacconi, J. Chem. Soc., Chem. Commun., (1981) 47.
124 M. Rakowski DuBois, M.L. VanDerveer, D.L. DuBois, R.C. Haltiwanger, and W.K. Miller, J. Am. Chem. Soc., 102 (1980) 7456.
125 P. Kathirgamanathan, M. Martinez, and A.G. Sykes, J. Chem. Soc., Chem. Commun., (1985) 1437, and references therein.
126 D.T. Richens and A.G. Sykes, Inorg. Chem., 21 (1982) 418.
127 M.T. Paffett and F.C. Anson, Inorg. Chem., 22 (1983) 1347.
128 P. Kathirgamanathan, M. Martinez, and A.G. Sykes, Polyhedron, 5 (1986) 505.
129 T. Shibahara, H. Hattori, and H. Kuroya, J. Am. Chem. Soc., 106 (1984) 2710.
130 T. Shibahara, T. Yamada, H. Kuroya, E.F. Hills, P. Kathirgamanathan, and A.G. Sykes, Inorg. Chim. Acta, 113 (1986) L19.
131 T. Shibahara, H. Miyake, K. Kobayashi, and H. Kuroya, Chem. Lett., (1986) 139.
132 P. Kathirgamanathan, M. Martinez, and A.G. Sykes, J. Chem. Soc., Chem. Commun., (1985) 953.
133 T. Shibahara and H. Kuroya, Polyhedron, 5 (1986) 357.
134 A. Müller and U. Reinsch, Angew. Chem. Int. Ed. Engl., 19 (1980) 72.
135 C. Howlader, G.P. Haight, Jr., T.W. Hambley, G.A. Lawrence, K.M. Rahmoeller, and M.R. Snow, Aust. J. Chem., 36 (1983) 377.
136 K. Wieghardt, W. Herrmann, A. Müller, W. Eltzner, and M. Zimmermann, Z. Naturforsch., Teil B, 39 (1984) 876.
137 A. Müller, R. Jostes, W. Eltzner, C-S. Nie, E. Diemann, H. Bögge, M. Zimmermann, M. Dartmann, U. Reinsch-Vogell, S. Che, S.J. Cyvin, and B.N. Cyvin, Inorg. Chem., 24 (1985) 2872.
138 P.J. Vergamini, H. Vahrenkamp, and L.F. Dahl, J. Am. Chem. Soc., 93 (1971) 6327.
139 W. Beck, W. Danzer, and G. Thiel, Angew. Chem., 85 (1973) 625.
140 F.A. Cotton, Z. Dori, R. Llusar, and W. Schwotzer, Inorg. Chem., 25 (1986) 3654.
141 W-H. Pan, M.E. Leonowicz, and E.I. Stiefel, Inorg. Chem., 22 (1983) 672.
142 J. Bernholc and E.I. Stiefel, Inorg. Chem., 24 (1985) 1323.
143 A. Müller, S. Pohl, M. Dartmann, J.P. Cohen, J.M. Bennett, and R.M. Kirchner, Z. Naturforsch., Teil B, 34 (1979) 434.
144 A. Müller, R. Jostes, W. Jaegermann, and R. Bhattacharyya, Inorg. Chim. Acta, 41 (1980) 259.
145 A. Müller, W. Eltzner, H. Bögge, and R. Jostes, Angew. Chem., Int. Ed. Engl., 21 (1982) 795.
146 T.C.W. Mak, K.S. Jasim, and C. Chieh, Inorg. Chem., 24 (1985) 1587, and references therein.
147 F.A. Cotton, M.P. Diebold, Z. Dori, R. Llusar, and W. Schwotzer, J. Am. Chem. Soc., 107 (1985) 6735.
148 T. Shibahara, E. Kawano, M. Okano, M. Nishi, and H. Kuroya, Chem. Lett., (1986) 827.
149 T. Shibahara, H. Kuroya, K. Matsumoto, and S. Ooi, J. Am. Chem. Soc., 106 (1984) 789.

150 T. Shibahara, H. Kuroya, K. Matsumoto, and S. Ooi, Inorg. Chim. Acta, 116 (1986) L25.
151 J.A. Bandy, C.E. Davies, J.C. Green, M.L.H. Green, K. Prout, and D.P.S. Rodgers, J. Chem. Soc., Chem. Commun., (1983) 1395.
152 P.D. Williams and M.D. Curtis, Inorg. Chem., 25 (1986) 4562.
153 F.A. Cotton, Z. Dori, R. Llusar, and W. Schwotzer, Inorg. Chem., 25 (1986) 3529.
154 H. Brunner, H. Kauermann, and J. Wachter, J. Organomet. Chem., 265 (1984) 189.
155 T. Shibahara, K. Kohda, A. Ohtsuji, K. Yasuda, and H. Kuroya, J. Am. Chem. Soc., 108 (1986) 2757.
156 S. Bhaduri and J.A. Ibers, Inorg. Chem., 25 (1986) 3.
157 E. Königer-Ahlborn and A. Müller, Angew. Chem. Int. Ed. Engl., 14 (1975) 573.
158 A. Müller, R.G. Bhattacharyya, E. Königer-Ahlborn, R.C. Sharma, W. Rittner, A. Neumann, G. Henkel, and B. Krebs, Inorg. Chim. Acta, 37 (1979) L493.
159 A. Müller, W. Rittner, A. Neumann, E. Königer-Ahlborn, and R.G. Bhattacharyya, Z. Anorg. Allg. Chem., 461 (1980) 91.
160 F. Secheresse, G. Lavigne, Y. Jeannin, and J. Lefebvre, J. Coord. Chem., 11 (1981) 11.
161 A. Müller, H. Bögge, E. Krickemeyer, G. Henkel, and B. Krebs, Z. Naturforsch., Teil B, 37 (1982) 1014.
162 A. Müller, W. Hellmann, C. Römer, M. Römer, H. Bögge, R. Jostes, and U. Schimanski, Inorg. Chim. Acta, 83 (1984) L75.